


Spring 2022

## Analysis of Bio-alcohols with Mie-scattering and LTC for Lowered Emissions in PCCI

Cesar E. Carapia

Follow this and additional works at: <https://digitalcommons.georgiasouthern.edu/etd>

 Part of the [Automotive Engineering Commons](#), [Energy Systems Commons](#), [Environmental Indicators and Impact Assessment Commons](#), [Heat Transfer, Combustion Commons](#), and the [Sustainability Commons](#)

---

### Recommended Citation

Carapia, Cesar E., "Analysis of Bio-alcohols with Mie-scattering and LTC for Lowered Emissions in PCCI" (2022). *Electronic Theses and Dissertations*. 2390.  
<https://digitalcommons.georgiasouthern.edu/etd/2390>

This thesis (open access) is brought to you for free and open access by the Jack N. Averitt College of Graduate Studies at Digital Commons@Georgia Southern. It has been accepted for inclusion in Electronic Theses and Dissertations by an authorized administrator of Digital Commons@Georgia Southern. For more information, please contact [digitalcommons@georgiasouthern.edu](mailto:digitalcommons@georgiasouthern.edu).

# ANALYSIS OF BIO-ALCOHOLS WITH MIE-SCATTERING AND LTC FOR LOWERED EMISSIONS IN PCCI

by

CESAR EULISES CARAPIA

(Under the Direction of Valentin Soloiu)

## ABSTRACT

An investigation was conducted on the optimal engine parameters for facilitating lower  $\text{NO}_x$  and soot emissions of PCCI combustion with either ethanol or n-butanol. The PFI fuels selected were tested at loads of 3, 4, and 5 Bar IMEP for a total of 28 total combustion tests with variations made to the EGR% and boost pressure for each test in order to find the optimal emissions strategy. A Mie-scattering spray fuel analysis was also conducted on the three fuels to gain insight on their influence on combustion/emissions characteristics. It was found that ethanol had a greater average Sauter Mean Diameter than n-butanol by 5  $\mu\text{m}$ . This indicated that if the intake temperature is not sufficiently high, ethanol may not form a complete homogenous air-fuel mixture compared to n-butanol. Although ethanol had a lower reactivity than n-butanol it was found that the PPRR and subsequent AHRR was dramatically increased at loads of 4 and 5 bar IMEP. At 4 bar IMEP, PCCI with ethanol had an increased PPRR of 39% to PCCI with n-butanol and an increase of 39.67% for max AHRR. At 5 bar IMEP, PCCI with ethanol had an increased PPRR from PCCI with n-butanol of 38.94% and an increase of max AHRR of 50.98%. In concerns to the emissions, it was found that PCCI with n-butanol had greater reductions of  $\text{NO}_x$  emissions than PCCI with ethanol while ethanol was found to greatly reduce soot emissions. At a load of 5 bar IMEP, PCCI with n-butanol had a simultaneous reduction of  $\text{NO}_x$  and soot emissions of 53.2% and 36.7% respectively from CDC while PCCI with ethanol had emissions reductions of 21.3% and 72.28% respectively from CDC. In addition to this, the environmental impact of PCCI with either ethanol or n-butanol was shown to be considerably reduced by as much as 58.9% as indicated by the lower renewable carbon index. PCCI with n-butanol if incorporated at higher loads and a proper EGR/boost strategy, is a greater method of choice for reducing both  $\text{NO}_x$  and soot emissions while reducing the environmental impact.

INDEX WORDS: Emissions,  $\text{CO}_2$ , Biofuels, Low temperature combustion, Premixed charged compression ignition,  $\text{NO}_x$ , N-butanol, Ethanol, Soot, Diesel, Renewable carbon index

ANALYSIS OF BIO-ALCOHOLS WITH MIE-SCATTERING AND LTC FOR LOWERED  
EMISSIONS IN PCCI

by

CESAR EULISES CARAPIA

B.S., Georgia Southern University, 2019

A Thesis Submitted to the Graduate Faculty of Georgia Southern University

in Partial Fulfillment of the Requirements for the Degree

MASTER OF SCIENCE

© 2022

CESAR EULISES CARAPIA

All Rights Reserved

ANALYSIS OF BIO-ALCOHOLS WITH MIE-SCATTERING AND LTC FOR LOWERED  
EMISSIONS IN PCCI

by

CESAR EULISES CARAPIA

Major Professor:  
Committee:

Valentin Soloiu  
Marcel Ilie  
Mosfequr Rahman

Electronic Version Approved:  
May 2022

## DEDICATION

I would like to dedicate this thesis to my family for always supporting me in my endeavors. I would especially like to thank my parents Jose and Juana Carapia for teaching me how to perceive and conquer life's challenges. I would also like to dedicate this thesis to my older brother Emanuel "Manolo" Carapia who helped guide me in my younger years and inspired my love of cars. I would also like to thank the lord for granting me the wisdom and strength to finish my college education, Proverbs 4:7.

## ACKNOWLEDGMENTS

I would like to start by acknowledging my advisor Dr. Valentin Soloiu for his time, mentorship, and continuous support throughout my undergraduate and graduate studies and research. His guidance helped increase my knowledge to multiple disciplines within engineering and as a result develop my professional skill set.

I would like to thank Dr. Marcel Ilie for his assistance and guidance throughout my tenure at Georgia Southern University. With his assistance and aid in my studies, I have gained much knowledge and insight.

I would also like to extend my gratitude to my entire thesis committee: Dr. Valentin Soloiu, Dr. Marcel Ilie, Dr. Mosfequr Rahman for their time, encouragement, and insightful feedback for this review process.

Finally, I would also like to thank my fellow lab mates here at Georgia Southern: Remi Gaubert, Jose Moncada, Tyler Wiley, Austin Brant, Richard ‘Chipper’ Smith III, Levi McKinney, David Obando Ortegon, Amanda Weaver, Shaen Mehrzed, Siraj, Mathew Musial, and Seth Nowak for all of the support, the discussions and conversations, and the continued encouragement throughout my graduate studies

## TABLE OF CONTENTS

ACKNOWLEDGMENTS .....	3
LIST OF TABLES .....	7
LIST OF FIGURES .....	8
LIST OF EQUATIONS .....	10
LIST OF ABBREVIATIONS .....	11
CHAPTER	
1 INTRODUCTION .....	14
Purpose of Research.....	14
Emissions Effect on the Environment/Human Health .....	14
Conventional Emissions Mitigation Strategies .....	16
Electric Powertrains Progress and Hurdles .....	20
Internal Combustion Engines Future .....	24
Purpose of Study .....	27
Statement of Hypothesis .....	27
2 LITERATURE REVIEW.....	28
Bio-alcohols .....	28
Green House Gas Emissions .....	31
Low Temperature Combustion Methods .....	34
3 METHODS.....	37
Overview .....	37
Development of an Improved Electrically Driven Centrifugal Supercharger System.....	37
Fuel Analysis .....	43
Lower Heating Value .....	44
Viscosity .....	46
TGA-DTA.....	47
Fuel Spray Analysis .....	48
Engine Testing and Instrumentation .....	49
Engine Parameters for Operating Test Points .....	51
Injection Parameters.....	53
Criteria for Success .....	55



4 DATA AND RESULTS ANALYSIS .....	56
Preliminary Results .....	56
Low Temperature Oxidation and Thermal Stability Analysis .....	56
Viscosity Analysis .....	58
Lower Heating Value Analysis .....	59
Mie-Scattering Fuel Spray Analysis .....	60
Preliminary Fired Engine Analysis .....	61
Preliminary NO <sub>x</sub> Emissions Results .....	62
Preliminary Soot Emissions Results .....	65
Preliminary Unburnt Hydrocarbon (UHC) Emissions Results .....	68
Fired Engine Analysis .....	71
Fired Engine Tests Lambda .....	71
Optimal CDC and PCCI Test Points per Load .....	72
Combustion Pressure and Pressure Rise Rate .....	73
Ringing Intensity .....	79
In-Cylinder Temperature .....	81
Apparent Heat Release Rate .....	84
Mass Fraction Burned .....	87
Heat Flux and Heat Losses .....	90
Emissions Analysis .....	93
Nitrogen Oxide Emissions .....	93
Soot Emissions .....	95
Unburnt Hydrocarbon Emissions .....	97
Carbon Monoxide Emissions .....	98
Formaldehyde and Aldehyde Emissions .....	99
Carbon Dioxide Emissions and Carbon Environmental Impact Index .....	101
Fuel Consumption and Efficiency .....	104
Energy Specific and Brake Specific Fuel Consumption .....	104
Indicated Thermal Efficiency .....	107
5 FINDINGS, CONCLUSION, AND RECOMMENDATIONS .....	109
Conclusions .....	109
Future Work .....	111

Special Thanks .....	111
REFERENCES .....	112

## LIST OF TABLES

Table 1: Specifications and Diameters of the Supercharger Transmission .....	40
Table 2: Thermo-physical Properties of Research Fuels (Elfasakhany and Mahrous 2016, Zheng et al. 2018, VP-Racing-Fuels 2019).....	44
Table 3: Engine Specifications .....	49
Table 4: Selected Measurement Accuracy .....	50
Table 5: Operating test points at a load of 3, 4, & 5 bar IMEP .....	52
Table 6: Engine Operation Parameters/Limits.....	53
Table 7: Injection Parameters at 3 Bar IMEP .....	54
Table 8: Injection Parameters at 4 Bar IMEP .....	54
Table 9: Injection Parameters at 5 Bar IMEP .....	55
Table 10: Volatility of researched fuels.....	57
Table 11: Viscosity of the researched fuels at 40 °C .....	59
Table 12: Calorimeter Results .....	60
Table 13: Particle Size Distribution by Volume ( $\mu\text{m}$ ).....	60
Table 14: Global Lambda for All Combustion Tests Conducted .....	71
Table 15: Selected Optimal Test Points per Load and Combustion/Fuel Method .....	72
Table 16: RI of 3 Optimal Points per Load Tested.....	80
Table 17: ID and CD for Optimal Points at 5 Bar IMEP.....	89
Table 18: Percent Losses of Optimal Points at 5 Bar IMEP.....	93
Table 19: NO <sub>x</sub> Emissions of Optimal Points.....	95
Table 20: Soot Emissions of Optimal Points .....	96
Table 21: UHC Emissions of Optimal Points .....	98
Table 22: CO Emissions of Optimal Points.....	99
Table 23: Formaldehyde Emissions of Optimal Points .....	100
Table 24: Aldehyde Emissions of Optimal Points.....	101
Table 25: CO <sub>2</sub> Emissions of All the Optimal Combustion Tests Conducted .....	103
Table 26: Renewable Carbon Index of All the Optimal Combustion Tests Conducted.....	104
Table 27: ESFC of Optimal Points .....	106
Table 28: BSFC of Optimal Points .....	107
Table 29: ITE of Optimal Points.....	108

## LIST OF FIGURES

Figure 1: NO <sub>x</sub> Emissions Transformation into Ozone (NOAA 2016) .....	15
Figure 2: Annual Wet Sulfate Deposition Prior to ULSD and After (EPA 2021a) .....	16
Figure 3: EGR System (Hannu Jääskeläinen 2020).....	17
Figure 4: Tier 4 CI Exhaust Aftertreatment System (Deere 2022) .....	18
Figure 5: CI vs SI Emissions Charecteristics (Maurya 2019, Pitz JW 2011) .....	19
Figure 6: Battery Pack Costs Since 2010 (Richter 2021) .....	20
Figure 7: SQM Lithium Mine in the Atacama Desert Chile (Ellsmoor 2019) .....	22
Figure 8: Cobalt demand from 2000 to 2015 with projections to 2025 (Frankel 2016) .....	22
Figure 9: Artisinal Mining Used in the Extraction of Cobalt (Frankel 2016) .....	23
Figure 10: Toyota's Plan for Solid State Batteries (VISNIC 2021) .....	24
Figure 11: PFI Injection of H <sub>2</sub> vs DI of H <sub>2</sub> (Gao et al. 2022, Babayev et al. 2021) .....	26
Figure 12: Criteria for Feasability of a Synthetic Fuel (Styring, Dowson, and Tozer 2021) .....	27
Figure 13. Annual CO <sub>2</sub> emissions per country (Roser 2020).....	31
Figure 14. Third Generation Biofuel Production Process (Maity et al. 2014).....	33
Figure 15: CDC vs PCCI vs RCCI combustion at 1 and 4 bar BMEP (Singh, Kumar, and Agarwal 2020) .....	35
Figure 16: Single Fuel vs Dual Fuel LTC Methods Performance Charecteristics (Shim, Park, and Bae 2020) .....	36
Figure 17: Previous Supercharger Pulley System.....	38
Figure 18: Supercharger Transmission System Schematic.....	39
Figure 19: Free Body Diagram of The Electric Motor to Intermediate Pulleys .....	41
Figure 20: CAD Model of New Supercharger Transmission System.....	42
Figure 21: Old vs New Supercharger System Boost .....	43
Figure 22. Parr Calorimeter Assembly Cross-Sectional View Source: (Parr Instrument Company, Series 1341 Plain Jacket Oxygen Combustion calorimeters n.d.) .....	45
Figure 23. Parr Calorimeter Temperature Rise Curve Source: (Parr Instrument Company, Series 1341 Plain Jacket Oxygen Combustion calorimeters n.d) .....	46
Figure 24. Brookfield DV-II +Pro Rotational Viscometer (Brookfield) .....	46
Figure 25. Shimadzu FTG-60 (Oceania) .....	47
Figure 26. Mie Scattering Spray Analysis Test Bed (Soloiu et al. 2019).....	48
Figure 27: Experimental Engine Setup .....	51
Figure 28: Thermogravimetric Analysis .....	56
Figure 29: Differential Thermal Analysis of the Researched Fuels. ....	58
Figure 30: Viscosity measurements for the researched fuels.....	59
Figure 31: Spray SMD distribution and development .....	61
Figure 32: NO <sub>x</sub> emissions at 3 bar IMEP, CDC (a), PCCI 45BU (b), PCCI 45ET (c) .....	63
Figure 33: NO <sub>x</sub> emissions at 4 bar IMEP, CDC (a), PCCI 45BU (b), PCCI 45ET (c) .....	64
Figure 34: NO <sub>x</sub> emissions at 5 bar IMEP, CDC (a), PCCI 45BU (b), PCCI 45ET (c) .....	65
Figure 35: Soot emissions at 3 bar IMEP, CDC (a), PCCI 45BU (b), PCCI 45ET (c) .....	66
Figure 36: Soot emissions at 4 bar IMEP, CDC (a), PCCI 45BU (b), PCCI 45ET (c) .....	67
Figure 37: Soot emissions at 5 bar IMEP, CDC (a), PCCI 45BU (b), PCCI 45ET (c) .....	68

Figure 38: UHC emissions at 3 bar IMEP PCCI 45BU (a) and PCCI 45ET (b) .....	69
Figure 39: UHC emissions at 4 bar IMEP PCCI 45BU (a) and PCCI 45ET (b) .....	70
Figure 40: UHC emissions at 5 bar IMEP PCCI 45BU (a) and PCCI 45ET (b) .....	70
Figure 41: Optimal Test Points Parameters at 3 Bar IMEP .....	73
Figure 42: In-cylinder Pressure and PRR of All Trials at 3 Bar IMEP .....	74
Figure 43: In-cylinder Pressure and PRR of The Best 3 Trials at 3 Bar IMEP .....	75
Figure 44: In-cylinder Pressure and PRR of All Trials at 4 Bar IMEP .....	76
Figure 45: In-cylinder Pressure and PRR of The Best 3 Trials at 4 Bar IMEP .....	77
Figure 46: In-cylinder Pressure and PRR of All Trials at 5 Bar IMEP .....	78
Figure 47: In-cylinder Pressure and PRR of The Best 3 Trials at 5 Bar IMEP .....	79
Figure 48: RI for All Combustion Tests Conducted at 3 bar IMEP .....	80
Figure 49: In-cylinder Temperature for Combustion Tests Conducted at 3 Bar IMEP.....	81
Figure 50: In-cylinder Temperature for Combustion Tests Conducted at 4 Bar IMEP.....	82
Figure 51: In-cylinder Temperature for Combustion Tests Conducted at 5 Bar IMEP.....	83
Figure 52: AHRR for Combustion Tests Conducted at 3 Bar IMEP.....	85
Figure 53: AHRR for Combustion Tests Conducted at 4 Bar IMEP.....	86
Figure 54: AHRR for Combustion Tests Conducted at 5 Bar IMEP.....	87
Figure 55: MFB of Optimal Points at 5 Bar IMEP.....	88
Figure 56: Heat Flux of Optimal Points at 5 Bar IMEP .....	91
Figure 57: Heat Losses of Optimal Points at 5 Bar IMEP .....	92
Figure 58: NO <sub>x</sub> Emissions of All Combustion Tests Conducted .....	94
Figure 59: Soot Emissions of All the Combustion Tests Conducted.....	96
Figure 60: UHC Emissions of All the Combustion Tests Conducted .....	97
Figure 61: CO Emissions of All the Combustion Tests Conducted .....	98
Figure 62: Formaldehyde Emissions of All the Combustion Tests Conducted.....	100
Figure 63: Aldehyde Emissions of All the Combustion Tests Conducted .....	101
Figure 64: CO <sub>2</sub> Emissions of All the Combustion Tests Conducted .....	102
Figure 65: ESFC of All the Combustion Tests Conducted.....	105
Figure 66: BSFC of All the Combustion Tests Conducted.....	106
Figure 67: ITE of All the Combustion Tests Conducted .....	107

## LIST OF EQUATIONS

Equation 1 .....	39
Equation 2 .....	39
Equation 3 .....	40
Equation 4 .....	40
Equation 5 .....	40
Equation 6 .....	40
Equation 7 .....	40
Equation 8 .....	41
Equation 9 .....	45
Equation 10 .....	79
Equation 11 .....	84
Equation 12 .....	90
Equation 13 .....	90
Equation 14 .....	103

## LIST OF ABBREVIATIONS

A	Cylinder Area
AFR	Air Fuel Ratio
AHRR	Apparent Heat Release Rate
ASTM	American Society for Testing and Materials
ATDC	After Top Dead Center
BMEP	Brake Mean Effective Pressure
BTDC	Bottom Dead Center
CA10	10% Mass Fuel Burned
CAD	Crank Angle Degree
CD	Combustion Duration
CDC	Conventional Diesel Combustion
CI	Compression Ignition
CO	Carbon Monoxide
COV	Coefficient of Variation
cP	centi Poise
CRDI	Common Rail Direct Injection
CVCC	Constant Volume Combustion Chamber
D	Cylinder Bore Diameter
DCN	Derived Cetane Number
DF-PCCI	Dual Fuel Premixed Charge Compression Ignition
DI	Direct Injection
DOC	Diesel Oxidative Catalysts
DSHC	Direct Sugar to Hydrocarbon
DTA	Differential Thermal Analysis
DV (10)	Largest Droplet Sauter Mean Diameter for 10% of Fuel Volume Spray
DV (50)	Largest Droplet Sauter Mean Diameter for 50% of Fuel Volume Spray
DV (90)	Largest Droplet Sauter Mean Diameter for 90% of Fuel Volume Spray

ECU	Engine Control Unit
EGR	Exhaust Gas Recirculation
EPA	Environmental Protection Agency
EU	European Union
FTIR	Fourier Transform Infrared
GHG	Green House Gas
H	Lower Heating Value
H <sub>c</sub>	Gross Heating Value
H <sub>net</sub>	Net Heating Value
HCCI	Homogenous Charge Compression Ignition
HTHR	High Temperature Heat Release
ICE	Internal Combustion Engine
ID	Ignition Delay
IMEP	Indicated Mean Effective Pressure
LHV	Lower Heating Value
LTC	Low Temperature Combustion
m <sub>air</sub>	Mass of air
MC	Motoring Curve
MFB	Mass Fraction Burned
Nox	Nitrogen Oxides
PAH	Poly Aromatic Hydrocarbons
PCCI	Premixed Charge Compression Ignition
PCCI 45BU	PCCI with 45% Fuel mass of n-butanol Port Fuel Injected
PCCI 45ET	PCCI with 45% Fuel mass of ethanol Port Fuel Injected
PFI	Port Fuel Injection
PID	Proportional Integral Derivative
PM	Particulate Matter
PPC	Partially Premixed Combustion



PPM	Parts per Million
PPRR	Peak Pressure Rise Rate
PRR	Pressure Rise Rate
$\dot{q}$	Overall Heat Flux
RCCI	Reactivity Controlled Compression Ignition
RCCI LRF	Reactivity Controlled Compression Ignition Low Reactive Fuel
RCI	Renewable Carbon Index
Re	Reynolds Number
RI	Ringing Intensity
RPM	Revolutions per Minute
S	Stroke
SI	Spark Ignition
SMD	Sauter Mean Diameter
SOI	Start of Injection
TA(10)	10% Fuel Mass Vaporized
TA(50)	50% Fuel Mass Vaporized
TA(90)	90% Fuel Mass Vaporized
THC	Total Hydrocarbons
$T_A$	Combustion Temperature
$T_w$	Wall Temperature
UHC	Unburnt Hydrocarbons
ULSD	Ultra-Low Sulfur Diesel
UV	Ultraviolet
V	Cylinder Volume
$\Delta\%$	Delta Percent
$\lambda_A$	Air Thermal Conductivity
$\sigma$	Stefan-Boltzman Constant

## CHAPTER 1

### INTRODUCTION

#### Purpose of Research

Society today has become more concerned about climate change and the impact of non-renewable carbon on the environment. As a result, governments worldwide have begun to enact policies for the reduction of Green House Gasses (GHG) through either passing even stricter emissions regulations or the outright banning of Internal Combustion Engine (ICE) powered passenger vehicles. With this recent shift, attention has been drawn on how to meet these stricter emissions and how to reduce ICE impact on the environment while simultaneously meeting energy demands. Currently as it stands, energy demands for the consumer and commercial transportation sector require a multi-faceted solution as electric powertrains are not yet suitable for all sectors of the market.

With this in mind, research is well underway on minimizing the impact ICE powered vehicles have on the environment with the utilization of advanced combustion techniques, exhaust after treatment systems, renewable biofuels, hydrogen combustion, and synthetic drop-in fuel replacements. As a result of which, promising solutions have emerged for future and past ICE platforms to tackle society's ever-increasing energy demands while overcoming the environmental challenges set before it. As such, for the foreseeable future ICE powered powertrains will remain an integral part of the transportation sector specifically in rural communities and the commercial sector.

#### Emissions Effect on the Environment/Human Health

Over the last couple of decades, concerns have been growing on the impact various gaseous emissions from ICE have on both the environment and human health. As a result, various studies have been conducted not only on how to mitigate these emissions but also their impact in general. The primary emissions of concern from Compression Ignition (CI) engines apart from Carbon Dioxide (CO<sub>2</sub>), are Nitrogen Oxide (NO<sub>x</sub>) and soot emissions. NO<sub>x</sub> emissions from combustion primarily end up in the lower troposphere where they are broken down by UV rays and form ozone as seen in Figure 1. As a result of this, smog develops in highly industrious/urban areas and has been shown to negatively affect human health particularly those with respiratory issues (Price et

al. 1997). In addition,  $\text{N}_2\text{O}$  has been shown to reduce stratospheric ozone as it is broken down by UV rays into nitric oxide and nitrogen which then reacts with ozone to form  $\text{NO}_2$ .

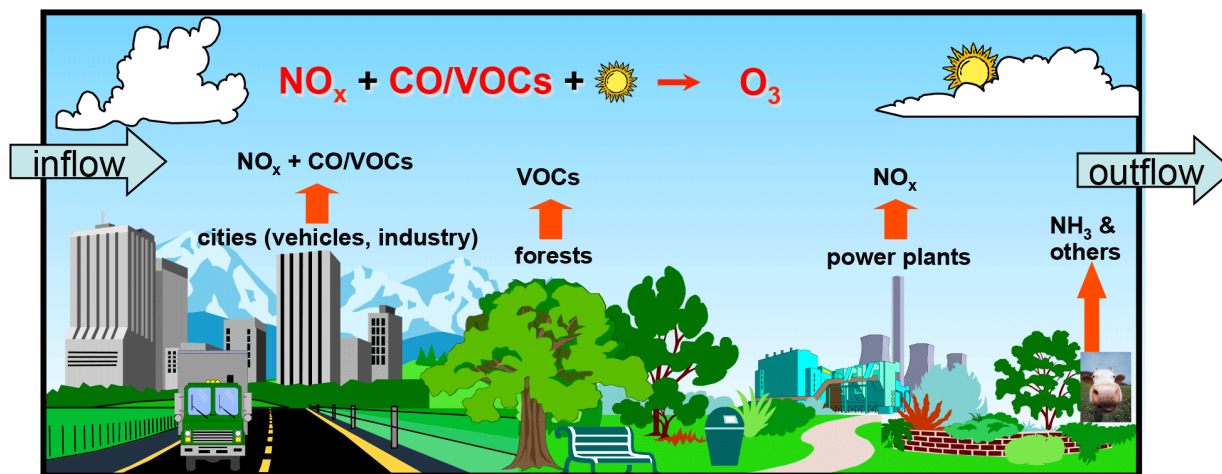


Figure 1:  $\text{NO}_x$  Emissions Transformation into Ozone (NOAA 2016)

In addition to effecting human health and the formation of tropospheric ozone,  $\text{NO}_x$  emissions have been shown to effect acid rain events due to the increase in hydroxyl-radicals formed in the troposphere (Lawrence and Crutzen 1999). However, acid rain events are predominately governed by the sulfur released into the atmosphere, this once was a major concern prior to the introduction of Ultra-Low Sulfur Diesel (ULSD) in 2006 (EPA 2021b). As a direct result of this, the quantity of sulfate deposition in bodies of water were shown to decrease from the high levels previously seen between 1989-1991 as shown in Figure 2.

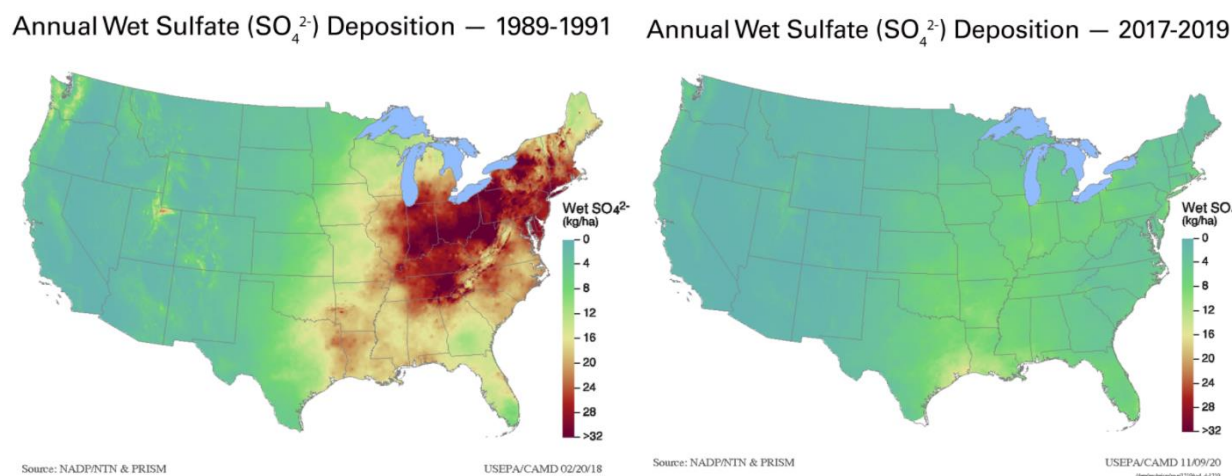


Figure 2: Annual Wet Sulfate Deposition Prior to ULSD and After (EPA 2021a)

Although soot emissions have a relatively low environmental impact when compared to other gaseous emissions emitted from combustion processes, they do however negatively impact human health, particularly those who have respiratory conditions (EPA 2021c). As a result of this investigations were done and continue to this day on how to mitigate their effect and how different particulate matter shape/sizes effect their impact on human health (H. Bockhorn 2009). It was found in investigations from Frampton et al. that when exposed to ultrafine carbon particles in concentration 10-100 times greater than most urban environment for prolonged periods of time, tests subjects exhibited minimal to no airway inflammation (Frampton et al. 2004). This study indicates that pure soot by itself may not negatively impact health although contaminants that are attached to the soot particles may cause issues (H. Bockhorn 2009). In addition, it was found that soot from bio-diesel combustion was less mutagenic than soot from ULSD combustion due to the reduction of poly aromatic hydrocarbons (PAH), indicating that apart from bio-diesels lesser impact on the environment it may also have lesser impact on human health (H. Bockhorn 2009).

### Conventional Emissions Mitigation Strategies

One of the first methods of mitigating emissions from CI engines was Exhaust Gas Recirculation (EGR) introduced in the 1970s and grew more prevalent starting in the 2000's (Hawley et al. 1999) an example of which can be seen in Figure 3. This method was primarily introduced for the reduction of  $\text{NO}_x$  emissions, however often at the cost of soot and UHC

emissions. EGR is able to reduce  $\text{NO}_x$  emissions due to its effect on increasing the specific heat of the intake air, lower peak Apparent Heat Release Rate (AHRR), and increasing the Ignition Delay (ID) thereby reducing combustion temperatures (Maiboom, Tazua, and H      2008).

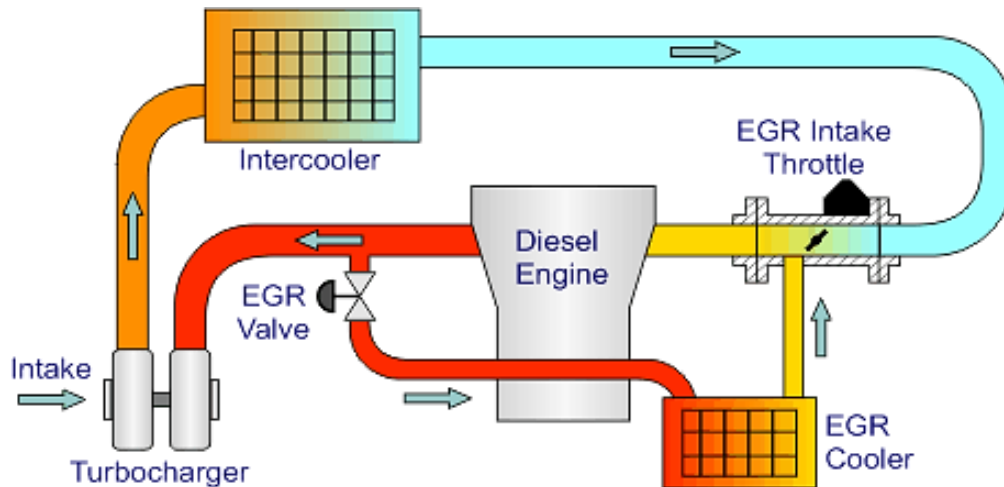


Figure 3: EGR System (Hannu J          2020)

However, EGR's negative effect on soot emissions and Brake Specific Fuel Consumption (BSFC) can be mitigated by employing a constant Air Fuel Ratio (AFR) strategy while simultaneously lowering  $\text{NO}_x$  emissions (Kouremenos, Hountalas, and Binder 2001).

Introduced soon after EGR, diesel exhaust aftertreatment systems began to be introduced into on-highway diesel engines starting in 2001 with Diesel Oxidative Catalysts (DOC) being the first (Hannu J          2020). This was done in order to meet more stringent  $\text{NO}_x$ , CO, soot, and UHC emissions regulations that could not be met with either injection strategy's or EGR. Unlike in their Spark Ignition (SI) counterparts, CI aftertreatment systems require multiple components with different materials, with each component targeting a specific exhaust component as seen in Figure 4.

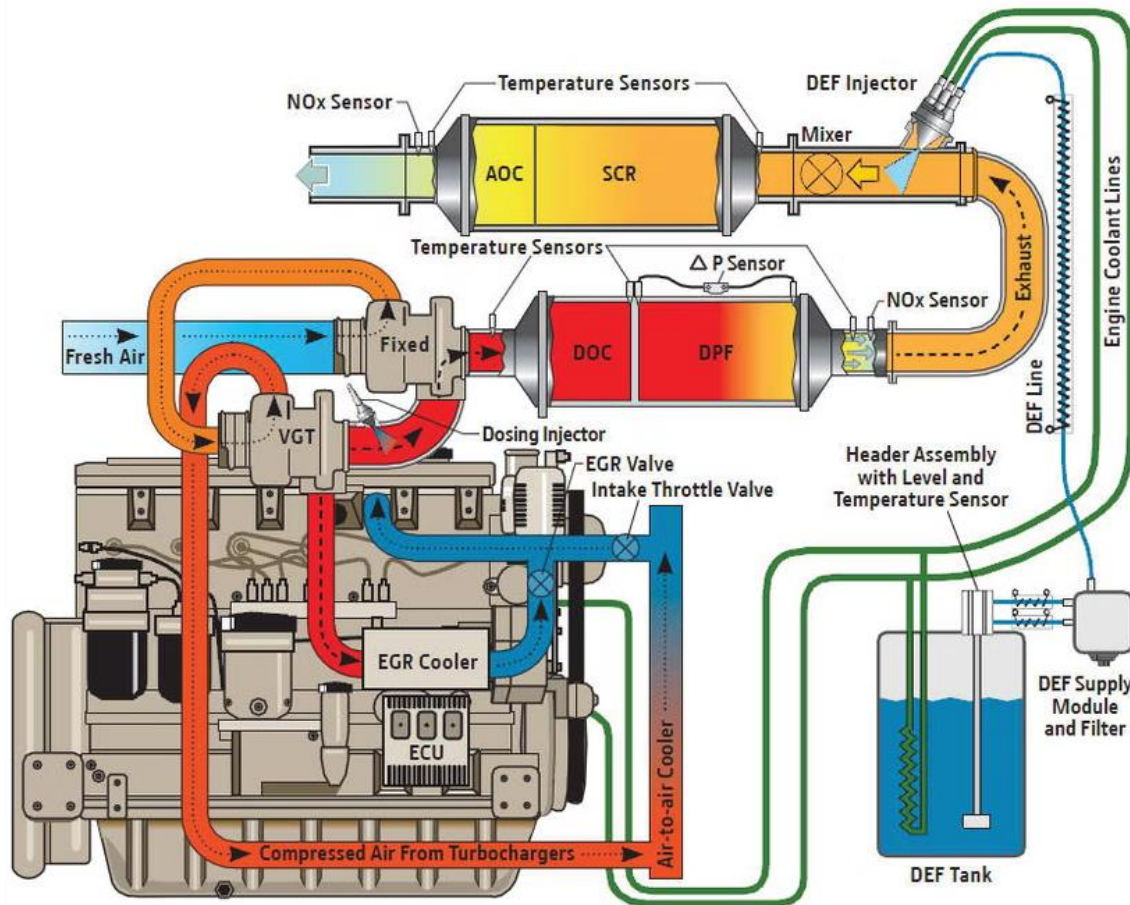


Figure 4: Tier 4 CI Exhaust Aftertreatment System (Deere 2022)

This is due to the fact of CI combustion typically having both a leaner AFR and lower exhaust temperatures than in SI combustion makes SI catalyst ineffective on reducing emissions on a CI platform (Majewski 2016). In addition to this CI engines typically have higher NO<sub>x</sub> and soot emissions than SI engines, thus increasing the complexity of the aftertreatment system needed as seen in Figure 5 where the combustion characteristics of each are visualized.

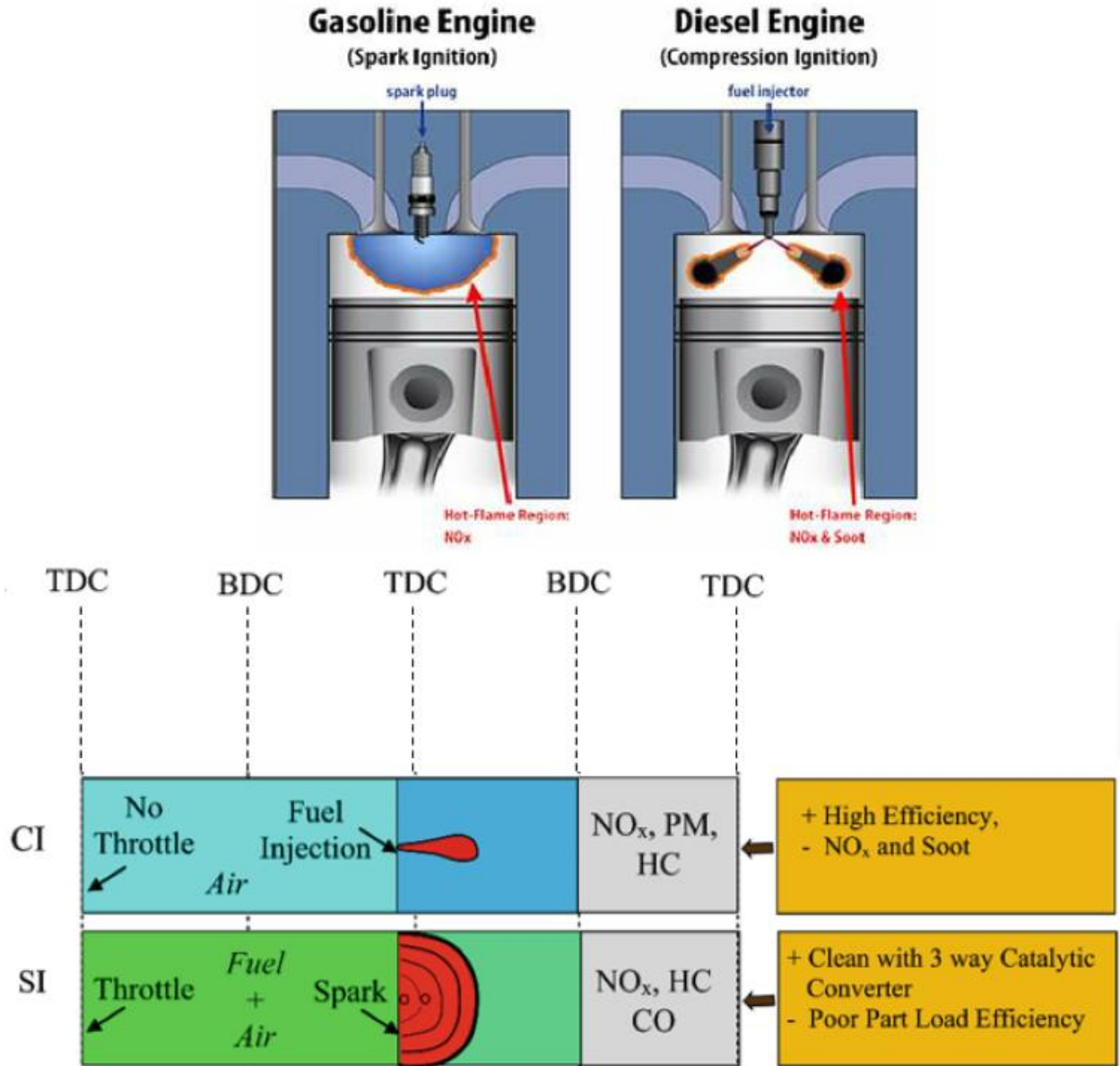


Figure 5: CI vs SI Emissions Characteristics (Maurya 2019, Pitz JW 2011)

Although these methods have been adequate for meeting current and near-term emissions standards, it is however not without its drawbacks. Primary of which is the added cost of these systems (primarily that of the exhaust after treatment system) to the overall cost of the vehicle. In addition to this, it adds another fluid that must be regularly replenished by the user for the system to function optimally.



## Electric Powertrains Progress and Hurdles

Electric vehicles have been gaining popularity in recent years as an alternative platform for the transportation sector. This in part is due to both advancements in battery tech, charging infrastructure, and increasing incentives by government bodies within consumer level vehicle platforms (Morgan 2019). However, for many particularly those not located in urban centers electric vehicles and their supporting infrastructure have not yet reached the maturity level wanted by these consumers (Altun et al. 2019).

Battery technology has made great advancements in recent years with decreasing costs of battery packs as well as increased range. Over the last 12 years the \$ per kWh of battery packs have decreased from \$1200 to just under \$200 per kWh as seen in Figure 6 (Richter 2021). This has dramatically reduced the costs of electric vehicles and as a result lowered the threshold at which consumers can obtain one with the price being brought lower by government incentives. Although the price of battery packs has lowered tremendously over the last decade, it appears in recent years to have leveled out indicating that the current battery technology (lithium-ion based) has reached its limits.

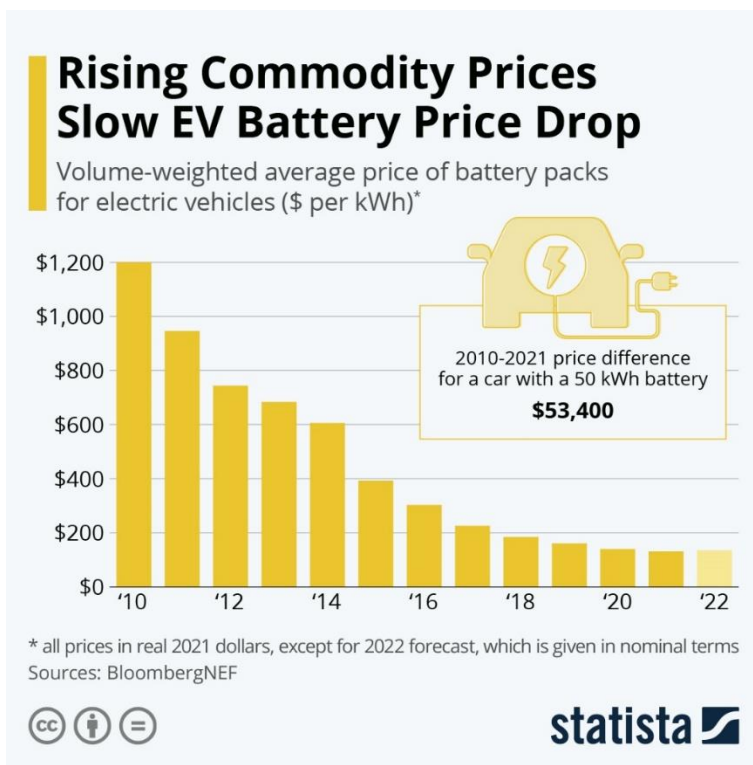


Figure 6: Battery Pack Costs Since 2010 (Richter 2021)



As much progress as battery technology has made over the last decade, more progress is needed to not only further reduce the cost per kWh of the battery packs used in vehicles but also the reduction of their environmental impact. Although from an end user perspective, electric cars in themselves are cleaner than their ICE powered counterparts. Be that as it may electric vehicles still have environmental concerns that must be addressed, primarily that of the sustainability of their batteries during the manufacturing stage and after their useful cycle life. Particularly the heavy metals required for the making of most electric vehicle battery packs, primarily lithium and cobalt.

Lithium is a vital component that forms the backbone of modern-day rechargeable batteries due to its energy density and life cycle compared to other battery technologies available in the market (Nickel cadmium, lead acid, etc.). Lithium although present in trace amounts throughout the world in most rocks and soils, is rarely found in concentrations necessary for industrial level extraction processes. This is due in no short part by the reactivity of lithium causing it to bind with other elements reducing its concentrations. Currently few locations in the world have the abundance of lithium necessary for industrial level extraction, the majority of which are located in Argentina, Bolivia, and Chile (DC Bradley 2018). Although other geological viable locations exist in the United States, China, and Australia, the vast majority of these deposits are in lower concentrations than the deposits found in South America.

However, the process in which lithium is obtained is highly damaging to the environment in both its extraction from the ground and the refinement of its ore (Kaunda 2020). As is the case with most mining operations, the extraction of the ore from the earth tends to be heavily destructive to the local environment with practices such as the usage of separation ponds as shown in Figure 7. The usage of this mining process can negatively impact the environment by not only contaminating the local watertable with various heavy metals that severely degrade biological functions but also uses a great quantity of water in order to mine the mineral (DC Bradley 2018).

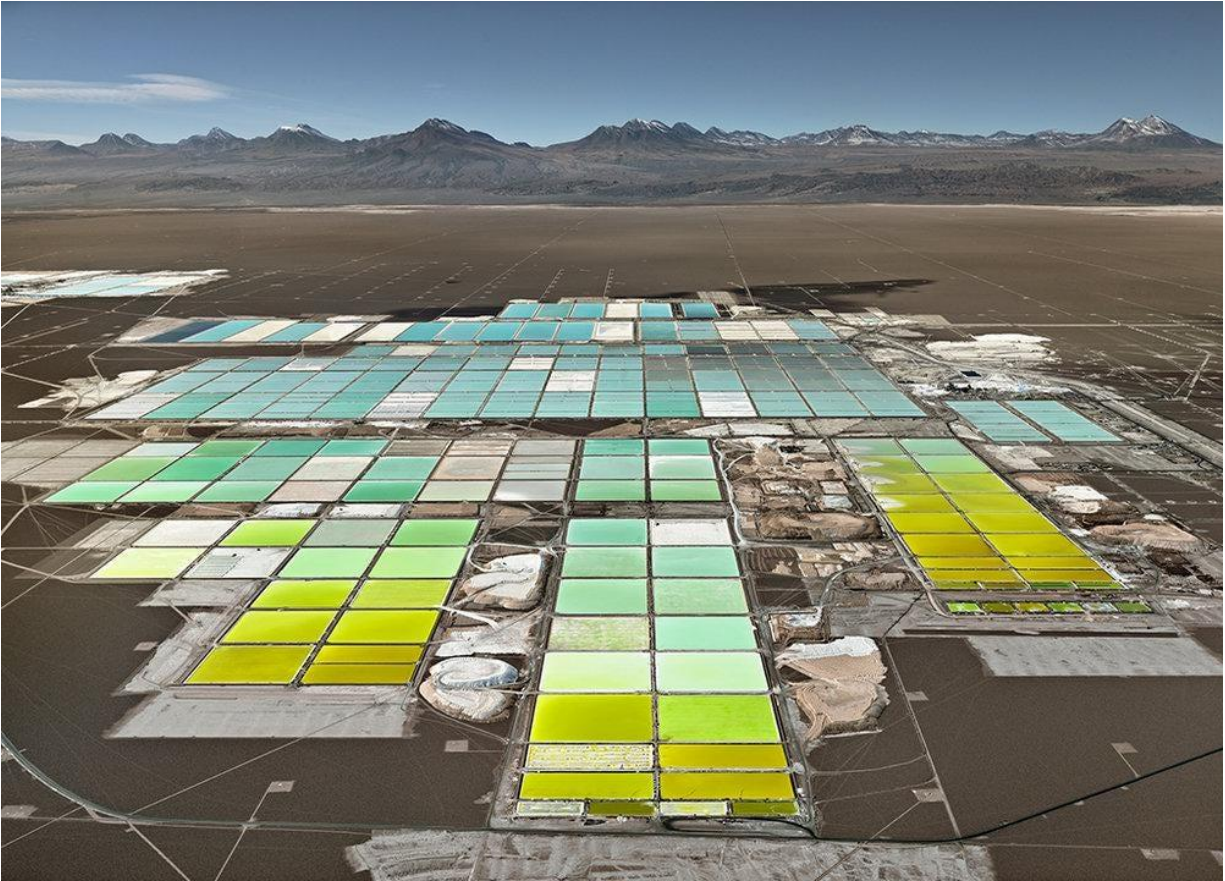


Figure 7: SQM Lithium Mine in the Atacama Desert Chile (Ellsmoor 2019)

In addition to this, cobalt another vital component of most modern-day battery technology has various issues related to not only its environmental impact but also the ethics associated with the extraction practices of most mining operations. Over the last two decades demand for cobalt has been increasing at an exuberant rate as consumers demand more potent portable devices in conjunction with the increased production of EVs as seen in Figure 8 below.

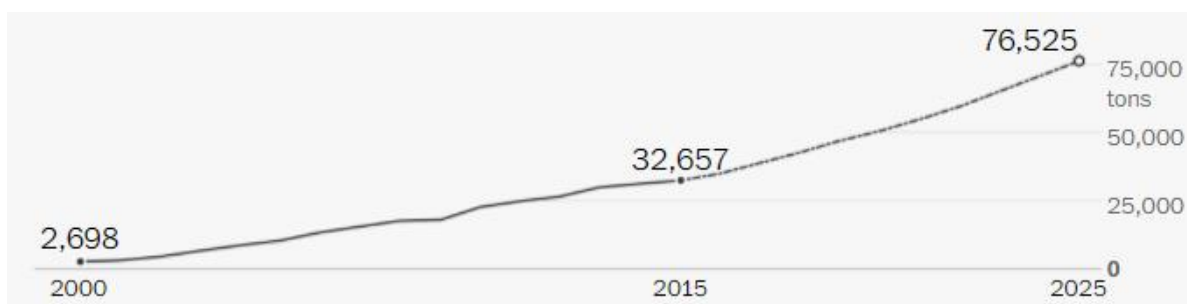


Figure 8: Cobalt demand from 2000 to 2015 with projections to 2025 (Frankel 2016)

Cobalt similar to lithium, is not widely available at high concentrations throughout the world except for a few locations primarily located in the Democratic Republic of the Congo. As a result of economic pressures, most mining operations in the DRC do not adhere to environmental or worker safety regulations typically seen in other countries in order to keep up with the increasing demand on the global market. Due to the lack of regulations and a system where only upon successful recovery of minerals are the miners paid, miners are forced to use artisanal mining practices as seen in Figure 9. All too often this leads to severe injuries or even fatalities, due to the lack of oversight of these operations most families are left paying the medical bills on their own.



Figure 9: Artisanal Mining Used in the Extraction of Cobalt (Frankel 2016)

With all of this in mind, research on solid state batteries is poised to help alleviate most of these issues while simultaneously increasing the versatility and energy density of rechargeable batteries (Albertus et al. 2021). Unlike lithium-ion batteries, solid state batteries utilize a solid electrolyte layer (primarily composed of either ceramics or polymers) rather than a liquid



electrolyte and as a result reduces the reliance upon metals like cobalt or lithium and increases the resilience of the battery cell. However, the manufacturing process of incorporating the solid electrolytes with the electrodes has been a major hurdle for mass production of this battery tech. Nevertheless, researchers from MIT have developed a sintering methodology for joining these materials together in a manner that can be scaled up to levels necessary for mass production (Chandler 2022). In recent years this technology has begun to mature to the point where major companies such as Toyota have begun to develop plans to mass produce them by the mid 2020's for their products (Miller 2022) as seen in their roadmap presentation in Figure 10.

## Next-generation lithium-ion battery

### [Aims]

**Longer service life**

**Greater energy density**

**More compact size**

**Lower cost**

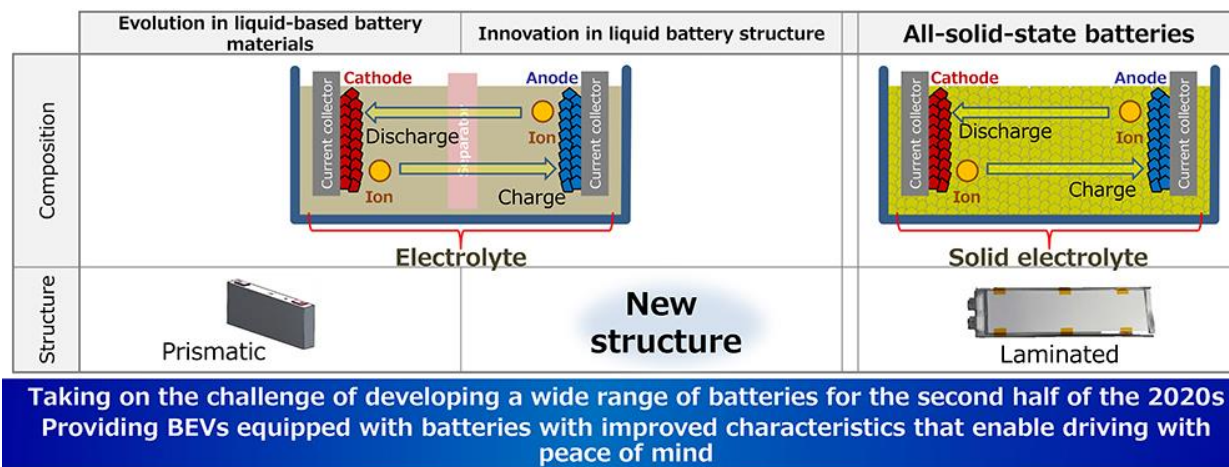


Figure 10: Toyota's Plan for Solid State Batteries (VISNIC 2021)

## Internal Combustion Engines Future

Although fierce competition has begun over the powertrain technology utilized in the passenger vehicle portion of the automobile industry, ICE will remain an integral solution for solving societies energy demands particularly in the commercial/industrial markets. Advancements on the reduction of emissions emitted from ICE have been made not only through research in advance combustion techniques but also the usage of alternative fuels either synthetic or biofuels. One advancement that has been gaining traction in recent years is the usage of

hydrogen as either a dual fuel or single fuel solution for reducing and/or eliminating CO<sub>2</sub> emissions and reduce NO<sub>x</sub> emissions in ICE mostly intended for commercial/industrial sectors (Hosseini and Wahid 2016). For example, studies have been conducted on the utilization of hydrogen for fueling gas turbines for providing quick electrical supply for the PowerGrid's instantaneous demand spikes. A study by Beita et al. investigated the usage of either natural/hydrogen gas mixtures and pure hydrogen gas for utilization in a gas turbine for minimizing the thermoacoustic instability characteristics and NO<sub>x</sub> emissions of the various mixtures (Beita et al. 2021). With the findings of this investigation and others related to this subject, hydrogen gas has a promising future for in the power generation industry as not only is its cleaner burning than natural gas but also simultaneously helps solves the power generation issues associated with renewables.

In conjunction with this, hydrogen has also been investigated for usage in CI engines in the commercial sector. The benefits seen in hydrogen combustion in gas turbines are also prevalent in CI engines, however work is underway for optimizing CI for utilization of hydrogen gas. Primarily the research is focused on optimizing the injection strategy and other various emission control methods (EGR and boost) for not only minimizing NO<sub>x</sub> emissions but also maintain a cycle-by-cycle combustion stability as seen in various studies (Gao et al. 2022, Babayev et al. 2021). As seen in Figure 11 below, a direct injection strategy is optimal for maintain stability of the combustion process as a PFI strategy has issues with backfire and/or pre-ignition.

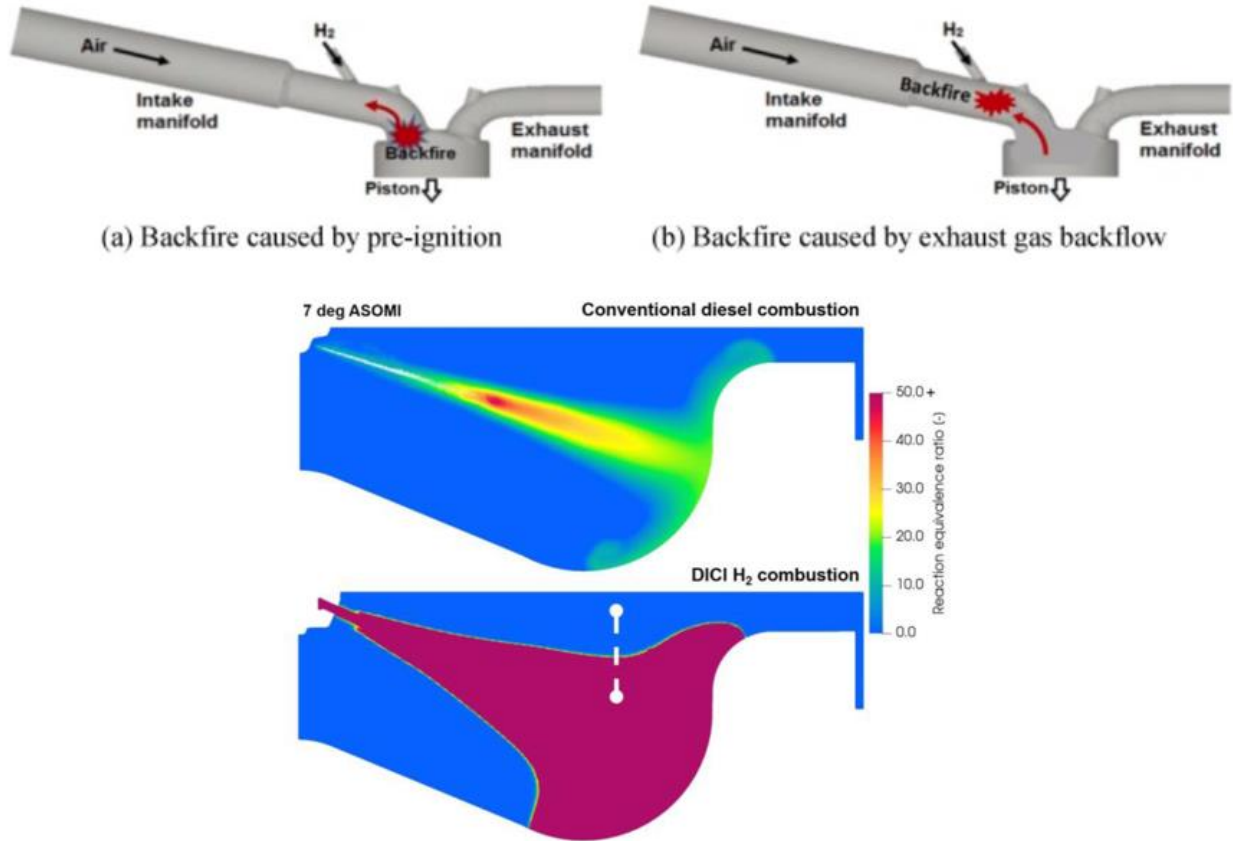


Figure 11: PFI Injection of H<sub>2</sub> vs DI of H<sub>2</sub> (Gao et al. 2022, Babayev et al. 2021)

In addition to hydrogen combustion, alternative synthetic fuels have been developed as drop-in replacements for fossil fuels utilized in either SI, CI, or aerospace jet engines (Styring, Dowson, and Tozer 2021, Boehm, Scholla, and Heyne 2021). This henceforth is meant to be utilized in existing ICE platforms as the transition is made to newer platforms that can utilize other alternative fuels. These synthetic fuels have similar combustion characteristics to their intended replacements, as of yet research is underway for increasing the production scale of these fuels. Though progress has been made on utilizing various catalysts for increasing efficiency in production of these fuels from various sources (Goh et al. 2022). A figure detailing the criteria utilized for measuring the feasibility of a synthetic fuel can be seen in Figure 12.

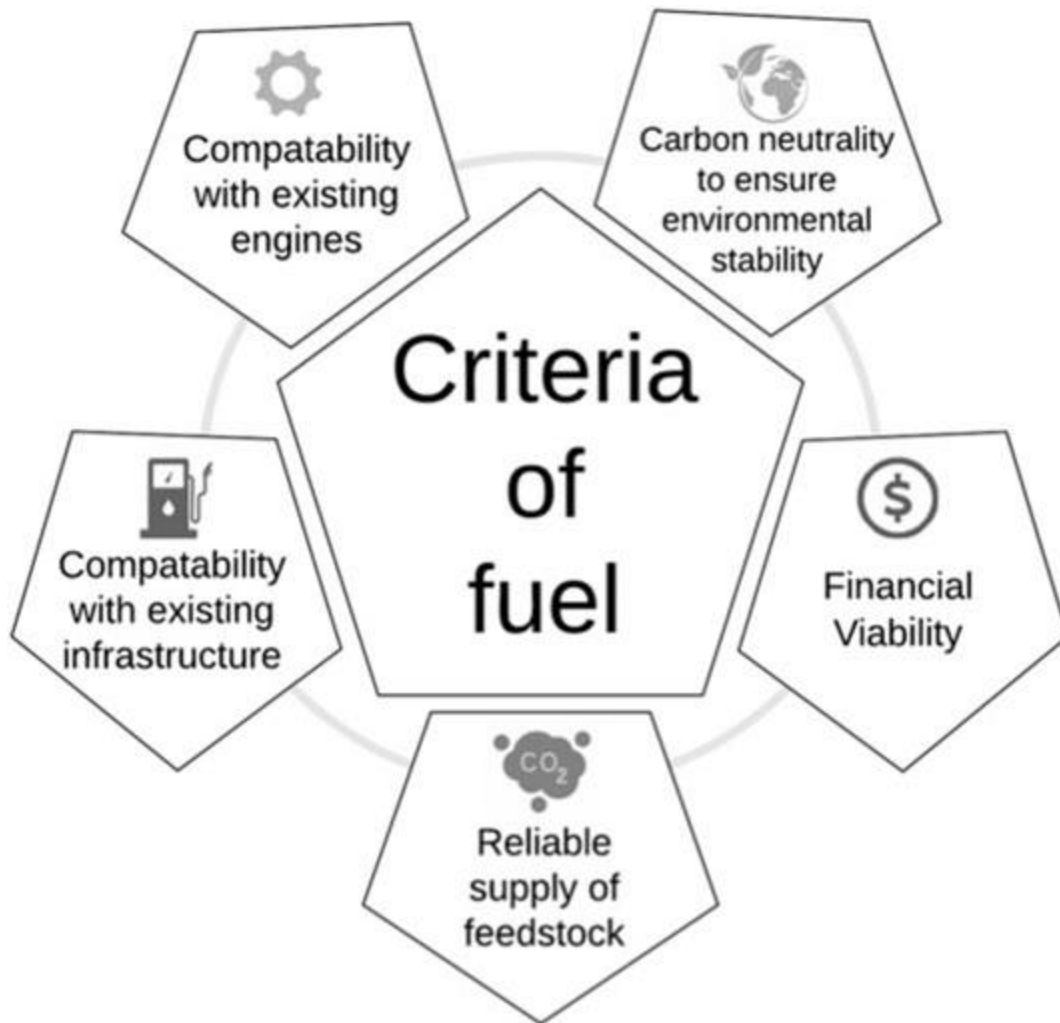


Figure 12: Criteria for Feasibility of a Synthetic Fuel (Styring, Dowson, and Tozer 2021)

### Purpose of Study

This study was conducted in order to gain insight on the optimal EGR and boost strategy necessary for lower NO<sub>x</sub> and soot emissions using PCCI with either 45% PFI of ethanol or n-butanol over various loads.

### Statement of Hypothesis

With an optimal EGR and boost strategy, PCCI can obtain a NO<sub>x</sub> and soot emissions reduction of at least 10% for 2 out of the 3 loads without the need of a non-neat ULSD#2 DI fuel.

## CHAPTER 2

### LITERATURE REVIEW

#### Bio-alcohols

Kasmuri et al. (2017) conducted a study on the generation of bio-alcohols utilizing various pyrolysis methods. It was observed that in order for bio-alcohols production conducted in this manner to be more profitable heavier considerations have to be made on the utilization of by-products created by pyrolysis in addition to what method is utilized. Of the three methods of pyrolysis (Conventional, Fast, and Flash), Flash pyrolysis is optimal for creating bio-alcohols. However, Flash pyrolysis requires higher heating rates ( $>1000\text{ }^{\circ}\text{C/s}$ ) than conventional pyrolysis ( $0.1\text{-}10\text{ }^{\circ}\text{C/s}$ ) and thus is more difficult to achieve, this however leads to an increase in produced bio-alcohol of 50% over conventional pyrolysis.

Weber et al. (2010) investigated on the production of second-generation bio-alcohols utilizing Lignocellulosic biomass rather than feedstock as is the case with first generation bio-alcohols (primarily ethanol). It was found that although bioethanol production has an established production infrastructure, more progress has been made on the production of second-generation bio-alcohols such as butanol for its potential for increased utilization of otherwise wasted biomaterials. As of 2010, production of second-generation bio-alcohols such as butanol are limited by the ability for micro-organisms to survive environments containing more than 7-8% butanol. As such, this study suggests for further feasibility of lignocellulosic bio-alcohol production, more efficient methods for extracting the butanol from the bio-mass reactor are needed in order to increase the mass-production of said bio-alcohols.

Hergueta et al. (2018) investigated the effect bio-alcohols have on morphology of particulate matter emitted from combustion in comparison to gasoline. It was found that ethanol and n-butanol fuel mixtures decreased the overall size of particulate matter emitted in comparison to gasoline. However, ethanol and n-butanol have differing particulate matter structures, ethanol fuel blends had particulate matter form in more chain like structures while as n-butanol fuel blends had more of a clump shape.

Han et al. (2019) conducted a study on the usage of bio-alcohols for the production of jet fuels via multiple processes. This study was conducted to counteract the carbon dioxide emissions associated with the aviation industries increasing output with carbon neutral sources. The



production of carbon neutral jet fuel was produced via several methods utilizing bio-alcohols and or their sourced biomass, these processes utilize the Sugar To Jet (STJ) method by catalytic upgrading and the conversion of either sugar or starches to hydrocarbons. In addition to this, biological organisms converting biomass directly to jet fuel with the addition of catalysts to convert the produced bio-alcohols (ethanol, n-butanol, methanol) into jet fuels via the Direct Sugar to Hydrocarbon (DSHC) process.

Kang et al. (2014) investigated the yields of second-generation methods for the production of bioethanol. Currently, commercially viable bio-ethanol production is limited to first generation methods (derived from food stock biomass) due to second generation bio-ethanol production (derived from non-food biomass, lignocellulosic) relatively low yields of 30%-50% ethanol from supplied biomass. However, it was found with the introduction of genetically modified *S. cerevisiae* and *Z. mobilis* and the reduction of steps involved in production, yields increased to 92% of the theoretical limit of bio-mass conversion to ethanol.

Yoshimoto et al. (2018) investigated the effects various bio-alcohol isomers (iso-butanol, n-butanol, iso-pentanol, n-pentanol) diesel fuel blends had on combustion properties in a supercharged diesel engine. It was found that regardless of the engine's operation with or without EGR or boost, all the tested bio-alcohol fuel blends were able to reduce  $\text{NO}_x$  and smoke emissions in comparison to conventional diesel combustion. The fuel blends consisting of either n-butanol or iso-butanol had the greatest reduction in smoke emissions when compared to iso-pentanol or n-pentanol due to the higher oxygen content of butanol. However, the bio-alcohol fuel blends were unable to make a considerable difference to emissions utilizing conventional combustion techniques.

Doustdar et al. (2021) conducted a study on the wear characteristics of various bio-alcohols either in neat fluids or as mixtures with diesel. It was found that all bio alcohols tested (butanol, pentanol, cyclopentanol, cyclopentanone) in their neat forms had lower roughness in their wear tracks than neat diesel. In addition to this, all the bio-alcohol diesel fuel blends (especially cyclopentanone) were shown to have lower wear scars than their neat counterparts due to the oxygenated fuels forming a protective lubricative layer between moving parts. This indicates that the longevity of high-pressure fuel systems could be extended with the usage of bio-alcohols.

Xiao et al. (2019) investigated the effects various n-butanol fuel blends would have on the emissions and combustion characteristics of a 4-cylinder engine under various loads. It was

observed that an increase in n-butanol lead to the reduction of soot formation as well as a decrease in combustion duration. Ignition delay was increased as n-butanol was added to the primary fuel. CO, UHC, and NOX emissions also increased as the concentration of n-butanol in the primary fuel was increased. This led to the conclusion that n-butanol should be added to ULSD in moderate quantities as not to increase harmful emissions too much.

Huang et al. (2019) researched alternative ways of producing n-butanol from low-cost sources. Cassava bagasse was utilized as the main biomass for the fermentation process for the production of n-butanol. It was observed that with selective breeding of a *Clostridium* bacteria strain that the production of n-butanol was increased by a considerable amount and if used properly within a bio-reactor setup, can lead to a viable industrial production of n-butanol from low-cost produce.

Liang et al. (2019) utilized a constant volume combustion chamber to analyze the reactivity of n-butanol and a diesel surrogate n-heptane at various combustion chamber temperatures. It was observed that n-butanol had a two-stage heat release associated with its combustion regardless of the temperature of the combustion chamber. It was also discovered that as the equivalence ratio of the air within the combustion chamber increased, so did the pressure and heat release rates by a substantial amount.

Tian et al. (2020) investigated the effects n-butanol would have on a Port Fuel Injected (PFI) Spark Ignition (SI) engine under various engine speeds. It was discovered that n-butanol increases engine power and torque considerably at low engine speeds but faces an inverse reaction as the speed is increased. However, the decrease in performance is not substantial and if used effectively, increases the thermal efficiency of the engine. This is done in conjunction with the reduction of CO and NOX emissions, however at the cost of increasing Hydrocarbon emissions. It was determined in this investigation that n-butanol can serve as a viable alternative to ethanol as a additive to gasoline for the desired performance.

Raganati et al. (2020) studied a viable process for the absorption of butanol from a fermentation process to reduce the die-off of bacteria within a solution to maintain the production at a steady state. It was observed that an amberlite material; mat was able to safely remove excess butanol from the system at a lowered energy process in comparison to traditional means. This study potentially revealed key steppingstone for the industrial scaled production of butanol needed to make it a marketable biofuel.

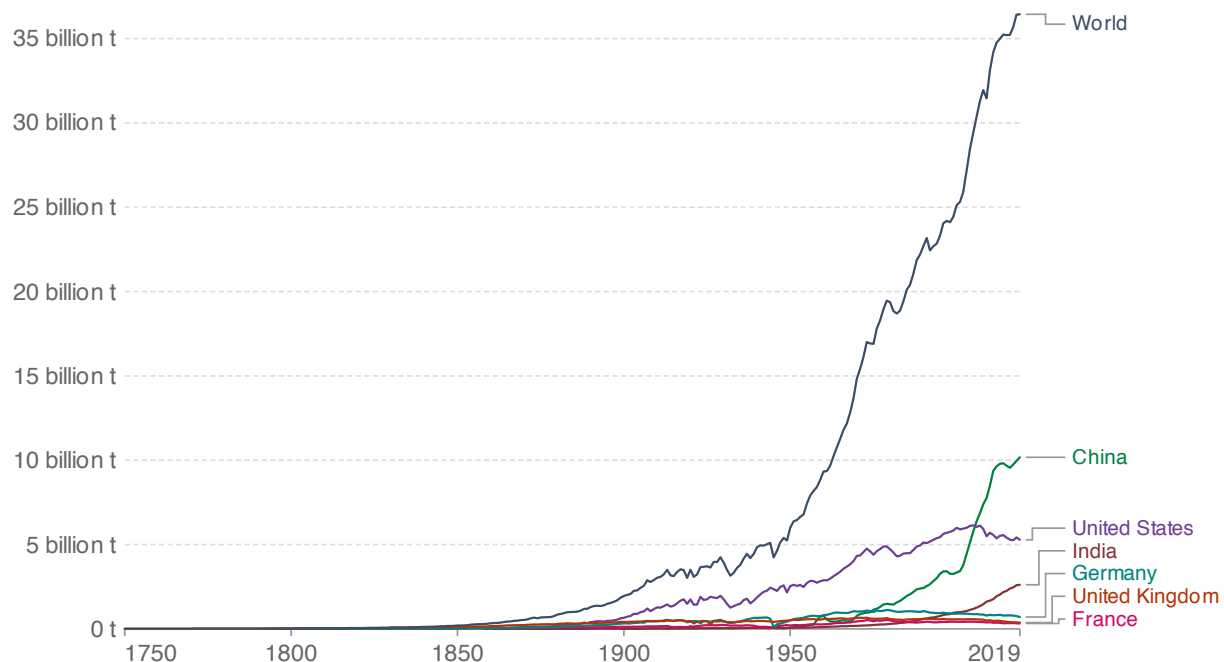
## Green House Gas Emissions

A study conducted by Roser (2020) analyzed the greenhouse gasses and other pollutants emitted from various countries from the beginning of the industrial era (1800) to the present (data available as of 2019). It was shown that although the United States had historically been a major contributor to worldwide CO<sub>2</sub> emissions, major strides have been made since 2006 for the reduction of CO<sub>2</sub> emissions emitted as seen in Figure 13. This observation is due in no short part to the investment in multiple carbon neutral energy sources (biofuels, nuclear, solar, wind, hydro, etc.) throughout various economic sectors.

### Annual CO<sub>2</sub> emissions

Carbon dioxide (CO<sub>2</sub>) emissions from the burning of fossil fuels for energy and cement production. Land use change is not included.

Our World  
in Data



Source: Global Carbon Project

OurWorldInData.org/co2-and-other-greenhouse-gas-emissions/ • CC BY

Note: CO<sub>2</sub> emissions are measured on a production basis, meaning they do not correct for emissions embedded in traded goods.

Figure 13. Annual CO<sub>2</sub> emissions per country (Roser 2020)

However, it can be observed that although the United States, Germany, United Kingdom, and France have reduced annual CO<sub>2</sub> emissions year by year, CO<sub>2</sub> emissions worldwide have continued to grow due to the exponential growth of CO<sub>2</sub> emitted by China. The growth in CO<sub>2</sub>

emissions by China has been shown to be on the rise since 2001 with only minimal changes to the rise in emissions seen between 2013-2017. This indicates that although great strides have been made in reducing CO<sub>2</sub> emissions from various countries worldwide, greater efforts have to be made for other countries to comply with this need otherwise CO<sub>2</sub> emissions will continue to rise despite the actions by most to reduce annual emissions levels.

A review conducted by Johnson et al. (2007) argued that although the agricultural sector contributed a sizable portion of GHG emissions, efforts can be made to not only reduce the impact agriculture has on GHG emissions but also reduce the GHG emitted by the energy sector. This can be accomplished by harnessing the waste products from various agricultural sectors for the production of biofuels. The utilization of otherwise discarded materials has been shown to have a positive impact for GHG reductions efforts as the biomass utilized for fuel production is a carbon neutral source.

Davis et al. (2012) conducted an investigation on the usage of second-generation biofuels for the reduction of both GHG emissions and nitrogen leeching instead of first-generation corn derived biofuels in the Midwest. It was found that second generation biofuels derived from perennial cellulosic feedstock had the potential for not only reducing GHG emissions by 29%-473% but also reduced nitrogen leeching by 15%-22%. The investigation also found that despite land use being diverted from corn growth to perennial cellulosic feedstock, a 4% growth in food grain occurred while increasing ethanol production by 82%. The findings of this investigation thereby conclude that if production methods were to switch from corn-based ethanol to perennial cellulosic feedstocks ethanol production, agricultural lands in the Midwest would benefit from greater nitrogen retention and lower land used diverted for fuel production per the same size of land.

Dwivedi et al. (2015) investigated the GHG impact of cellulosic ethanol production from corn stover, switchgrass, and miscanthus in various soil qualities found in the Eastern United States. It was discovered that the highest GHG reduction yields were derived from miscanthus and switchgrass derived bioethanol throughout most soil types in comparison to corn. It was shown that GHG emissions had the potential to be reduced by as much as 130%-156% with the utilization of miscanthus while switchgrass shown a reduction of GHG of 97%-135%. This study concluded that with the usage of second-generation bioethanol, GHG emissions can be reduced despite the

varying soil grades found in the east coast and can serve as a viable option for transitioning fuel consumption from gasoline to ethanol.

In a study conducted by Maity et al. (2014), an analysis was done on the effect third generation biofuels would have on GHG emissions. Third generation biofuels when compared to second- and first-generation biofuels are shown to not only require less farming area than previous generations but also provide greater energy yields per volume of feedstock. However, unlike first- and second-generation biofuel production, third generation biofuels are produced from the harvesting of algae in bioreactors. It was shown in this study that biofuel production yields were as high as 91% of the biomass utilized thus making it a more efficient pathway for GHG emissions reduction with the additional benefit of treating wastewater further reducing GHG emissions by reducing energy required in other sectors of society as seen in Figure 14.

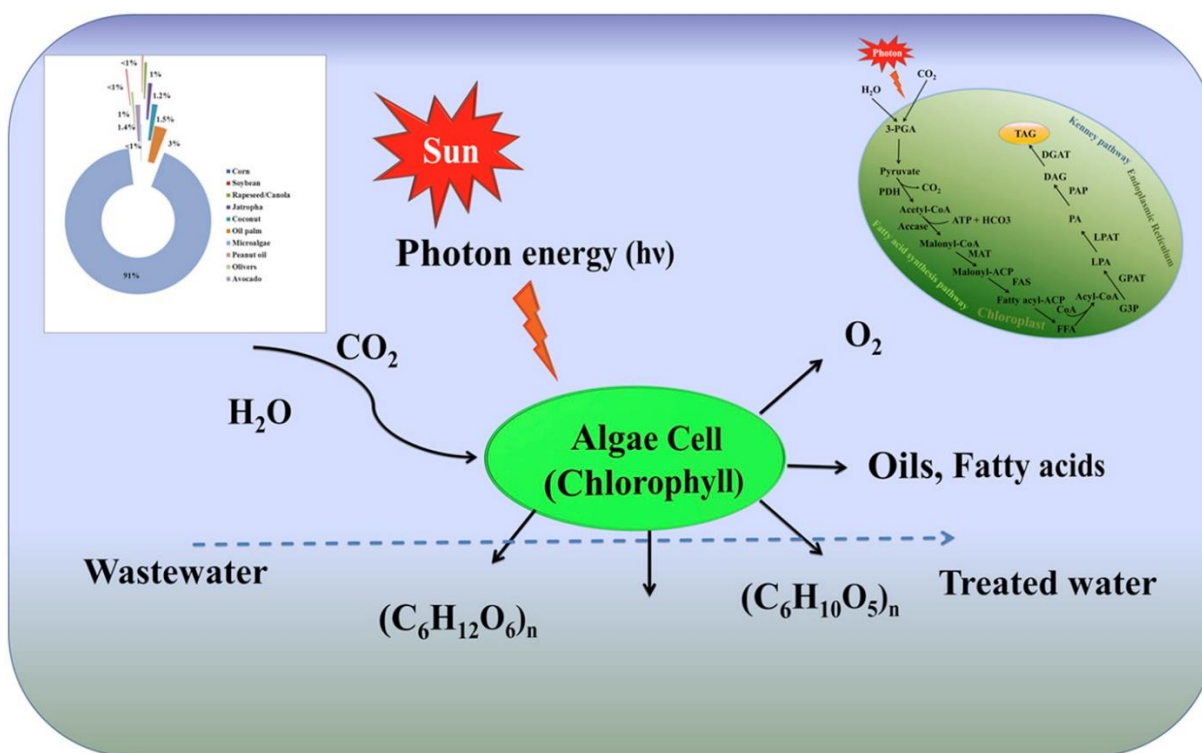


Figure 14. Third Generation Biofuel Production Process (Maity et al. 2014)

Ho et al. (2011) conducted an analysis of utilizing microalgae systems for CO<sub>2</sub> sequestration systems. It was found that the utilization of microalgae bioreactors not only was more economical from a land usage perspective but also from its versatility in providing multiple

products from its biomass such as medicinal products, food additive production, animal nutrition products, cosmetics, and various biofuels. The investigation found for further improvements of the system careful considerations have to be made for the species to be utilized in the bioreactors as the optimal specimen will have higher growth rate, high CO<sub>2</sub> sequestration, and low contamination risk.

### Low Temperature Combustion Methods

Soloiu, Moncada, Gaubert, Knowles, et al. (2018) investigated RCCI combustion with Methyl-oleate and n-butanol for the reduction of harmful emissions. It was observed that RCCI with the usage of these two alternative fuels was capable of reducing NOX and soot emissions of an engine at a low load to almost non-existent levels. It was also observed that the ringing intensity was severely reduced by 70% and has the potential for increasing the longevity of the engine with the reduction of stresses to the engine components. The efficiency of the engine improved with the higher usage of methyl-oleate due to its unsaturated components.

Liu et al. (2019) did a detailed investigation on the kinetics of RCCI combustion utilizing an optical engine. It was observed that combustion occurred in multiple stages of low temperature heat release and high temperature heat release. The initial flame front observed in the optical engine was located at the edge of the piston at the location of quench and lead to the dual combustion phasing typically observed in RCCI.

Raut, Irdmoussa, and Shahbakhti (2018) conducted a study on creating a dynamic model capable of predicting RCCI's performance under various transient engine conditions. This modeling was done to better understand how RCCI performs under non-steady state conditions to rate the viability of the combustion strategy for transportation usage. It was found that RCCI is capable of running under various conditions but struggles under extreme loading conditions.

Ansari, Shahbakhti, and Naber (2018) investigated the viability of implementing a dual fuel combustion strategy into a production vehicle. It was observed that RCCI was best for stationary operations but is cable of being implemented on mobile platforms. This outcome was found that if the RCCI process is well optimized for a particular application, that it can be viable as a future transportation propulsion method.

Li et al. (2018) investigated the effect initial fuel properties have on the performance of RCCI. It was found that for methanol ULSD applications of RCCI, boost is not a viable parameter to obtain higher efficiency as the combustion process becomes unstable. The only way of

controlling RCCI with these selected fuels is to control the injection timing and EGR % used for combustion.

Cao et al. (2020) investigated the effect of injection pressure on NOx and PM emissions of PCCI combustion. It was found that higher injection pressures increased the engine performance and increased combustion stability while lowering NOx and PM emissions.

Hoang (2020) conducted a study on the optimization of PCCI combustion with the usage of a modified DI narrower injection spray pattern. This was done so in order to inject the fuel within the piston bowl for advanced injection timing combustion strategies and reduce the wall wetting that occurs from a non-optimized spray pattern. It was found that the narrow angle DI spray was able to reduce PM, UHC, and CO emissions from PCCI/PPC combustion.

Singh, Kumar, and Agarwal (2020) investigated RCCI and PCCI combustion versus CDC utilizing mineral diesel and methanol (for RCCI LRF) as their fuel source. It was found that RCCI and PCCI were able to reduce NOx emissions and smoke opacity in comparison to CDC at both low and high loads. However as can be seen in Figure 15 below, RCCI combustion is also able to reduce PPRR and BSFC.

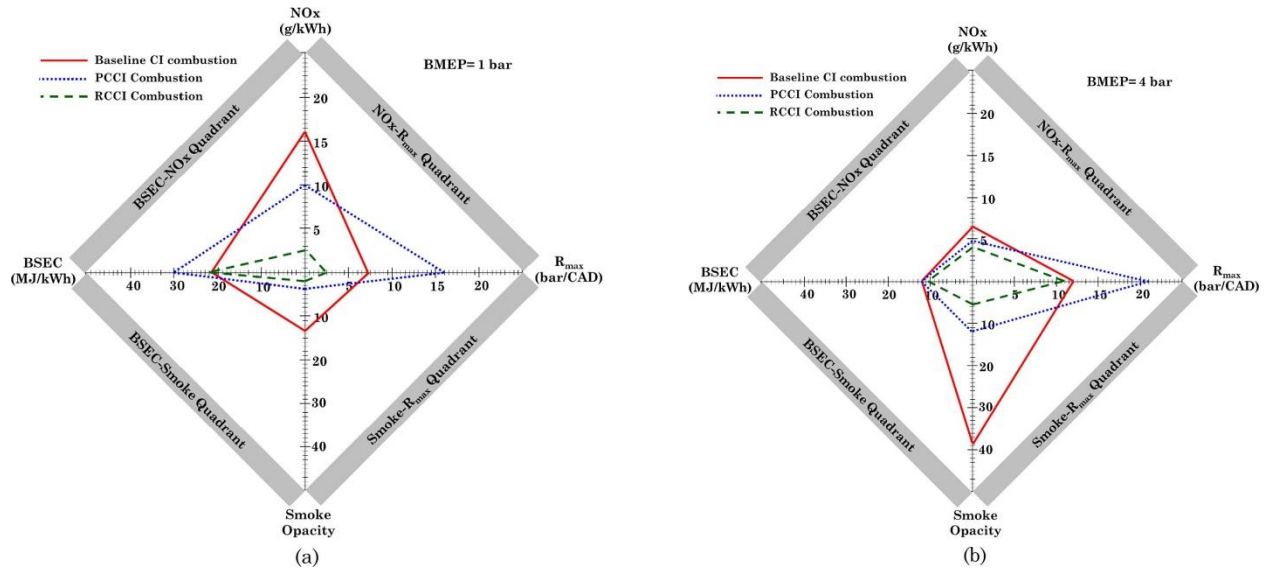


Figure 15: CDC vs PCCI vs RCCI combustion at 1 and 4 bar BMEP (Singh, Kumar, and Agarwal 2020)

Shim, Park, and Bae (2020) conducted a study on HCCI, PCCI, and DF-PCCI combustion/emission characteristics in comparison to CDC. It was seen in this investigation that

DF-PCCI had superior thermal efficiencies than the other LTC methods. In addition to this NO<sub>x</sub> and PM emissions were able to meet EU-VI regulations without the usage of an aftertreatment system, however CO and THC emissions were higher than CDC. Further studies are needed for optimizing the engine parameters in order to increase the combustion efficiency of PCCI, the performance characteristics of these LTC methods can be seen in Figure 16.

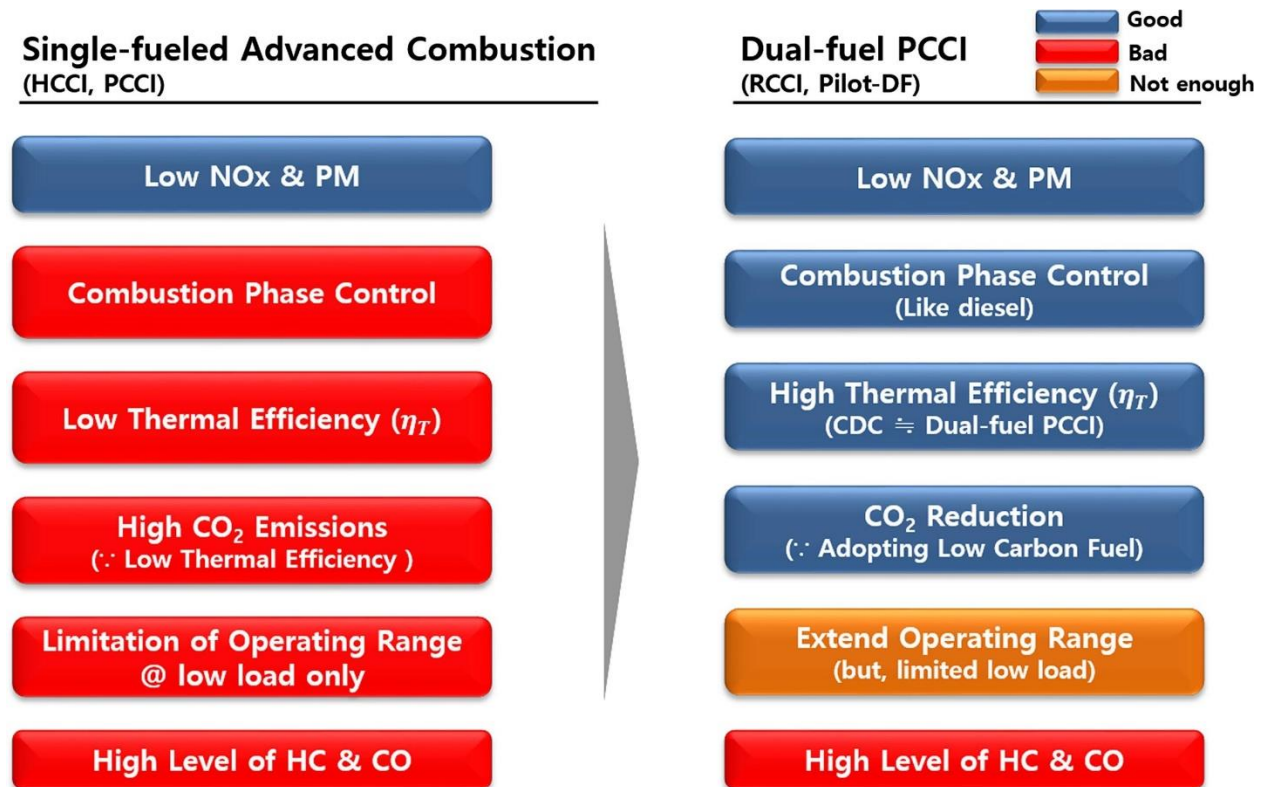


Figure 16: Single Fuel vs Dual Fuel LTC Methods Performance Characteristics (Shim, Park, and Bae 2020)

Pan et al. (2020) investigated a novel technique of employing a neural network for the optimization of PCCI combustion. It was found that the neural network was successful in predicting the non-linear relationship between various engine parameters and the emissions of PCCI. This model was trained on previously existing data sets of PCCI, and the results of which were experimentally verified within a high confidence. This technique is an indication of a future trend of LTC research and development being optimized with neural networks in order to achieve the desired results of lowered emissions and combustion efficiencies comparable to CDC.



## CHAPTER 3

### METHODS

#### Overview

The methods for the analyses' utilized to determine the properties relevant to combustion of the chosen fuels are included within this section. The lower heating value, viscosity, thermal gravimetric analysis, differential thermal analysis, fuel spray development, derived cetane number, and apparent heat release rate is used in this study.

#### Development of an Improved Electrically Driven Centrifugal Supercharger System

An electronically controlled supercharger system was previously developed for providing the desired quantity of boost to the engine regardless of the load and/or speed of the engine. However, the previous design did not achieve the desired boost necessary for more advanced control over various LTC methods investigated in the single cylinder CI engine. This was a result of the previous system not having the necessary transmission ratio in order to achieve the desired rpm at the supercharger pulley. In Figure 17, the previous transmission system can be seen where (A) is the pulley that is mounted on the electric motor, (B) is the intermediate shaft that transfers power from (A) to (D) pulleys, (C) is the belt tensioner for the supercharger belt, and (D) is the supercharger pulley.

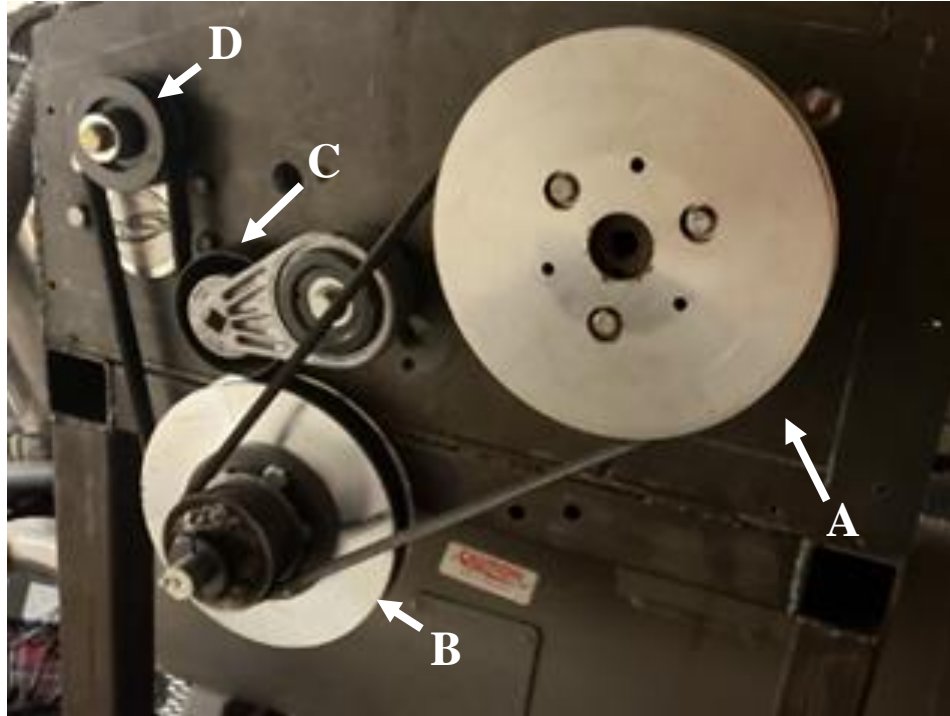


Figure 17: Previous Supercharger Pulley System

The system shown in Figure 17 had a transmission ratio from the supercharger pulley to the electric motor of 7.37:1 and produced 0.339 bar of boost at a peak motor speed of 1800 RPM. In-order to achieve greater boost pressures, a new system was developed to increase the transmission ratio sufficient enough in order to obtain greater boost pressures from the supercharger. The schematic of the system is shown in Figure 18 were the variables used for the calculation of the new transmission operating speeds from the newly installed pulleys. The pulleys that were changed are  $\theta_1$  at the electric motor and  $\theta_2$  of the intermediate shaft.

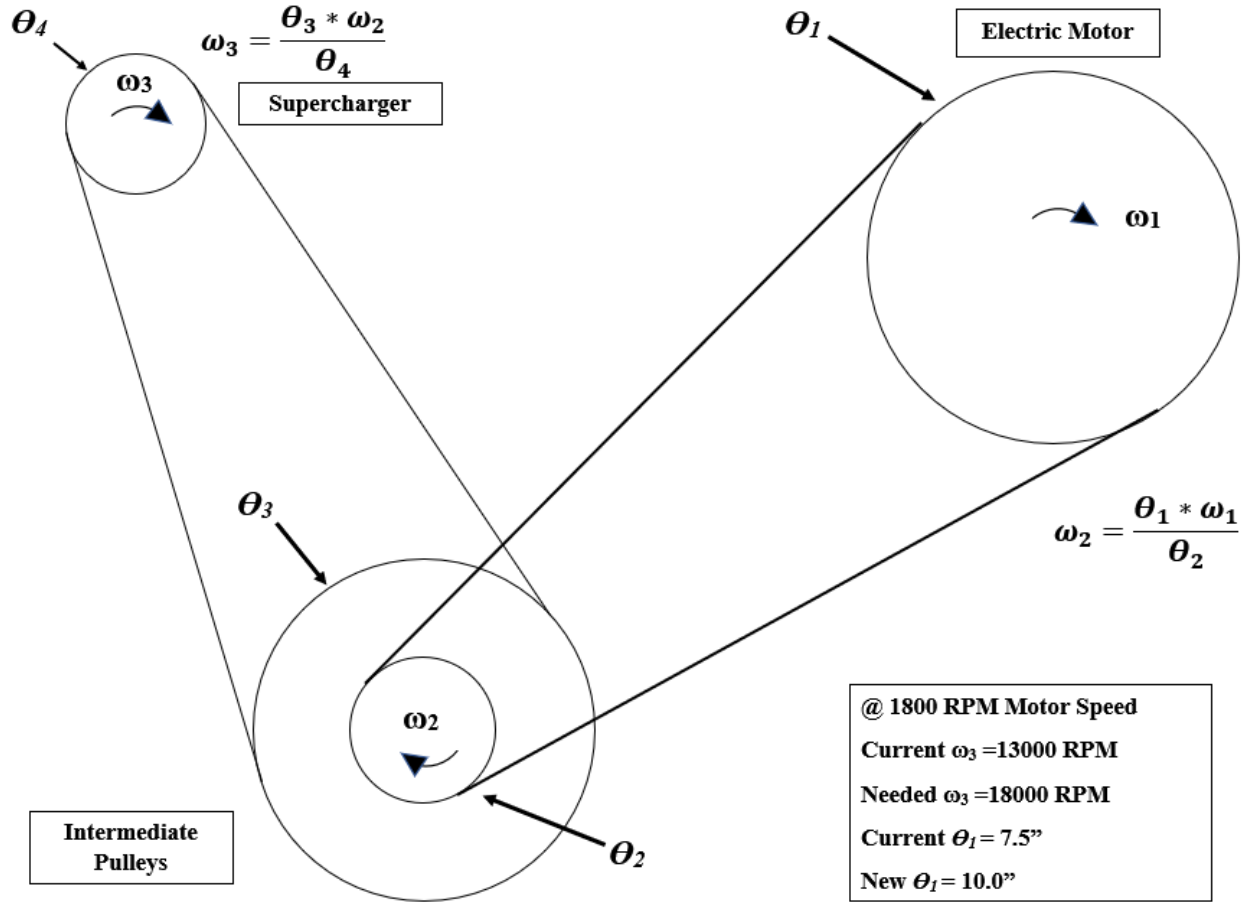


Figure 18: Supercharger Transmission System Schematic

The diameter of the new pulleys that were chosen with the criteria of maximizing the diameter of the motor pulley, minimizing the diameter of the intermediate shaft pulley, the compatibility of the new pulleys with the current hardware, and the availability of the chosen parts and belt from authorized vendors. The equations for calculating the speed of the intermediate shaft Equation 1, and the supercharger pulley Equation 2 based off the chosen diameters can be seen below. The diameters of all the pulleys chosen/used, the maximum calculated speed, and maximum boost of the system can be seen in Table 1.

$$\omega_2 = (\theta_1 \times \omega_1) \div \theta_2 \quad \text{Equation 1}$$

$$\omega_3 = (\theta_3 \times \omega_2) \div \theta_4 \quad \text{Equation 2}$$

Table 1: Specifications and Diameters of the Supercharger Transmission

	Old System	New System
$\theta_1$	6.810 (in)	10.000 (in)
$\theta_2$	2.900 (in)	2.640 (in)
$\theta_3$	7.500 (in)	7.500 (in)
$\theta_4$	2.625 (in)	7.500 (in)
<b>Max Supercharger RPM</b>	18250.00 (RPM)	18250.00 (RPM)
<b>Max <math>\omega_1</math></b>	1800.00 (RPM)	1800.00 (RPM)
<b>Max <math>\omega_2</math></b>	4643.18 (RPM)	6206.90 (RPM)
<b>Max <math>\omega_3</math></b>	13266.23 (RPM)	17734.00 (RPM)
<b>Pulley Ratio</b>	7.37:1	9.85:1
<b>Max Boost</b>	0.339 (bar)	0.829 (bar)

With the selection of the new pulleys, calculations on the tension required by the belt for maintaining adequate contact with the pulleys were done in order to ensure the longevity of the system and minimize downtime. A free body diagram of the newly selected pulleys is shown in Figure 19, where the forces that are acting on the system can be observed. Equation 3 - Equation 8 were utilized for calculating the required tension necessary for the belt to maintain grip on the pulleys with the maximum torque (MT) of the motor applied to the system.

$$\theta_{1a} := 180 + \left( 2 \cdot \left( \arcsin \left( \frac{r_{aft} - r_{bft}}{L_{ft}} \right) \right) \right) \quad \text{Equation 3}$$

$$\beta_a := \theta_{1a} \cdot \left( \frac{\pi}{180} \right) \quad \text{Equation 4}$$

$$x := 2.718^{\mu_b \cdot \beta_a} \quad \text{Equation 5}$$

$$F := \frac{MT}{r_{aft}} \quad \text{Equation 6}$$

$$T_{rest} := \left( \frac{F}{(x - 1)} \right) \quad \text{Equation 7}$$

$$T_{Max} := F - T_{rest}$$

Equation 8

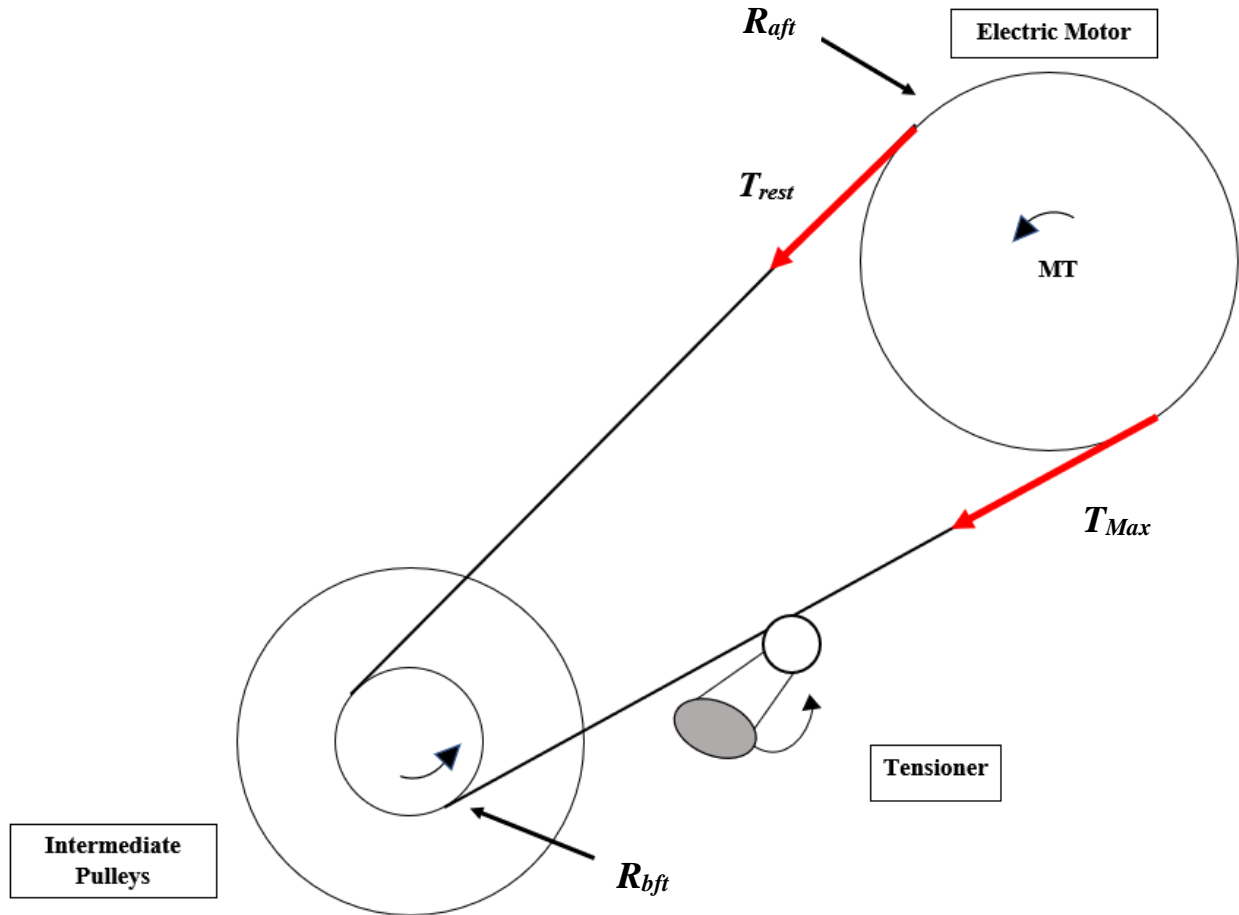


Figure 19: Free Body Diagram of The Electric Motor to Intermediate Pulleys

The new transmission system for the electrically driven supercharger system shown in Figure 20, had a 25% increase in RPM at any given motor speed as the transmission ratio was increased to 9.85.

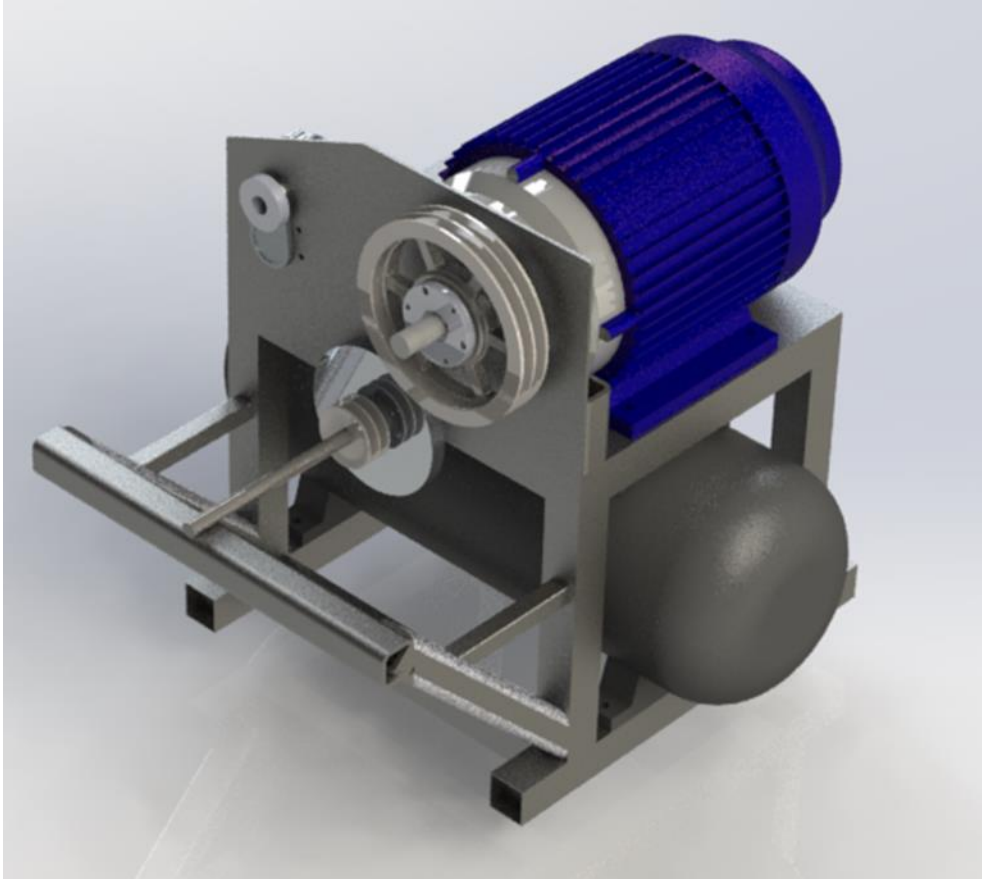


Figure 20: CAD Model of New Supercharger Transmission System

Although the speed of the pulleys was increased by 25%, the maximum achievable boost of the system increased by 59%. This is due to the exponential relationship between a centrifugal superchargers rotational speed and the quantity of boost that is produced as seen in Figure 21. Although the new system can achieve a higher quantity of boost compared to the old system, precaution is needed for operating the electric motor at speeds past 1350 RPM as the gearbox of the centrifugal supercharger begins to climb above safe operational temperatures. With this in mind it was noted that the usage of the system should not exceed 50 seconds at speeds greater than 1350RPM. In addition, the maximum speed of the electric motor should not exceed 1650 RPM as this exponentially increases the chance of catastrophic failure of the centrifugal supercharger gearbox.

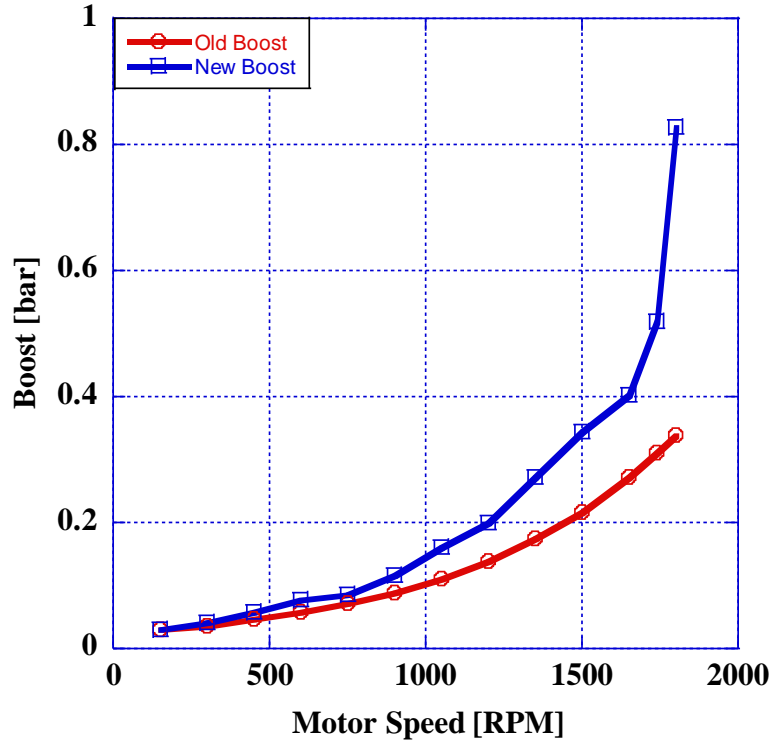


Figure 21: Old vs New Supercharger System Boost

### Fuel Analysis

Multiple studies were conducted on the thermo-physical properties of ULSD #2, n-butanol, and ethanol (represented as E98) in order to ensure safe operation of PCCI with the proper selection of engine operating parameter. These investigations also provided insight into the emissions/combustion characteristics of the chosen fuels prior to any fired engine analysis. The lower heating value, viscosity, low temperature oxidation, thermal stability, and spray development properties of the fuels were investigated within the scope of this study as will be seen in future sections.

The thermo-physical properties of ULSD#2, n-butanol, and ethanol that were not investigated inhouse but were deemed pertinent to the operation of PCCI were gathered from various sources and can be seen in Table 2. An attempt to investigate the reactivity of ethanol (at a 98% concentration) was deemed inconclusive as the ethanol was not able to combust in the PAC CID 510 Constant Volume Combustion Chamber (CVCC) while adhering to ASTM- D7668-14a protocol. However, this indicated that E-98 had an adequate low reactivity for PCCI combustion

however combustion efficiency may be affected at lower loads without the addition of boost. The greater oxygen content of ethanol in comparison to n-butanol should be favorable for reducing soot emissions which will be seen in a future section.

Table 2: Thermo-physical Properties of Research Fuels (Elfasakhany and Mahrous 2016, Zheng et al. 2018, VP-Racing-Fuels 2019)

	ULSD #2	n-butanol	E98
DCN	47.4	16.4	8
Octane	-	96	111.5
Density [g/mL]	0.85	0.81	0.79
% O <sub>2</sub>	-	21.6%	34.7%

### Lower Heating Value

The Parr 1341 constant volume calorimeter, as seen below in Figure 22, was used to determine the lower heating value of the selected fuels. A Ni-alloy fuse wire was strung across two electrodes and was used to ignite a 0.5 g sample of research fuel in the crucible below. The stainless-steel chamber was filled with 25 atm of O<sub>2</sub> before being submerged in a jacket containing 2 kg of deionized water. A stirrer was utilized for mixing the water in the water jacket and a k-type thermocouple was submerged in the jacket in order to determine the change of temperature of the water. The rise in temperature during combustion and was used to determine the gross heating value of the fuel.



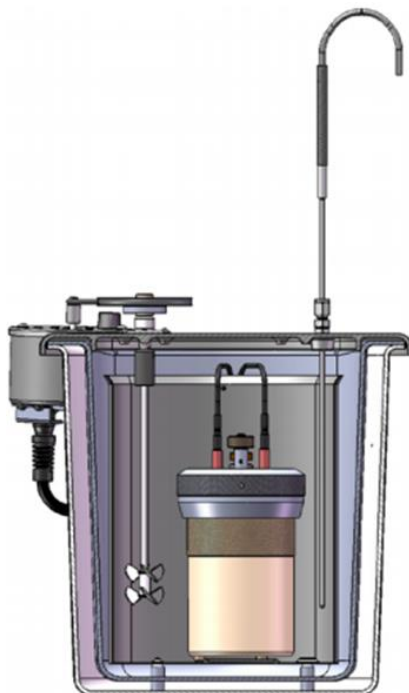


Figure 22. Parr Calorimeter Assembly Cross-Sectional View Source: (Parr Instrument Company, Series 1341 Plain Jacket Oxygen Combustion calorimeters n.d.)

Equation 9 is utilized for calculating the heat release of combustion with the measured increase in jacket water temperature. This temperature rise typically occurs within the first 20 seconds after combustion as can be observed within Figure 23.

$$H_{net} = 1.8H_C - 91.23H$$

Equation 9

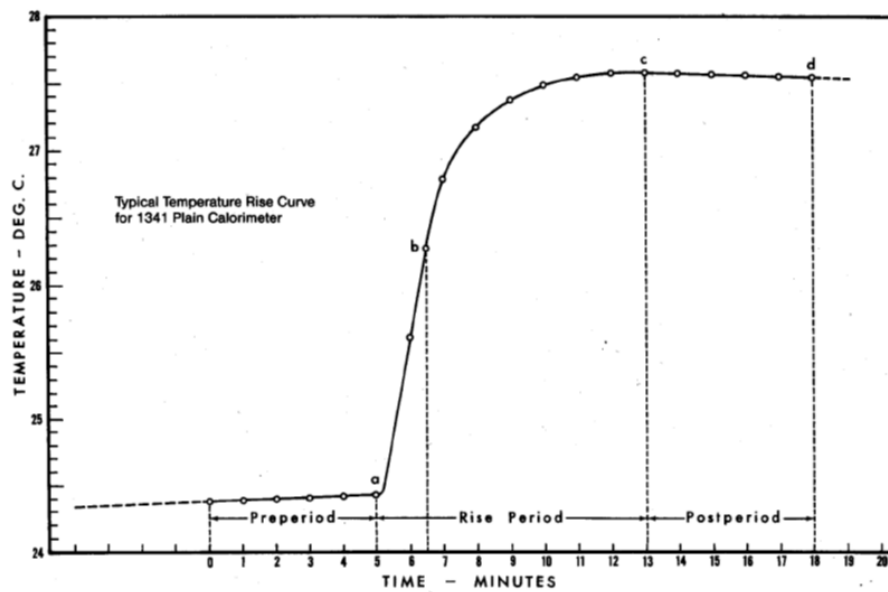


Figure 23. Parr Calorimeter Temperature Rise Curve Source: (Parr Instrument Company, Series 1341 Plain Jacket Oxygen Combustion calorimeters n.d)

### Viscosity

A Brookfield DV-II Pro Type Viscometer was used to measure the viscosity of the selected fuels over a temperature range typically observed within fuel systems from 26°C – 90°C as seen in Figure 24. The viscosity of a fuel is an important physical property that dictates the compatibility/performance of a fuel delivery/injection system and partially influences how well the fuel atomizes. Viscosity measurements were taken at 2°C increments utilizing a spindle rotating at 200 RPM with a 7.0 ml sample size. The temperature of the sample was controlled externally via a PID controlled liquid to liquid heat exchanger system.

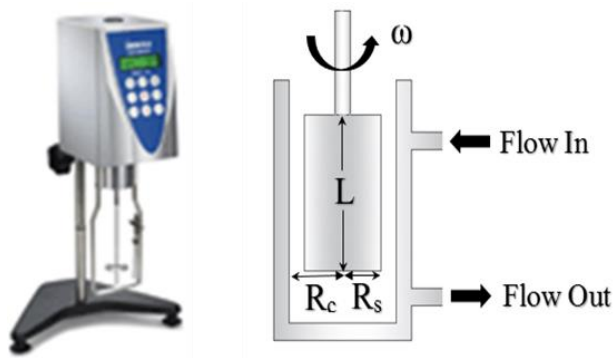


Figure 24. Brookfield DV-II +Pro Rotational Viscometer (Brookfield)

## TGA-DTA

A Shimadzu DTG-60 was utilized to conduct a Thermal Gravimetric Analysis (TGA) as well as a Differential Thermal Analysis (DTA) to obtain the energy release and rate of vaporization characteristics of the selected fuels. The research apparatus, as shown in Figure 25 below, consists of a high precision balance (measuring 0.01 mg) introduced into a furnace that heats the sample from 20 °C to 600 °C at a rate of 20 °C/min. As the sample was heated, the chamber was constantly purged with compressed air at a rate of 5 ml/min. Inside the furnace there are two stems mounted to a scale, one stem was reserved for an inert baseline powder, while the other was for the fuel sample. During the testing, the mass of the fuel sample was constantly monitored as the sample increased in temperature.

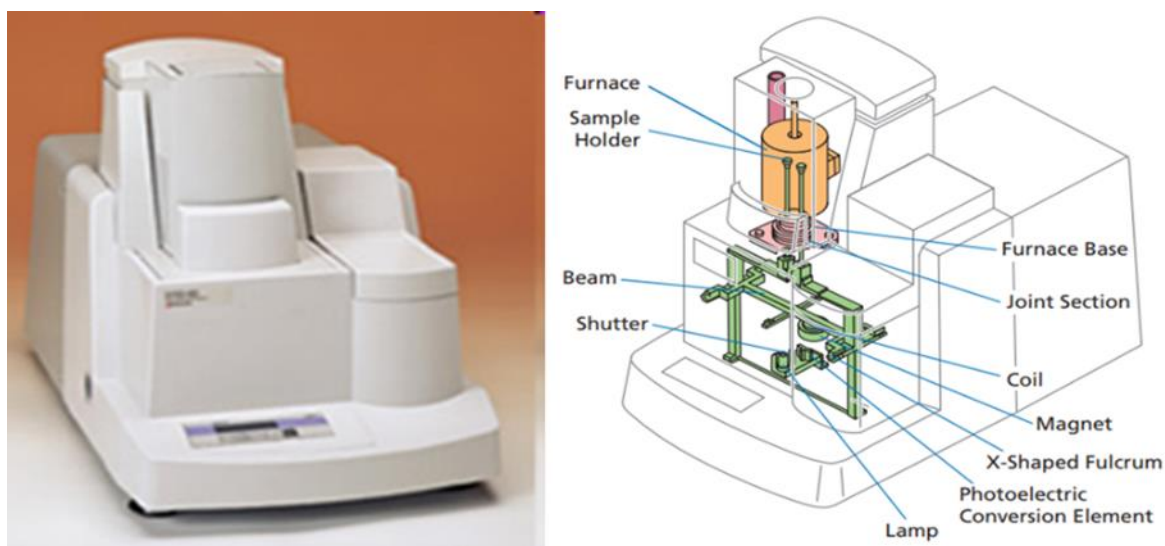


Figure 25. Shimadzu DTG-60 (Oceania)

The TGA is utilized for determining the fuel's thermal stability and the vaporization characteristics of the fuel post injection. This is pertinent to determining a fuel's performance in regard to its wall wetting characteristics and penetration into the cylinder. In addition, the DTA study reveals the quantity of heat absorption that occurs from the vaporization of the fuel and the energy given off with oxidation.

### Fuel Spray Analysis

A Spraytec Mie Scattering He-Ne Laser apparatus was used to analyze the spray development of the fuels by measuring the Sauter Mean Diameter (SMD) of the sprays droplets over time as shown in Figure 26. A single orifice pintle injector is placed 150 mm away from the laser beam, the injection event is then initiated via a pneumatic system that pressurizes the fuel rail pressure to 180 bar at the time of injection.

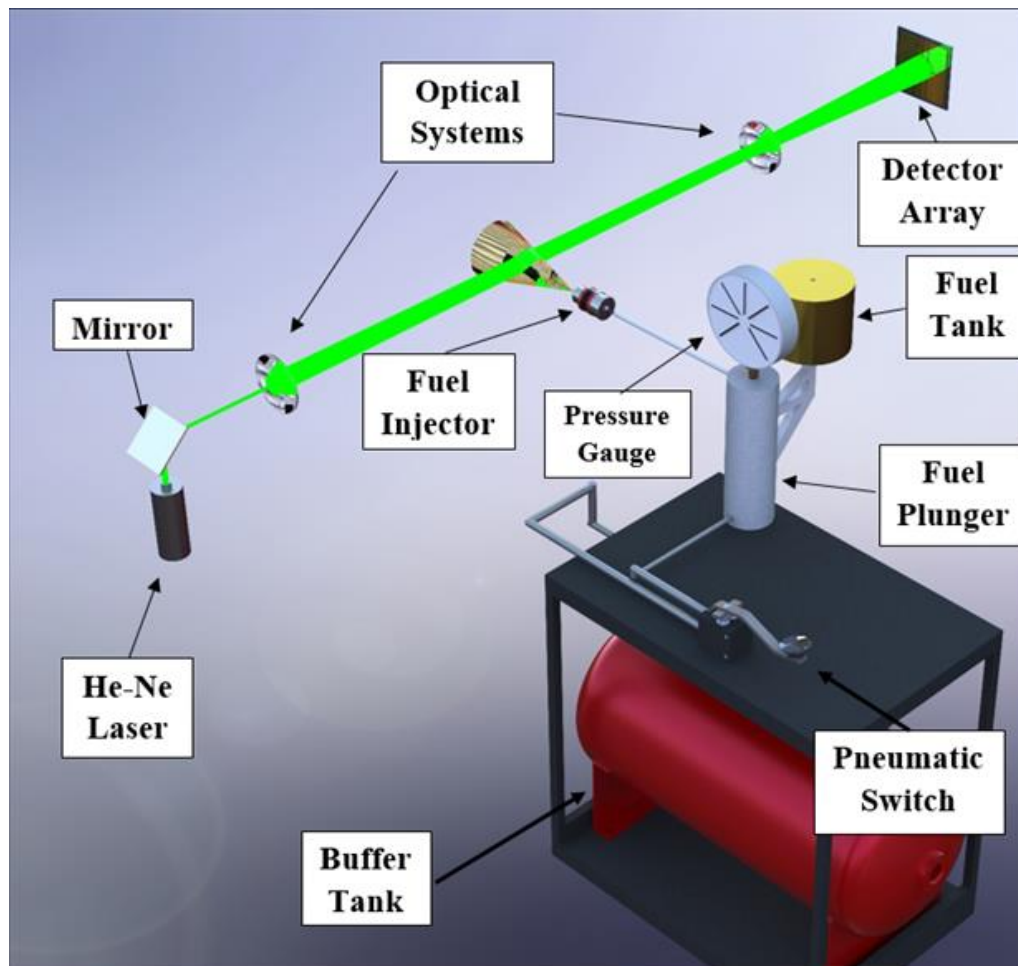


Figure 26. Mie Scattering Spray Analysis Test Bed (Soloiu et al. 2019)

The Malvern Spraytec records the diffraction of the spray droplets utilizing a He-Ne laser shot across a collimating optic lens and focusing lens onto a 32-detector array. The data is collected between 0.1 ms to 5 ms after injection at a sampling rate of 10 kHz, where it is then interpreted utilizing the Fraunhofer Diffraction theory.

### Engine Testing and Instrumentation

A 1.1L single cylinder experimental CI engine was instrumented in order to conduct an optimization study of PCCI combustion emissions utilizing either n-butanol or ethanol. This study was conducted at 3 loads of 3 bar, 4 bar, and 5 bar IMEP. A common rail piezo injection system has been outfitted on to the engine to enable greater flexibility on quantity of injection events and injection timing. The specifications of the engine and fuel injection DI and PFI systems are shown in Table 3.

Table 3: Engine Specifications

Parameter	Value
<b>Peak Power</b>	17kW @ 2200RPM
<b>Peak Torque</b>	77.5 Nm @ 1400 RPM
<b>Rated Power</b>	17 kW
<b>Bore X Stroke</b>	112 mm x 115 mm
<b>Displacement</b>	1.1L
<b>Number of Cylinders</b>	1
<b>Valves per Cylinder</b>	2
<b>Compression Ratio</b>	16:1
<b>Number of Strokes</b>	4
<b>Injector nozzle</b>	7x 0.115 mm
<b>Common Rail Pressure Range</b>	800 bar – 1200 bar
<b>PFI Pressure</b>	2.8 bar
<b>PFI Timing</b>	20 CAD (after intake starts)
<b>Speed</b>	1500 RPM

An NI Drivven ECU was selected to control the engine speed, DI injection timing, common rail pressure, PFI % by fuel mass. The speed and rotational position of the crankshaft was measured with a 3600 pulse Omron rotary encoder and was used by the ECU, AVL Indicor, and Yokogawa DL850 high-speed data acquisition system. The engine speed was set at 1500 RPM and was maintained by the Proportional Integral Derivative (PID) speed controller of the ECU by controlling the pulse width of the primary DI event.

A Kistler 6053cc pressure transducer with a 5010B Dual Mode Amplifier system was utilized to measure in-cylinder pressure and recorded by a Yokogawa DL850 high speed data

acquisition system for post processing. In addition, the pressure signal was utilized by an AVL Indicom for real time monitoring of pressure, AHRR, PPRR, and COV. An AVL Model 483 Micro Soot analyzer was used to measure soot emissions for each trial along with a AVL SESAM FTIR 30 species emissions analyzer for the gaseous emissions of the trials conducted. Mass flow rate for the intake air, DI system, and PFI system were measured with a Meriam Z50MC2-c Laminar Flow meter, 213 Maxx flow meter, P001 Maxx flow meter respectively, Table 4 includes the accuracy of the measurement devices utilized. A schematic of the experimental engine setup is shown in Figure 27 as well.

Table 4: Selected Measurement Accuracy

<b>Instrument</b>	<b>Measured Parameter</b>	<b>Accuracy</b>
<b>TQ513 Torque Sensor</b>	Torque	$\pm 0.06$ %
<b>Meriam Z50MC2-2 Laminar Flow Meter</b>	Air Mass Flow Rate	$\pm 0.72$ %
<b>213 Maxx Flow Meter</b>	Common Rail Fuel Flow Rate	$\pm 0.2$ %
<b>P001 Maxx Flow Meter</b>	PFI Fuel Flow Rate	$\pm 0.2$ %
<b>Kulite-175-190 M Intake Pressure Transducer</b>	Intake Pressure	$\pm 0.1$ %
<b>Kistler 6053cc Piezoelectric Pressure Transducer</b>	In-Cylinder Pressure	$\pm 0.19$ %
<b>AVL 483 Micro Soot Sensor</b>	Soot Concentration	$\pm 3.8$ %
<b>AVL SESAM FTIR V4</b>	NO <sub>x</sub> Concentration UHC Concentration CO Concentration CO <sub>2</sub> Concentration Formaldehyde Concentration	$\pm 2.0$ % of PPM Auto range

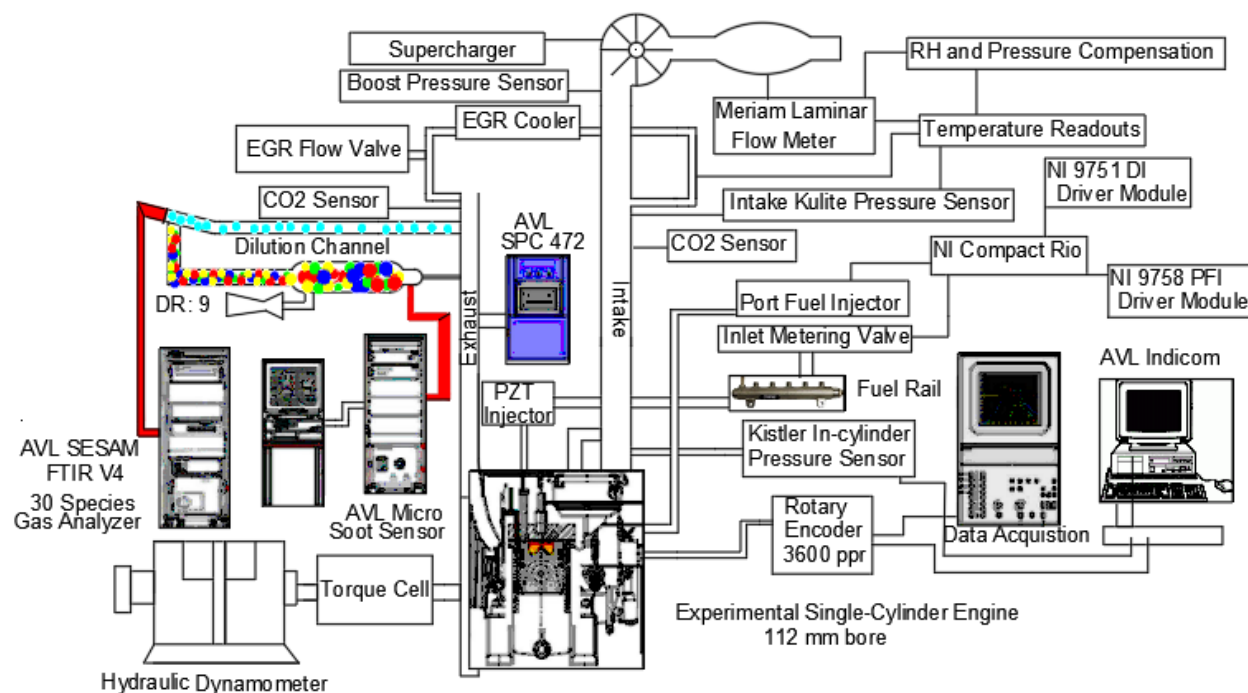


Figure 27: Experimental Engine Setup

### Engine Parameters for Operating Test Points

A preliminary analysis was conducted over several operating points per load and PFI fuel in order to obtain the optimal test points for the greatest reduction of NO<sub>x</sub>, soot, and UHC emissions in PCCI combustion. The results of the preliminary study were compiled into multiple contour maps that were utilized for determining the 27 operating points to be conducted at 3, 4, and 5 bar IMEP as seen in Table 5. An additional test point was conducted at 3 bar IMEP for PCCI 45ET as it was found during the investigation that adding greater EGR% and boost led to a simultaneous reduction of both NO<sub>x</sub> and soot.

Table 5: Operating test points at a load of 3, 4, &amp; 5 bar IMEP

Load	Optimization Parameter	Combustion Method	Boost [bar]	EGR [%]
<b>3 Bar</b>	NO <sub>x</sub>	CDC	0.160	17.5
	Soot	CDC	0.160	20
	UHC	CDC	0.265	15
	NO <sub>x</sub>	PCCI 45BU	0.328	15
	Soot	PCCI 45BU	0.265	20
	UHC	PCCI 45BU	0.265	10
	NO <sub>x</sub>	PCCI 45ET	0.328	15
	Soot	PCCI 45ET	0.265	20
	UHC	PCCI 45ET	0.328	10
	NO <sub>x</sub> /Soot	PCCI 45ET	0.328	25
<b>4 Bar</b>	NO <sub>x</sub>	CDC	0.160	15
	Soot	CDC	0.234	15
	UHC	CDC	0.214	15
	NO <sub>x</sub>	PCCI 45BU	0.265	20
	Soot	PCCI 45BU	0.378	15
	UHC	PCCI 45BU	0.378	10
	NO <sub>x</sub>	PCCI 45ET	0.328	20
	Soot	PCCI 45ET	0.214	15
	UHC	PCCI 45ET	0.378	115
<b>5 Bar</b>	NO <sub>x</sub>	CDC	0.328	25
	Soot	CDC	0.328	20
	UHC	CDC	0.328	15
	NO <sub>x</sub>	PCCI 45BU	0.265	20
	Soot	PCCI 45BU	0.265	10
	UHC	PCCI 45BU	0.265	15
	NO <sub>x</sub>	PCCI 45ET	0.328	15
	Soot	PCCI 45ET	0.265	15
	UHC	PCCI 45ET	0.265	5

The engine operational parameters and safety limits were adhered to for all the tests conducted over the 3 loads tested and can be observed in Table 6. All of the test points were conducted with an intake temperature of 65° C within a tolerance of  $\pm 5^{\circ}\text{C}$ . This was done in order to maximize the vaporization of the PFI fuels and to promote a more homogenous air/fuel mixture in order to further reduce UHC emissions. The other operating temperatures/limits seen in Table 6 were adhered to in order to ensure both the health of the engine and to ensure consistency between the test points that were conducted.



Table 6: Engine Operation Parameters/Limits

Parameter	Unit	Value
COV	%	0-5
Oil Temperature	°C	$70 \pm 10^{\circ}\text{C}$
Engine Coolant Temperature	°C	$75 \pm 6^{\circ}\text{C}$
Dyno Oil Temperature	°C	$32 \pm 2^{\circ}\text{C}$
Intake Temperature	°C	$65 \pm 5^{\circ}\text{C}$
PPRR Limit	Bar/CAD	8.00
Supercharger Gearbox Max Temperature	°C	$65^{\circ}\text{C}$

### Injection Parameters

The DI injection parameters for each test was determined experimentally in order to ensure COV was beneath 5%, PPRR remained below 8 bar/CAD, and the indicated CA50 from the AVL Indicom remained at 2 CAD ATDC. For 5 of the PCCI tests conducted at 3 bar IMEP, no pilot injection was utilized in order to maintain COV beneath 5%. This adjustment was needed in order to control the cycle per cycle combustion stability of the low reactivity PFI fuels as they were more prone to misfiring at low loads. The CRDI system utilized an injection pressure of 800 bar for a load of 3 bar IMEP and increased in increments of 200 bar per bar of increased IMEP load. The PFI duration per PCCI test was selected for maintaining PFI at 45% fuel mass injected with a tolerance of  $\pm 1.5\%$ . The pilot injection event is denoted as SOI-1 and the second injection event is denoted as SOI-2, the timing and duration of each per test conducted can be seen in Table 7 for a load of 3 bar IMEP, Table 8 for a load of 4 bar IMEP, and Table 9 for a load of 5 bar IMEP.

Table 7: Injection Parameters at 3 Bar IMEP

Test Name	SOI-1 Timing [CAD] BTDC	SOI-1 Duration[ms]	SOI-2 Timing [CAD] BTDC	SOI-2 Duration[ms]	PFI Duration [ms]	Rail Pressure [bar]
CDC NO <sub>x</sub>	60	0.2	12	0.562	-	800
CDC Soot	60	0.2	10	0.474	-	800
CDC UHC	60	0.2	12	0.514	-	800
PCCI 45BU NO <sub>x</sub>	60	0.2	11	0.396	2.07	800
PCCI 45BU Soot	60	0.2	10	0.431	2.02	800
PCCI 45BU UHC	60	-	11	0.400	1.95	800
PCCI 45ET NO <sub>x</sub>	60	-	12	0.450	2.20	800
PCCI 45ET Soot	60	-	12	0.450	2.25	800
PCCI 45ET UHC	60	-	12	0.450	2.10	800
PCCI 45ET NO <sub>x</sub> /Soot	60	-	12	0.460	2.10	800

Table 8: Injection Parameters at 4 Bar IMEP

Test Name	SOI-1 Timing [CAD] BTDC	SOI-1 Duration[ms]	SOI-2 Timing [CAD] BTDC	SOI-2 Duration[ms]	PFI Duration [ms]	Rail Pressure [bar]
CDC NO <sub>x</sub>	60	0.2	11	0.561	-	1000
CDC Soot	60	0.2	12	0.508	-	1000
CDC UHC	60	0.2	12	0.507	-	1000
PCCI 45BU NO <sub>x</sub>	60	0.2	7	0.320	2.80	1000
PCCI 45BU Soot	60	0.2	7	0.360	2.80	1000
PCCI 45BU UHC	60	0.2	7	0.380	2.70	1000
PCCI 45ET NO <sub>x</sub>	60	0.2	11	0.400	3.10	1000
PCCI 45ET Soot	60	0.2	10	0.420	3.10	1000
PCCI 45ET UHC	60	0.2	11	0.390	3.10	1000

Table 9: Injection Parameters at 5 Bar IMEP

Test Name	SOI-1 Timing [CAD] BTDC	SOI-1 Duration[ms]	SOI-2 Timing [CAD] BTDC	SOI-2 Duration[ms]	PFI Duration [ms]	Rail Pressure [bar]
<b>CDC NO<sub>x</sub></b>	60	0.2	12	0.540	-	1200
<b>CDC Soot</b>	60	0.2	12	0.530	-	1200
<b>CDC UHC</b>	60	0.2	11	0.552	-	1200
<b>PCCI 45BU NO<sub>x</sub></b>	60	0.2	6	0.350	3.45	1200
<b>PCCI 45BU Soot</b>	60	0.2	6	0.350	3.45	1200
<b>PCCI 45BU UHC</b>	60	0.2	6	0.350	3.46	1200
<b>PCCI 45ET NO<sub>x</sub></b>	60	0.2	9	0.375	3.70	1200
<b>PCCI 45ET Soot</b>	60	0.2	9	0.370	3.60	1200
<b>PCCI 45ET UHC</b>	60	0.2	9	0.350	3.55	1200

#### Criteria for Success

The criteria for success of this study are for NO<sub>x</sub> and soot emissions to be reduced by at least 30% for at least one PCCI test per load. An additional criteria for success is for a minimum of 10% reduction of non-renewable carbon in all PCCI combustion when compared to CDC.

## CHAPTER 4

## DATA AND RESULTS ANALYSIS

## Preliminary Results

Multiple investigations were conducted on the fuels utilized for CDC and PCCI combustion to ascertain their performance, emissions indicators, and compatibility with the PFI and CRDI fuel systems.

## Low Temperature Oxidation and Thermal Stability Analysis

The TGA measures the volatility of the researched fuels by recording the change in mass of the sample as the temperature is increased in the furnace chamber. As seen in Figure 28, E98 loses mass at a higher rate than both ULSD and n-butanol, this indicates that E98 when PFI would create a more homogeneous air/fuel mixture than n-butanol due to its higher volatility.

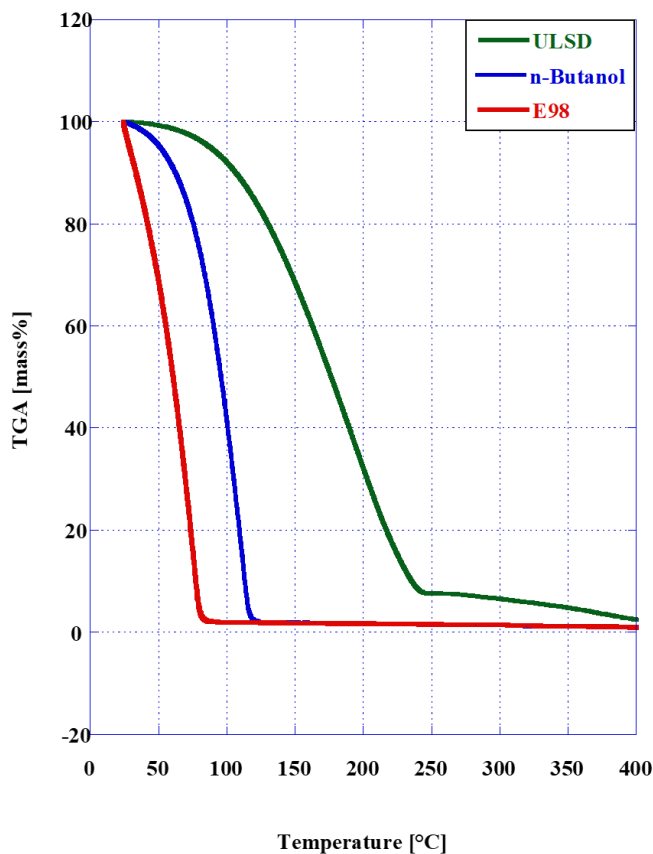


Figure 28: Thermogravimetric Analysis

In Table 10 the temperature at which 10 %, 50 %, and 90 % of the fuel mass was vaporized can be found, denoted by TA(10), TA(50), and TA(90). The extreme volatility of E98 is apparent as the TA(90) of the fuel is approximately 18°C lower than n-butanol. This indicates that E98 when compared to n-butanol more readily vaporizes when PFI into the intake manifold of the engine creating a more homogeneous air/fuel mixture. While ULSD has a TA90 that is 32 °C higher than E98, its volatility is inefficient for a PFI process.

Table 10: Volatility of researched fuels

<b>TA %</b>	<b>ULSD</b>	<b>n-butanol</b>	<b>E98</b>
<b>TA(10)</b>	110.0 °C	54.3 °C	33.4 °C
<b>TA(50)</b>	180.0 °C	80.8 °C	60.6 °C
<b>TA(90)</b>	240.0 °C	95.4 °C	77.3 °C

The DTA analysis, as seen in Figure 29, is a study of the endothermic and exothermic reactions of the fuel during the vaporization and low temperature oxidation process. The endothermic reaction was represented by the negative slope in the DTA curve while the positive slope represents the exothermic reactions. As such, during the experiment the endothermic reaction of the fuel increases until no more energy can be absorbed by the sample and begins to oxidize. E98 was shown to have the steepest negative and positive slopes as well as the largest endothermic reaction, thus emphasizing its higher volatility compared to that of n-butanol and ULSD.

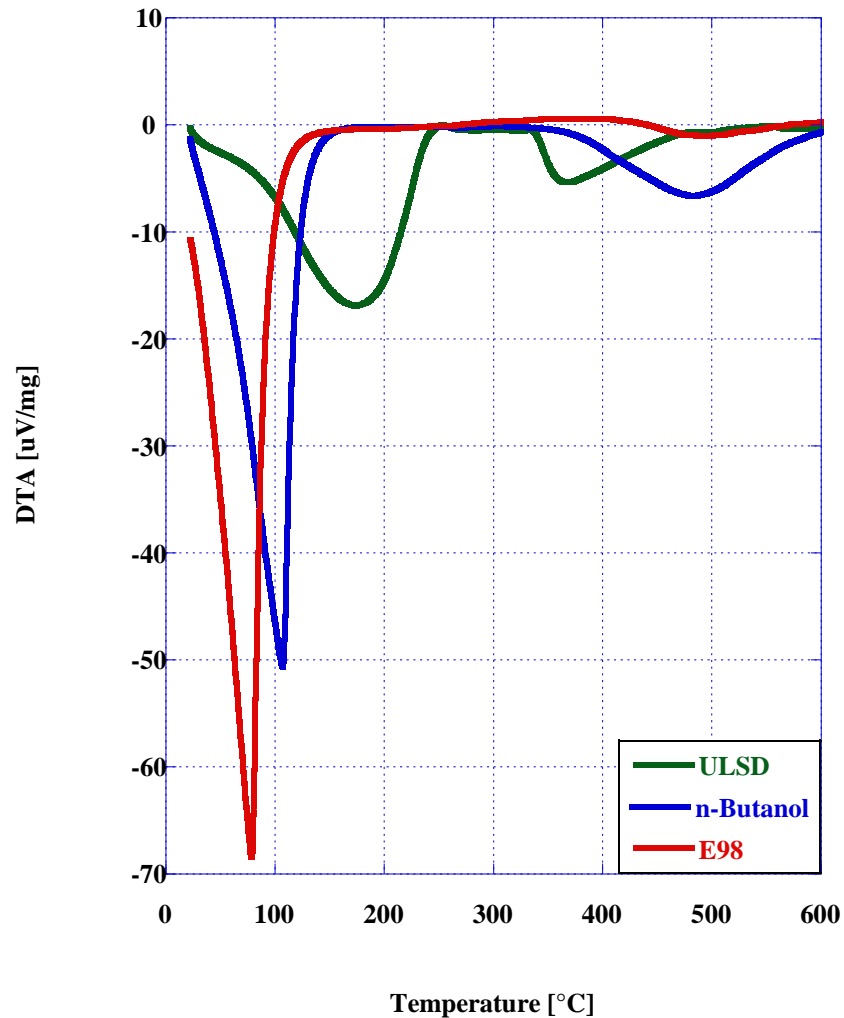


Figure 29: Differential Thermal Analysis of the Researched Fuels.

The greater endothermic reaction of E98 indicates that when PFI, the intake air temperature should decrease further than with n-butanol due to its greater latent heat of vaporization and thus in-cylinder temperatures should subsequently decrease. This was confirmed during fired engine research as will be seen in the next sections.

### Viscosity Analysis

As the temperature of the fuel increased the shear stress between the water jacket and spindle was seen to decrease, thus resulting in a lower viscosity. Figure 30 below shows the viscosity curve for the researched fuels with respect to temperature.

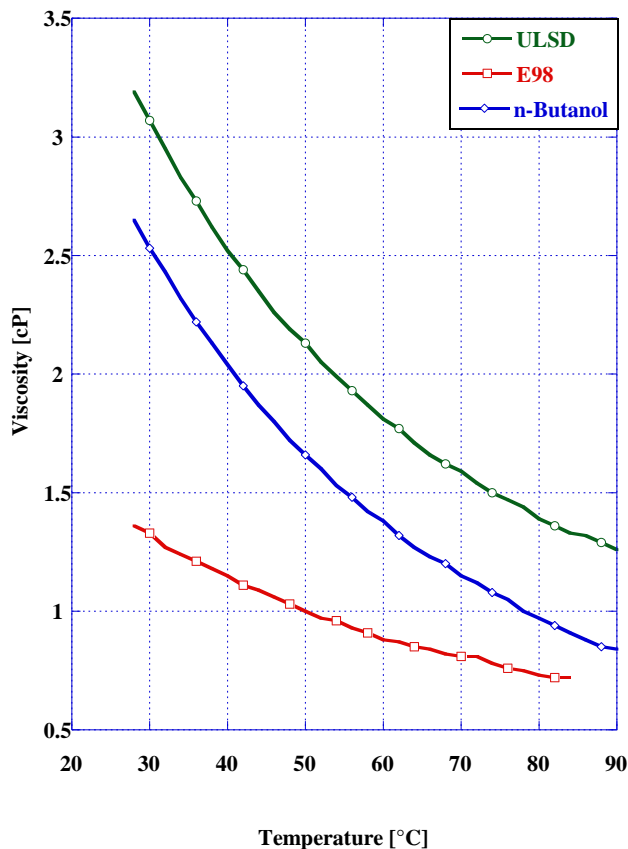


Figure 30: Viscosity measurements for the researched fuels

During the viscosity test, E98 was unable to reach 90 °C due to the fuel completely vaporizing before the test could be concluded. As seen in Table 11 below, ULSD was observed to have the highest viscosity of the research fuels with 2.52 cP at 40 °C. N-butanol had the second highest viscosity with 2.04 cP at 40 °C, followed by E98 with 1.15 cP at 40 °C.

Table 11: Viscosity of the researched fuels at 40 °C

	ULSD	n-butanol	E98
<b>Viscosity @ 40 °C (cP)</b>	2.52	2.04	1.15

### Lower Heating Value Analysis

The average lower heating value of the researched fuels can be seen in Table 12 below. USLD was seen to have the highest lower heating value at 45.1 (MJ/kg), followed by n-butanol with 32.0 (MJ/kg), and finally E98 at 24.7 (MJ/kg). The lower energy content of both n-butanol

and E98 indicates that greater fuel consumption may occur for PCCI combustion than CDC due to the increased fuel mass required for the same amount of work. As a result, increases in BSFC is expected with the greatest changes occurring for PCCI with ethanol.

Table 12: Calorimeter Results

Fuel	Lower Heating Value (MJ/kg)
ULSD	45.1
n-butanol	32.0
E98	24.7

### Mie-Scattering Fuel Spray Analysis

The Mie-scattering spray analysis was conducted for ULSD#2, n-butanol, and ethanol to study the atomization characteristics of the three fuels and compare them to one another. Across the three fuels, n-butanol had the smallest average SMD over time compared to the other fuels. It was found that there was a correlation between n-butanol and ethanol's lower viscosity to the smaller droplet diameters measured in comparison to ULSD #2. The most frequently measured droplet diameter for n-butanol sprays was 30  $\mu\text{m}$ , which consisted of 7.6 % of the spray by volume. By comparison, 8.5 % of ethanol's spray by volume was composed of droplets with a diameter of 30  $\mu\text{m}$ . The spray volume percentiles based on droplet SMD are displayed in Table 13 and the results show that n-butanol has an average of 5  $\mu\text{m}$  smaller SMD compared to ethanol for the same injection parameters.

Table 13: Particle Size Distribution by Volume ( $\mu\text{m}$ )

	ULSD	n-butanol	E98
DV (10)	12.5	12.23	24.8
DV (50)	40.1	34.2	65.3
DV (90)	131.1	88.21	91.0

DV (10) denotes the diameter that 10 % of the spray droplets by volume are less than or equal to in size. DV (50) is the corresponding diameter for 50 % of the spray volume and DV (90) denotes the same for 90 % of the spray volume. The ethanol sprays exhibited a droplet size distribution that is noticeably more concentrated about the most frequent droplet diameter, whereas n-butanol and diesel droplets are more distributed over different ranges of diameters as



seen in Figure 31. Ethanol does however still contain droplets that are larger than that of n-butanol for 90 % of the spray volume. This may be explained due to ethanol's higher volatility at room temperatures leading to smaller fuel droplets vaporizing prior to crossing the laser's beam as was observed in the TGA analysis.

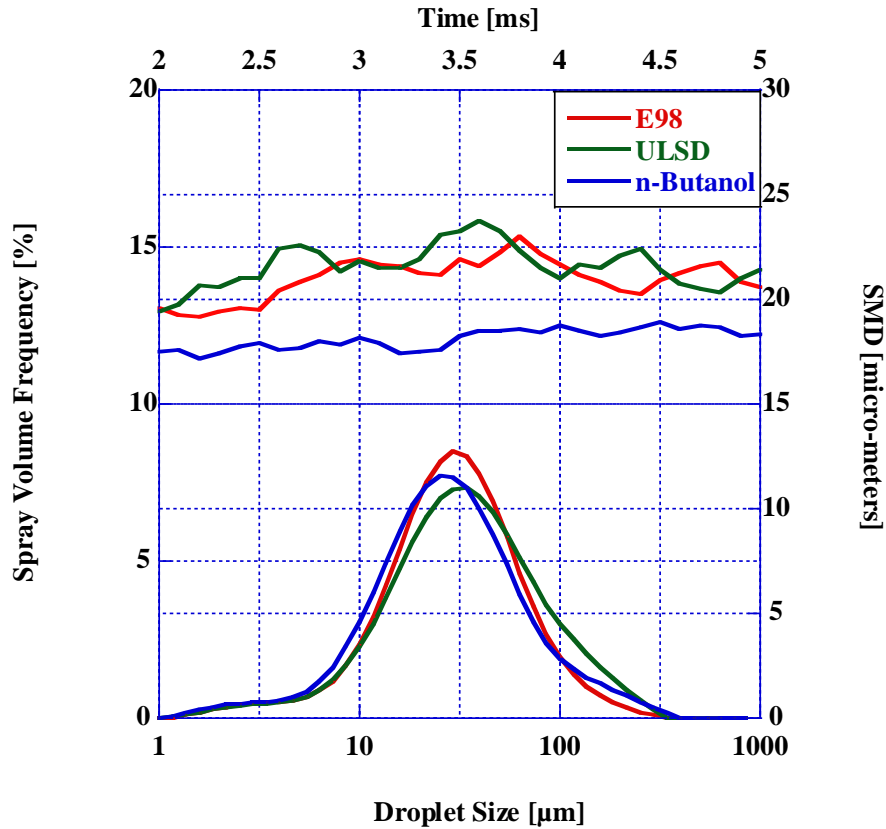


Figure 31: Spray SMD distribution and development

#### Preliminary Fired Engine Analysis

A fired engine preliminary study was conducted on identifying the optimal boost and EGR parameters for reducing  $\text{NO}_x$ , Soot, and UHC emissions while maintaining PPRR within acceptable parameters for CDC and PCCI with either ethanol or n-butanol. During this investigation DI timing/duration of the pilot and main injection event were changed accordingly to maintain COV below 5% and achieve an indicated CA50 of 2 °ATDC, PCCI was conducted with a PFI of 45% by fuel mass. During the execution of this study, the operating points were only held for one minute to stabilize readings without inducing excessive operating hours and wear and

tear of the experimental engine and emissions analysis equipment. As a result of this, an in-depth combustion analysis was not done on the points utilized for constructing the 3D maps of the preliminary analysis. However, the data gathered from this investigation was sufficient for determining the 27 operating points to determine the optimal parameters for PCCI.

### Preliminary NO<sub>x</sub> Emissions Results

EGR % and boost was changed simultaneously over several points in order to measure NO<sub>x</sub> emissions at 3 bar IMEP for CDC, PCCI 45BU, and PCCI 45ET. This was done in order to gain insight on the optimized studied parameters relation to NO<sub>x</sub> emissions as seen in Figure 32. It was observed at 3 bar IMEP that CDC had less NO<sub>x</sub> emissions as boost was decreased to 0.16 bar. Simultaneously optimal EGR % was shown to be at 17.5% at a boost of 0.16 bar with a second optimal point occurring at 25% EGR. However contrary to CDC, PCCI was observed to have lower NO<sub>x</sub> emissions as boost was increased to 0.328 bar at 15 % EGR for both n-butanol and ethanol. In addition, it was observed that PCCI 45ET had a secondary point in which NO<sub>x</sub> emissions were reduced with 20% EGR and 0.265 bar of boost.

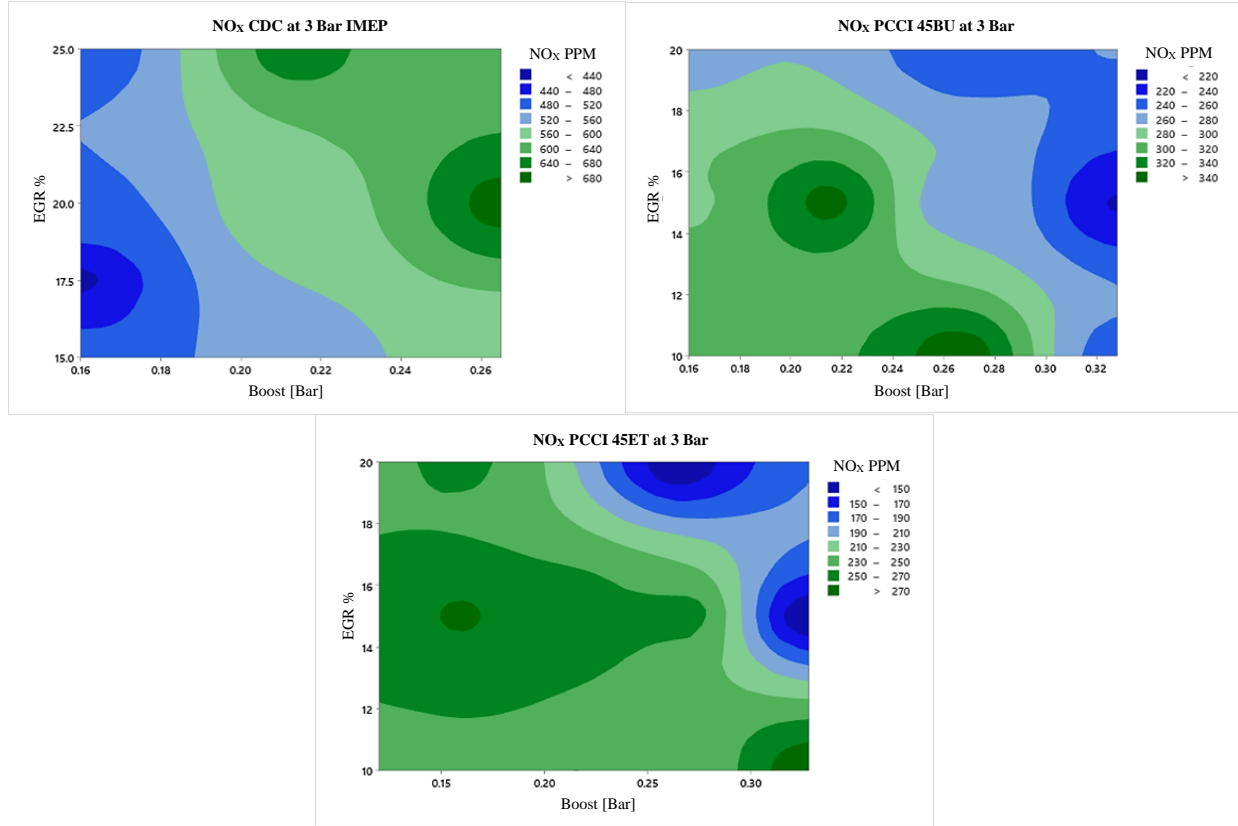


Figure 32: NO<sub>x</sub> emissions at 3 bar IMEP, CDC (a), PCCI 45BU (b), PCCI 45ET (c)

The observations made for PCCI 45ET indicate that lower boost could be used for lower NO<sub>x</sub> emissions than PCCI 45BU. However, due to ethanol's lower reactivity than n-butanol this may cause UHC to increase if less boost is utilized.

As the load was increased to 4 bar IMEP, it can be seen in Figure 33 that CDC had lower NO<sub>x</sub> emissions at a lower EGR % than at 3 bar IMEP at 15% and that boost remained the same at 0.16 bar. PCCI exhibited greater changes to the NO<sub>x</sub> emissions map than CDC as PCCI 45BU had its optimal point shift to 0.265 bar of boost and an EGR % of 20%. In addition to this, PCCI 45ET had even greater changes to the map in comparison to 3 bar IMEP where NO<sub>x</sub> emissions were seen to be greatly reduced throughout the operating points encompassing boost from 0.15 – 0.378 bar and EGR % greater than 14% and less than 20%. PCCI 45ET had its lowest NO<sub>x</sub> emissions occur at 0.328 bar of boost and 20% EGR. The trend indicated that as the load was raised PCCI with n-butanol required less boost and more EGR to sustain the NO<sub>x</sub> emissions reductions while PCCI with ethanol had less stringent requirements for reducing

NO<sub>x</sub> emissions at 4 bar IMEP. This could be as a result of ethanol's lower reactivity than n-butanol reducing peak in-cylinder combustion temperatures so long as sufficient boost and EGR is supplied to adequately control the combustion process. This observation however will be verified with the combustion analysis that will be conducted in a future section.

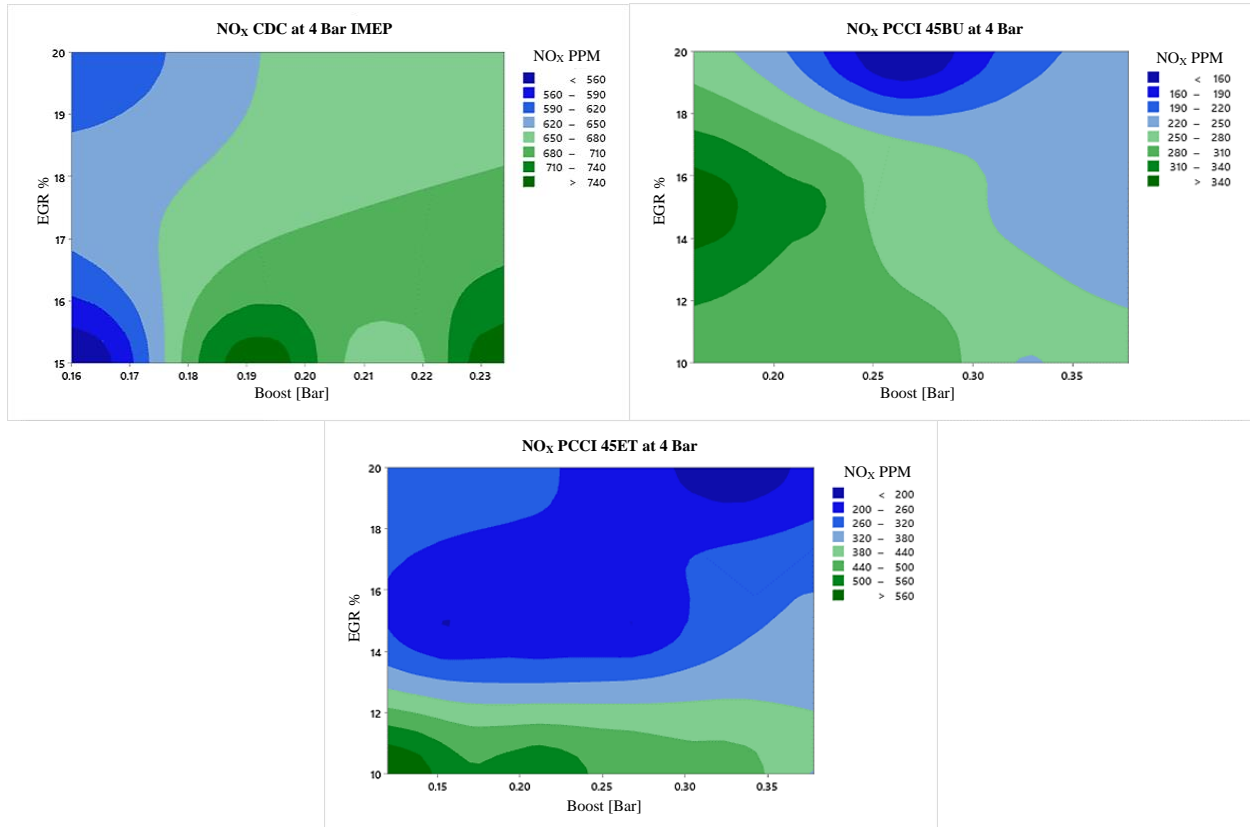


Figure 33: NO<sub>x</sub> emissions at 4 bar IMEP, CDC (a), PCCI 45BU (b), PCCI 45ET (c)

At a load of 5 bar IMEP, it was observed in Figure 34 that CDC, PCCI 45ET, and PCCI 45BU had considerable changes to the NO<sub>x</sub> emissions map when compared to tests conducted at 3 and 4 bar IMEP. At a load of 5 bar IMEP CDC was shown to require more EGR % and boost than PCCI 45BU and more EGR% than PCCI 45ET to lower NO<sub>x</sub> emissions. It was observed that PCCI with ethanol required more boost and less EGR % in order to reduce NO<sub>x</sub> emissions than PCCI with n-butanol due to ethanol's lower reactivity. However as was previously stated, ethanol's lower reactivity may lead to increased UHC emissions in comparison to n-butanol as will be observed in a future section. The optimal points regarding NO<sub>x</sub> emissions for CDC was indicated

to be at 0.328 bar of boost and 25% EGR while PCCI 45BU was at 0.265 bar of boost and 20% EGR and PCCI 45ET at 0.328 bar of boost and 15% EGR.

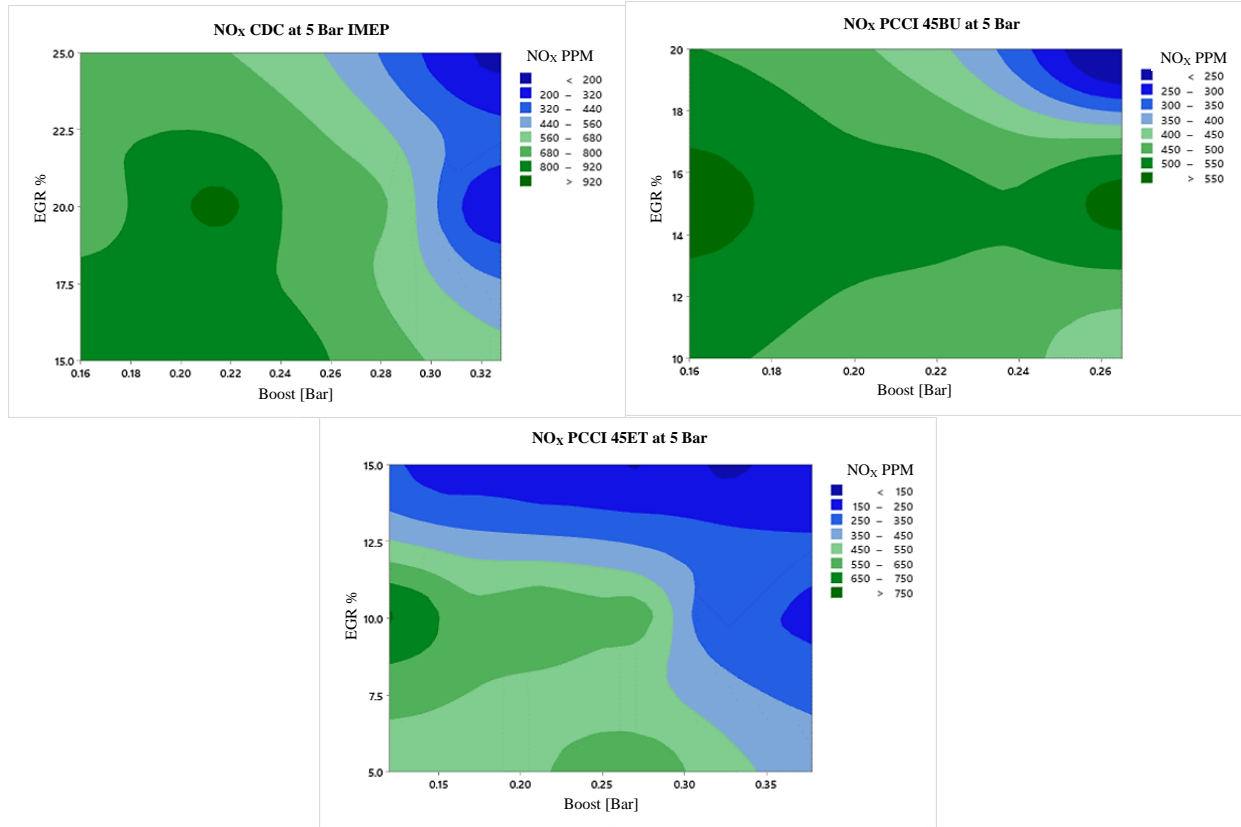


Figure 34: NO<sub>x</sub> emissions at 5 bar IMEP, CDC (a), PCCI 45BU (b), PCCI 45ET (c)

### Preliminary Soot Emissions Results

Several operating points were conducted in order to construct a preliminary study on the soot emissions map for CDC, PCCI 45BU, and PCCI 45ET at a load of 3 bar IMEP. The 3D maps constructed on boost and EGRs effect on soot emissions for each of the combustion methods can be observed in Figure 35. CDC had lower soot emissions with either low EGR % at any boost pressure or at low boost pressure (0.16 bar) with EGR % ranging from 17.5% - 20%. Whereas PCCI 45BU was shown to have lower soot emissions with higher boost pressure (0.328 bar) and EGR % at 10% or 15% with an additional ideal operating point located at 0.265 bar of boost pressure and 20% EGR. A similar trend was observed for PCCI 45ET where multiple points exhibited lower soot emissions located at 15% EGR and 0.16 bar of boost, 0.328 bar of boost and

15% EGR, and the greatest reductions occurring at 0.265 bar of boost and 20% EGR. The preliminary results gathered from this analysis indicate that at a low load of 3 bar IMEP, PCCI with either ethanol or n-butanol required higher boost and EGR than CDC for optimal soot emissions reduction.

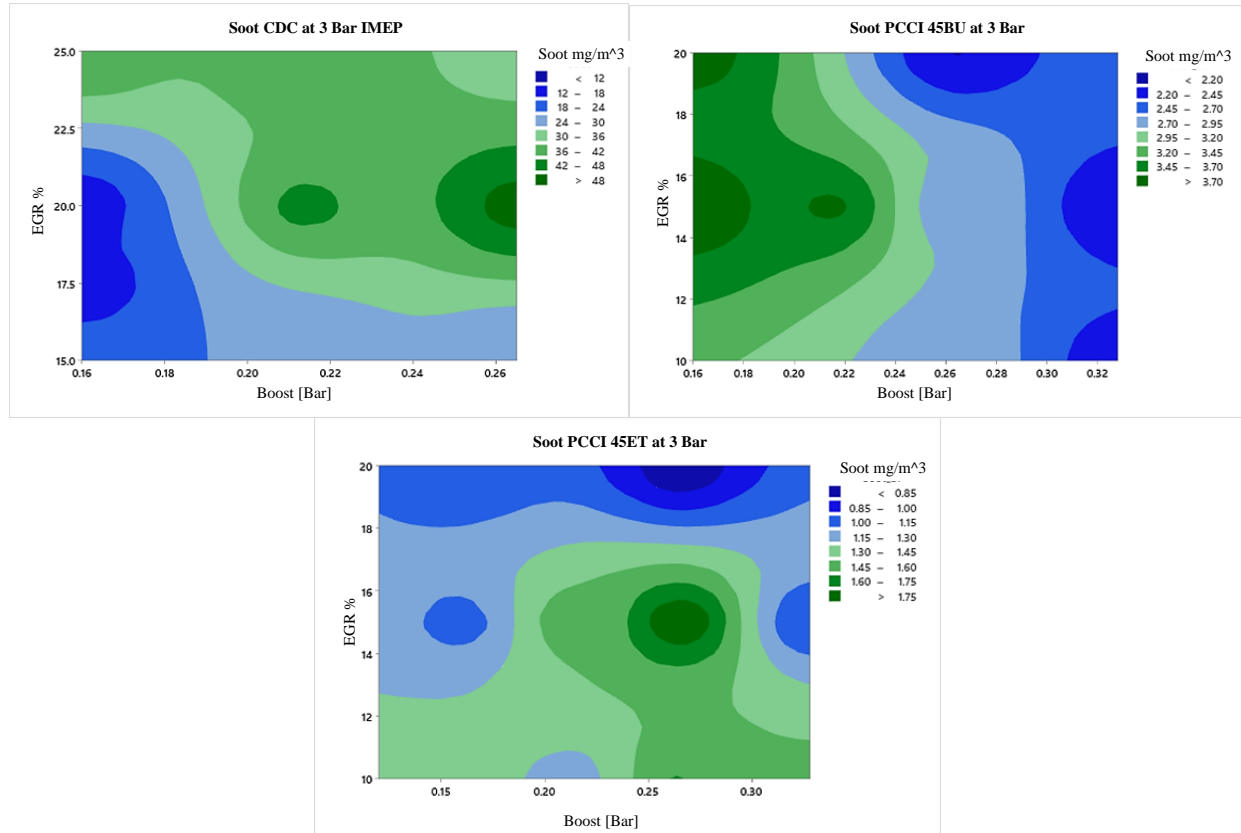


Figure 35: Soot emissions at 3 bar IMEP, CDC (a), PCCI 45BU (b), PCCI 45ET (c)

The soot emissions measured for operating points conducted at 4 bar IMEP were compiled into the contour maps seen in Figure 36. It was observed that PCCI 45BU had 3 ideal operating points where soot emissions were minimized while CDC had one point and PCCI 45ET had only one as well. This indicates that PCCI with n-butanol had less stringent requirements for minimizing soot emissions while CDC and PCCI with ethanol had more localized areas on the map where soot was minimized. CDC had soot emissions minimized as boost was increased to 0.234 bar of boost and was minimal at 15% EGR. PCCI 45ET had a larger area of the map where soot emissions were minimized encompassing operating points between 0.16 bar to 0.214 bar of boost and EGR

between 14% and 17.5%. PCCI 45BU on the other hand, had the largest area of lower soot emissions of the three combustion methods tested. This indicates that although PCCI with ethanol has lower soot emissions than n-butanol, PCCI with n-butanol has less rigorous conditions for soot reduction optimization.

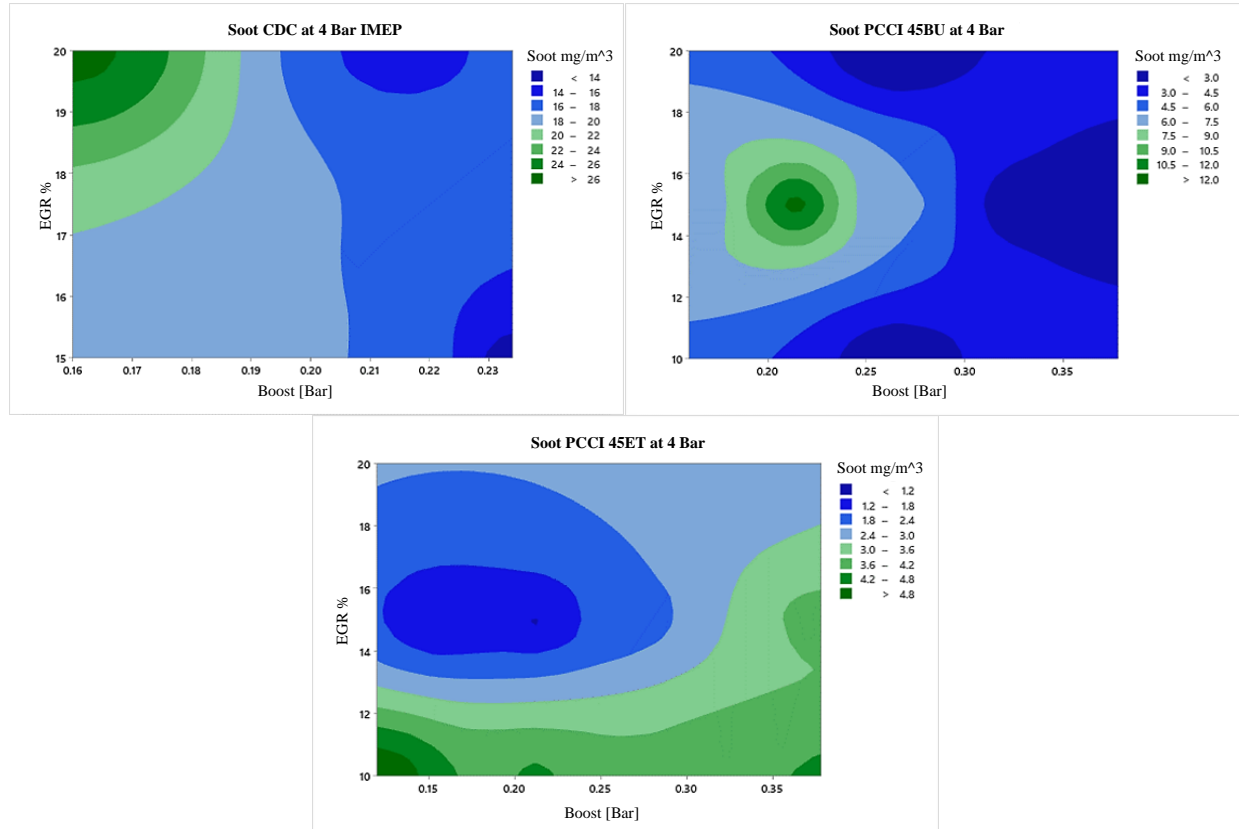


Figure 36: Soot emissions at 4 bar IMEP, CDC (a), PCCI 45BU (b), PCCI 45ET (c)

As the load was increased to 5 bar IMEP, it was observed in Figure 37 that CDC's soot emission map had minimally changed with the peak reduction point occurring at 0.328 bar of boost and 20% EGR. Inverse of the trend observed at 4 bar IMEP, PCCI 45BU had a larger portion of the map with lowered soot emissions indicating that PCCI with n-butanol has less stringent conditions for lowered soot emissions with the optimal point at 0.265 bar of boost and 10% EGR. However, PCCI 45ET had the opposite effect where a small area of the map had the lowest soot emissions at 15% EGR and 0.265 bar of boost. In addition, although a smaller portion of the map had optimal emissions, overall ethanol had lower soot emissions than either n-butanol or CDC.

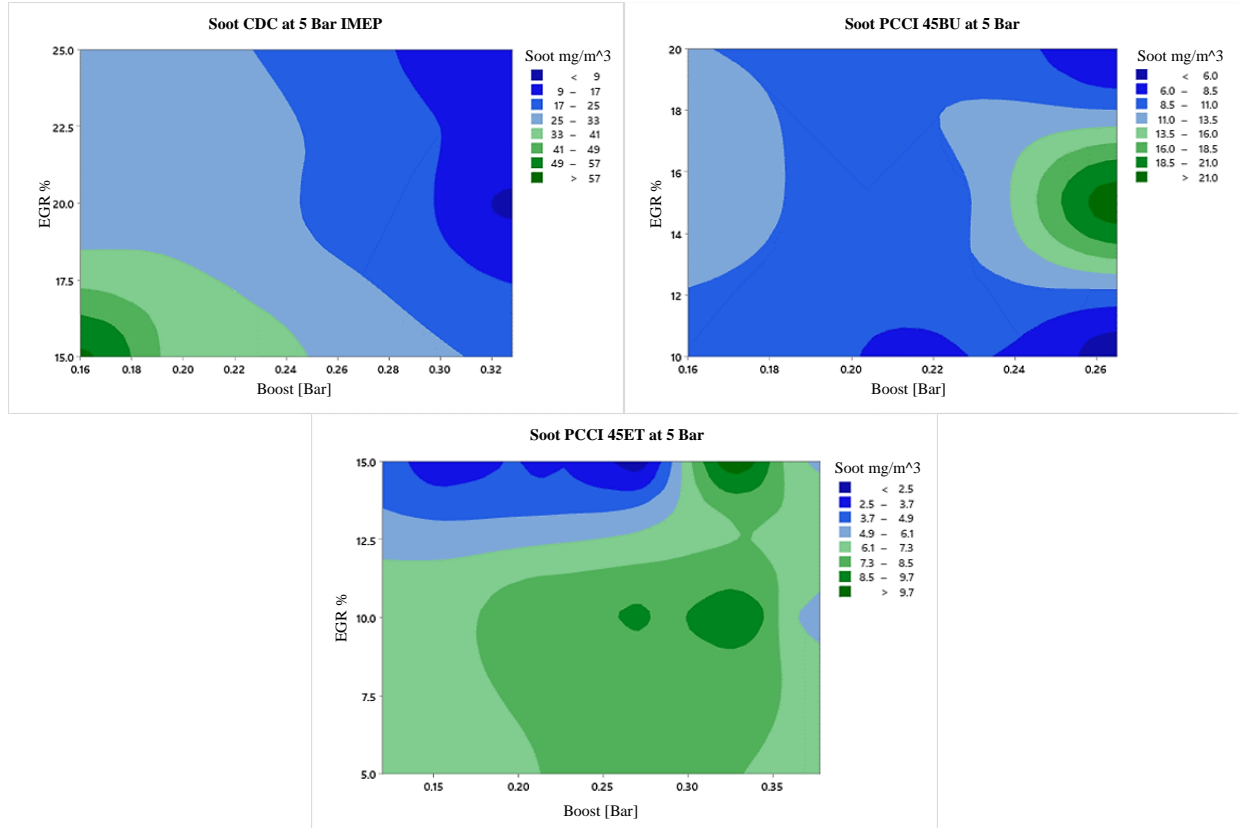


Figure 37: Soot emissions at 5 bar IMEP, CDC (a), PCCI 45BU (b), PCCI 45ET (c)

### Preliminary Unburnt Hydrocarbon (UHC) Emissions Results

Unburnt hydrocarbons emissions are an important concern for alternative combustion techniques/bio-alcohols as they are typically elevated when compared to CDC. However, this can be mitigated through the optimization of several engine operating parameters primarily boost and EGR. With this in mind, a preliminary investigation was conducted on the UHC emitted from PCCI 45BU and PCCI 45ET over several operating points of differing boost pressures and EGR% in order to gain insight on what parameters are needed for less UHC emissions.

At a load of 3 bar IMEP, it was observed in Figure 38 that UHC were lower for a greater area of the map for PCCI 45BU at boost pressures greater than 0.24 bar and throughout the EGR range of 10% - 20%. Within this range there were 3 optimal operating points at 0.265 bar of boost and 10% EGR, 0.328 bar of boost and 15% EGR, and 0.265 bar of boost and 20% EGR. In contrast, PCCI 45ET had a much smaller area of the map where UHC were lowered and only one optimal operating point at 10% EGR and 0.328 bar of boost. The observation obtained from this



preliminary investigation indicate that n-butanol's higher reactivity led to less stringent operating parameters necessary for reducing UHC when compared to ethanol's lower reactivity. PCCI with ethanol however, at a low load required boost and low EGR to achieve lower UHC.

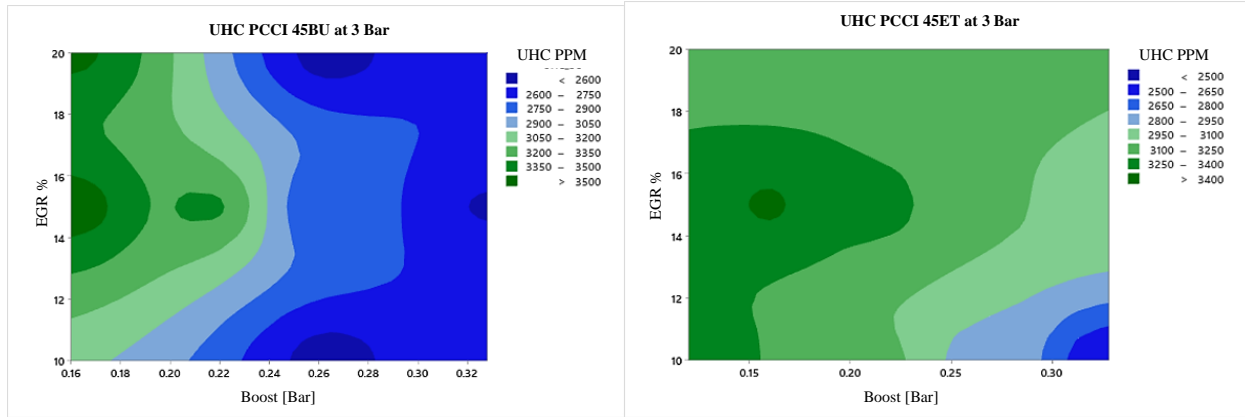


Figure 38: UHC emissions at 3 bar IMEP PCCI 45BU (a) and PCCI 45ET (b)

At a load of 5 bar IMEP, the behaviors previously observed at 3 bar IMEP were reversed as PCCI with n-butanol had a diminished area of the map where UHC emissions were reduced as seen in Figure 39. As for PCCI 45ET, the area of the map with greater UHC emissions reductions had expanded predominately at lower EGR%. However, for both PCCI 45BU and PCCI 45ET only one optimal operating point existed for the reduction of UHC emissions. As is the case, PCCI 45 BU had lower UHC emissions at 15% EGR and 0.378 bar of boost while PCCI 45ET had lower UHC emissions at 10% EGR and 0.378 bar of boost. The observations made at the load of 4 bar IMEP indicate that PCCI with either ethanol or n-butanol requires higher boost pressures to sustain lower UHC emissions with the reactivity of the PFI fuel of choice influencing the quantity of EGR% needed.

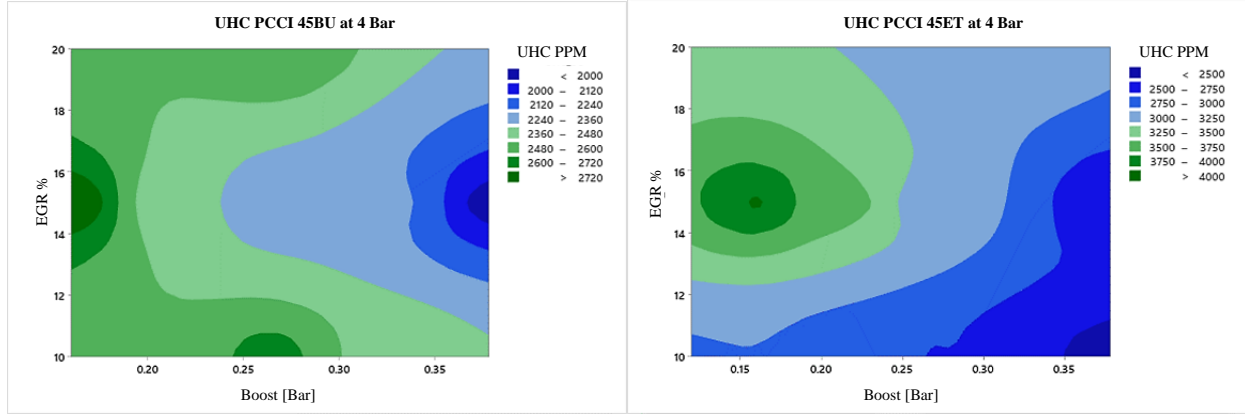


Figure 39: UHC emissions at 4 bar IMEP PCCI 45BU (a) and PCCI 45ET (b)

As the load of the engine was increased to 5 bar IMEP, it was observed in Figure 40 that lower boost pressures were needed for sustaining lower UHC emissions for both PCCI 45BU and PCCI 45ET. In addition, less EGR % was required for ethanol with optimal UHC emissions occurring at 5% EGR and 0.265 bar of boost while n-butanol needed the same boost pressure but at the same EGR% as the load 4 bar IMEP at 15% EGR. The trend observed at 5 bar IMEP reveals that at a higher load less boost pressure is needed for lower UHC emissions and that in particular ethanol requires minimal EGR% in order for this to occur.

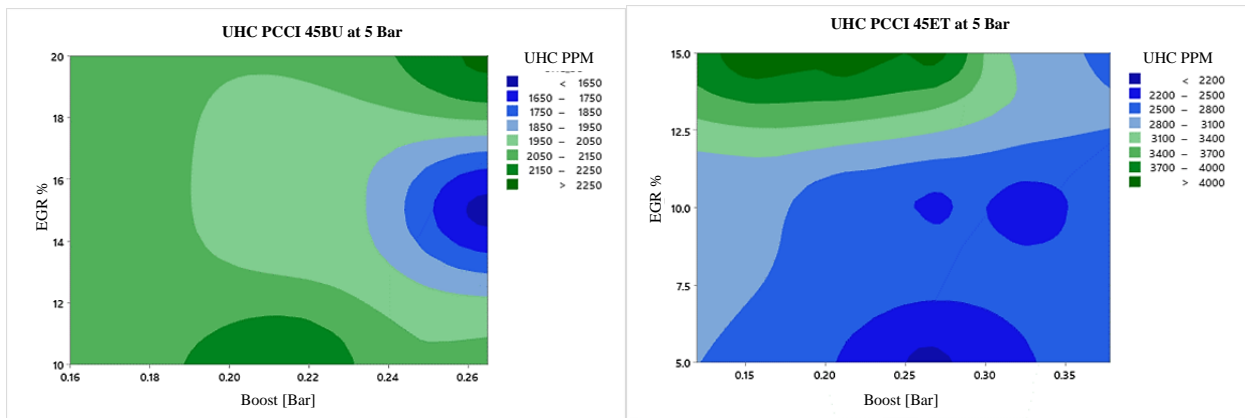


Figure 40: UHC emissions at 5 bar IMEP PCCI 45BU (a) and PCCI 45ET (b)

When comparing PCCI 45BU to PCCI 45ET, PCCI with n-butanol has lower UHC emissions than ethanol due to its lower reactivity, this could prove to be advantageous for increasing PCCI's combustion efficiency. Moreover, during the course of this investigation, the

general trend for PCCI 45BU was that as load was increased EGR% needed for lower UHC emissions increased from 10% - 15% while boost remained the same for 3 and 5 bar IMEP at 0.265 bar and only rose to 0.328 bar at 4 bar IMEP. PCCI 45ET UHC emissions on the other hand, had the opposite occur for EGR% as it lowered from 10% to 5% as load was increased. Concurrently the boost pressure needed for lower UHC emissions had a similar trend to PCCI 45BU where additional boost was needed for lower loads and less was required at a higher load of 5 bar IMEP.

### Fired Engine Analysis

Multiple studies were conducted on the combustion/emission characteristics of the 28 trials conducted over the loads 3 bar, 4 bar, and 5 bar IMEP. The names for each of the tests points is denoted by the combustion method, the PFI% by mass, the PFI fuel initials, and the emissions parameter of which it was optimized for. For each one of the loads studied, the optimal test point for CDC, PCCI 45ET, and PCCI 45BU were then further discussed for each one of the studies conducted. These test points were determined based off of their performance in NO<sub>x</sub>, soot, UHC, and combustion efficiency.

The studies conducted on the combustion characteristics of the tests conducted were done so utilizing the in-cylinder pressure, DI and PFI fuel flow rate, boost pressure, EGR, and intake manifold temperature in order to calculate the various engine performance metrics in this study. As for the emissions studies, an AVL Microsoot 483 was used for measuring the soot while the other gaseous emissions were measured with an AVL SESAM FTIR v4.

### Fired Engine Tests Lambda

The Lambda's for all of the combustion tests conducted in this study can be seen in Table 14, where a general trend was spotted of PCCI with ethanol having leaner global air-fuel ratios than all of the other tests conducted per their perspective load. Followed by this, PCCI with n-butanol had a leaner air-fuel mixture in comparison to CDC, PCCI leaner global lambda is attributed to the molecular oxygen provided by the PFI fuels. As is the case, generally as the % oxygen content of the fuel is raised so to will the lambda increase per given load. This is a strong indicator of diminished soot emissions which will be further discussed in future sections.

Table 14: Global Lambda for All Combustion Tests Conducted

Test Name	Lambda at 3 Bar	Lambda at 4 Bar	Lambda at 5 Bar
	IMEP	IMEP	IMEP
CDC NO <sub>x</sub>	8.04	5.10	6.22
CDC Soot	6.41	5.61	4.51
CDC UHC	6.87	5.31	5.07
PCCI 45BU NO <sub>x</sub>	8.51	6.68	5.00
PCCI 45BU Soot	8.31	7.06	4.44
PCCI 45BU UHC	8.09	7.48	4.94
PCCI 45ET NO <sub>x</sub>	9.31	6.77	5.79
PCCI 45ET Soot	8.60	6.07	5.48
PCCI 45ET UHC	8.60	7.04	5.06
PCCI 45ET Extra	9.12	-	-

#### Optimal CDC and PCCI Test Points per Load

During the course of this investigation, of the 28 tests conducted, only 3 combustion tests were chosen per load for CDC, PCCI with n-butanol, and PCCI with ethanol. These test points were chosen based off their performance in NO<sub>x</sub> emissions, soot emissions, Combustion Efficiency, and UHC emissions. The chosen optimal test point names of the 28 tests conducted are shown in Table 15 for each load and combustion method.

Table 15: Selected Optimal Test Points per Load and Combustion/Fuel Method

Load Bar IMEP	CDC	PCCI 45BU	PCCI 45ET
3	CDC Soot	PCCI 45BU NO <sub>x</sub>	PCCI 45ET Extra
4	CDC UHC	PCCI 45BU Soot	PCCI 45ET Soot
5	CDC Soot	PCCI 45BU Soot	PCCI 45ET UHC

In Figure 41 the various performance metrics of the optimal combustion tests points can be observed. The graphics were created based off the assessment of their performance in each category relative to the highest maximum value for that parameter at the chosen load. A more detailed analysis on each performance/emissions metric will be discussed in future sections.

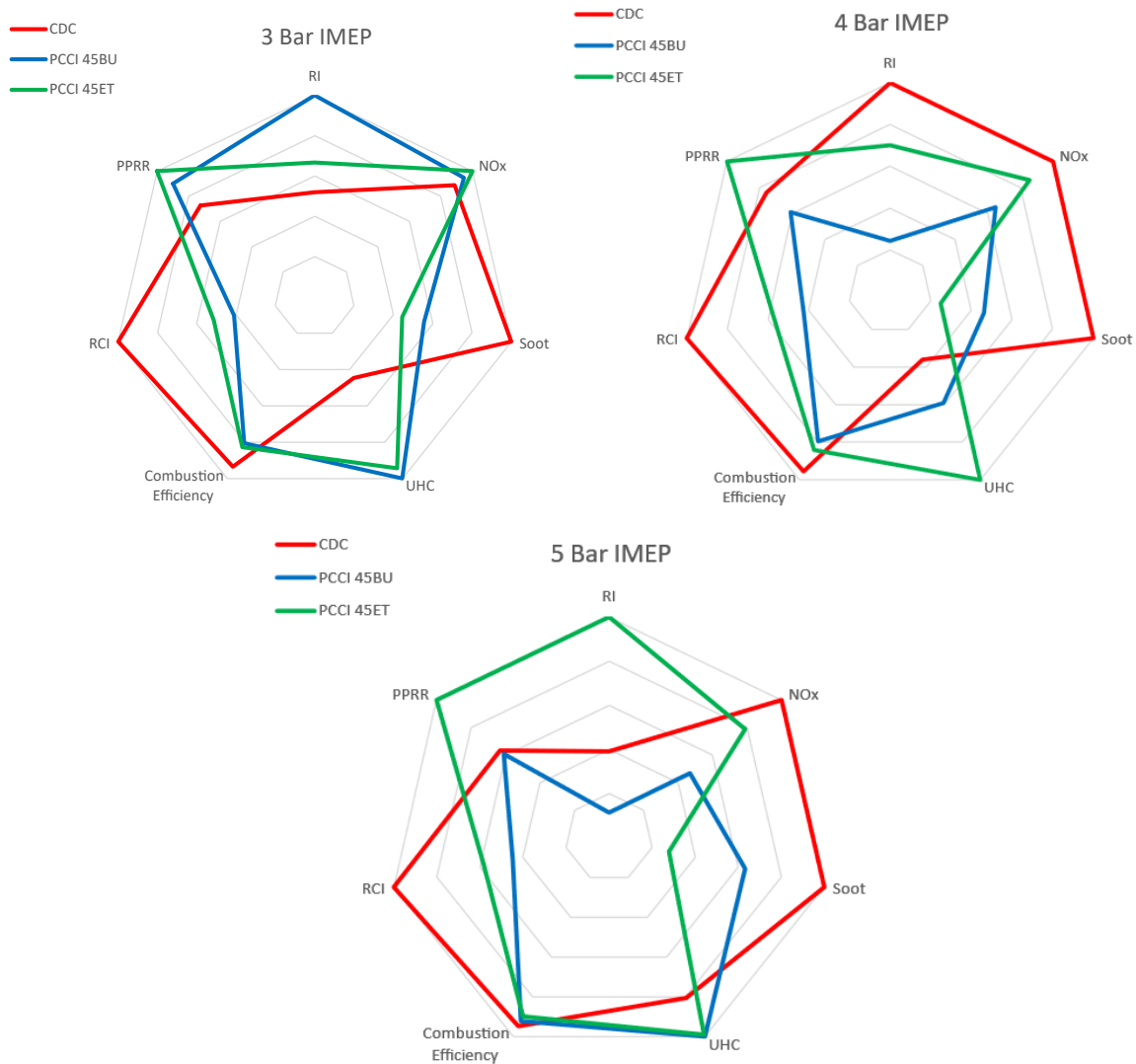


Figure 41: Optimal Test Points Parameters at 3 Bar IMEP

### Combustion Pressure and Pressure Rise Rate

The in-cylinder pressure and PRR for all the tests conducted at 3 bar IMEP can be seen in Figure 42 where a general trend was observed that PCCI tests with either ethanol or n-butanol had higher peak pressures and PRR than most CDC tests conducted. Apart from the increase in intake pressure (up to 0.31 bar of boost) used by some of the trials for a load of 3 bar IMEP, the increase

in-cylinder pressure observed for PCCI can be attributed to the combustion event initiated closer to TDC than CDC.

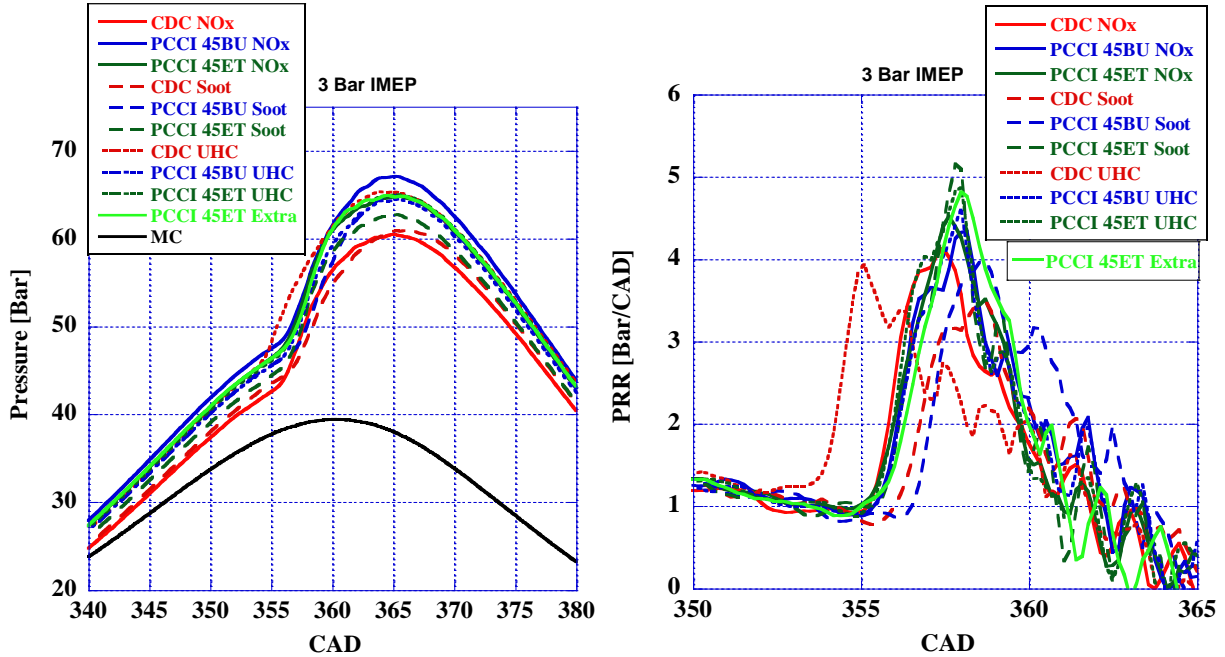


Figure 42: In-cylinder Pressure and PRR of All Trials at 3 Bar IMEP

The optimal test points found at a load of 3 bar IMEP was determined to be CDC Soot, PCCI 45ET Extra, and PCCI 45BU NO<sub>x</sub>. The combustion test “PCCI 45ET Extra” operating parameters were determined experimentally where it was observed that increasing the EGR% of the operating parameters of PCCI 45ET NO<sub>x</sub> to 25% was optimal for multiple combustion/emissions parameters. It was observed in Figure 43, that CDC had the lowest in-cylinder pressure and PPRR of the 3 optimal combustion tests at 3 bar IMEP. This was a result of the lower boost pressure and lessened intensity of combustion observed from CDC due to the absence of oxygenated fuels. PCCI 45ET Extra was observed to have less peak pressure than PCCI 45BU NO<sub>x</sub> as a result of a higher EGR% utilized and the lower reactivity of ethanol preventing greater combustion intensity as indicated by the in-cylinder pressure. However, it was observed that PCCI with ethanol had the greatest PPRR of the 3 tests followed by PCCI with n-butanol, indicating that at a low load of 3 bar IMEP the oxygen provided from the fuel rapidly increases pressure once combustion reaches a critical threshold.

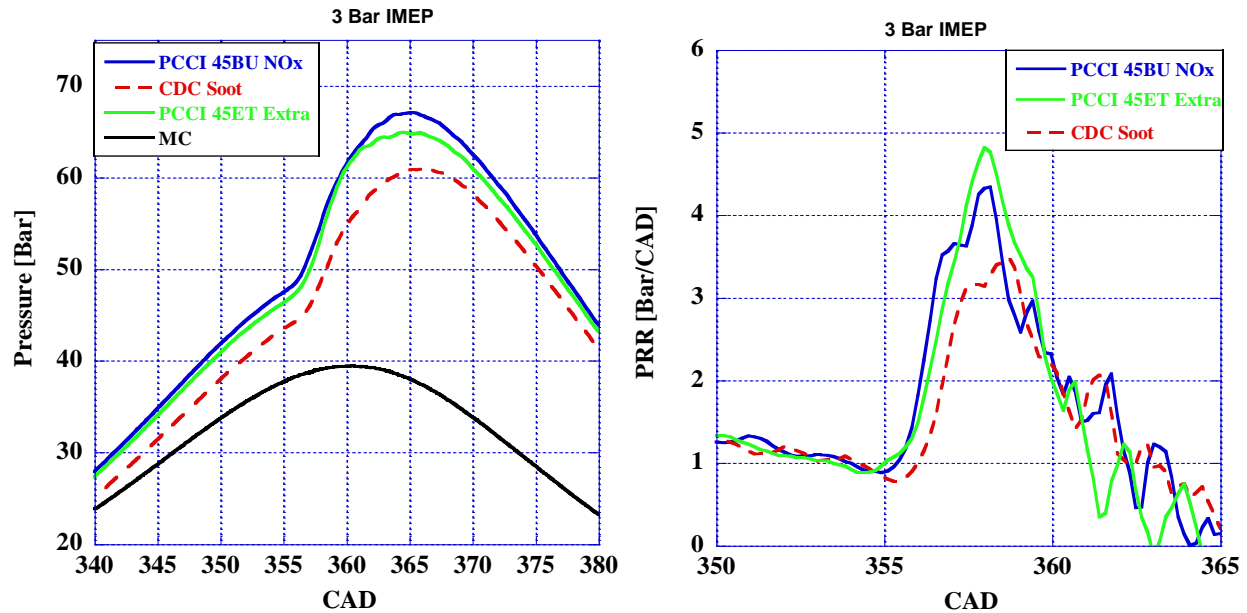


Figure 43: In-cylinder Pressure and PRR of The Best 3 Trials at 3 Bar IMEP

In Figure 44, it can be seen that CDC had the least variation in pressure amongst the 3 CDC tests conducted at 4 bar IMEP, while PCCI with ethanol had greater variation in pressure amongst the 3 tests conducted. In conjunction to this, most PCCI test had greater in-cylinder pressure than CDC as observed previously at a load of 3 bar IMEP due to the benefit of the oxygenated fuel. Further to this, PCCI with ethanol had a greater PPRR than all of the tests conducted exhibiting a single sharp peak. This is in contrast to the observation made with PCCI with n-butanol having a similar PPRR to that of CDC.

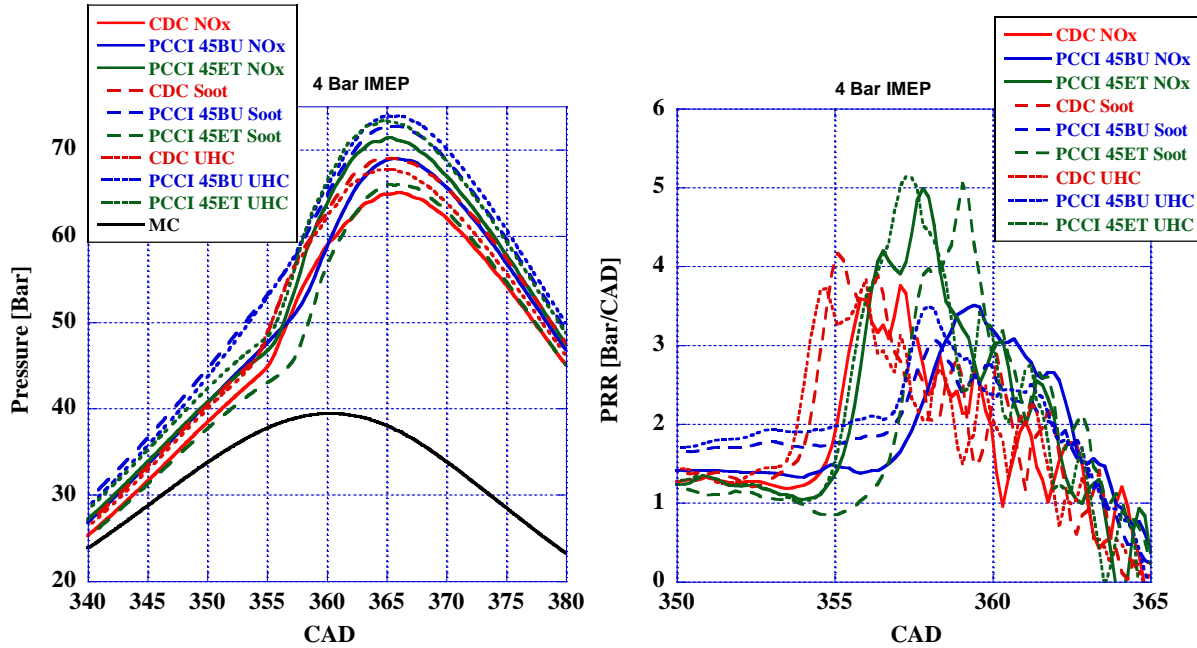


Figure 44: In-cylinder Pressure and PRR of All Trials at 4 Bar IMEP

However, when a more in-depth analysis is conducted on the 3 optimal points for 4 bar IMEP, PCCI 45ET Soot had the lowest pressures of the three tests conducted as seen in Figure 45 contradictory to the observation made at 3 bar IMEP. Although CDC UHC had less boost than PCCI 45ET Soot and the same EGR%, PCCI 45ET Soot had lower in-cylinder pressure throughout the observed range as a result of the increased PFI mass injected. Although PCCI 45BU Soot had the same PFI% by mass as PCCI 45ET Extra, the volume of fuel injected was greater for ethanol due to its lower density. In conjunction ethanol has a greater heat of absorption than n-butanol resulting in a further intake temperature decrease thus decreasing in-cylinder pressure. Apart from the decrease of in-cylinder pressure, PCCI 45ET Extra exhibited a greater PPRR than the other tests and occurs closer to TDC than the other tests. Despite having less boost than PCCI 45BU Soot, the decreased reactivity of ethanol and greater oxygen content had a greater effect on the location of the increase PPRR than boost. This indicates that for PCCI with ethanol, a greater quantity of energy from the diffusion combustion of DI ULSD#2 must be absorbed by the homogenous air-fuel mixture of ethanol in order to free the molecular oxygen from ethanol for combustion. This was indicated previously by the DTA study where ethanol had a greater endothermic reaction than n-butanol prior to oxidation and thus once ethanol releases its oxygen, helps expediate the combustion of the remaining fuel as seen by the sharp PPRR.



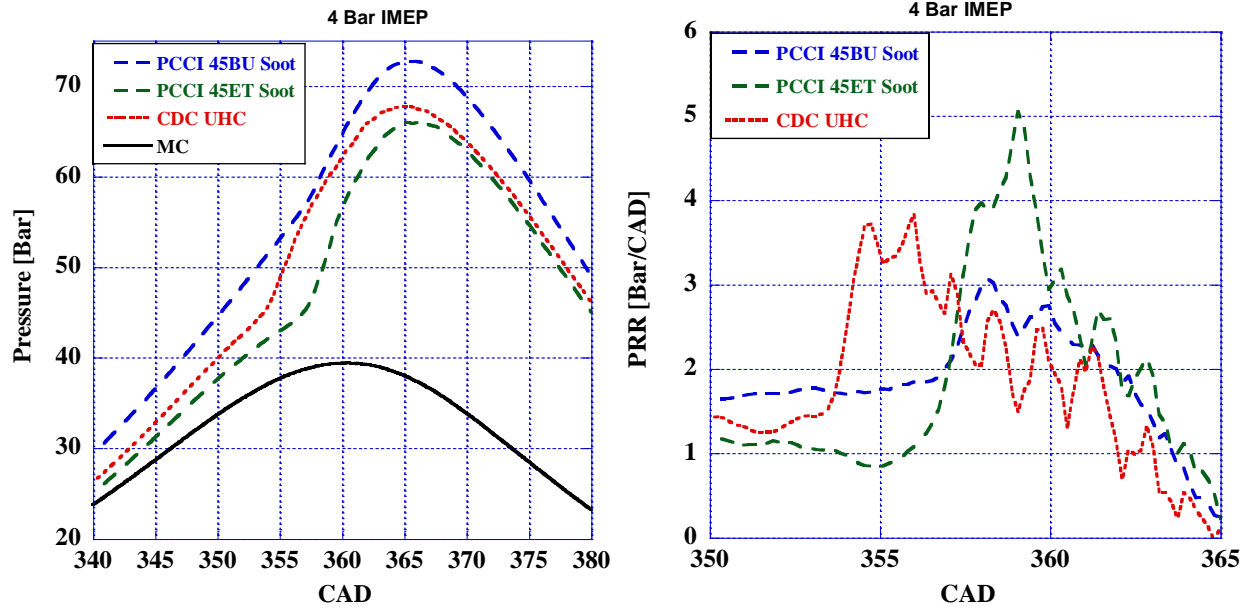


Figure 45: In-cylinder Pressure and PRR of The Best 3 Trials at 4 Bar IMEP

As the load was increased to 5 bar IMEP it was observed that the variation of the in-cylinder pressure was decreased between the tests conducted as seen in Figure 46. CDC was observed to have the greatest in-cylinder pressure of all the tests conducted both at its peak and during the compression stroke while most PCCI tests had lower pressure throughout the observed range. Yet it was further observed that PCCI with ethanol had a delayed PPRR in comparison to the other tests as was previously observed at lower loads, indicating despite the increase in load, ethanol's lower reactivity has greater control of the combustion process and may be more suitable for engines with higher compression ratios and/or greater boost. Furthermore, despite the lower reactivity of ethanol, due to its higher oxygen content once combustion hits a critical mass burned the remaining fuel mass is burned at an expedited rate.

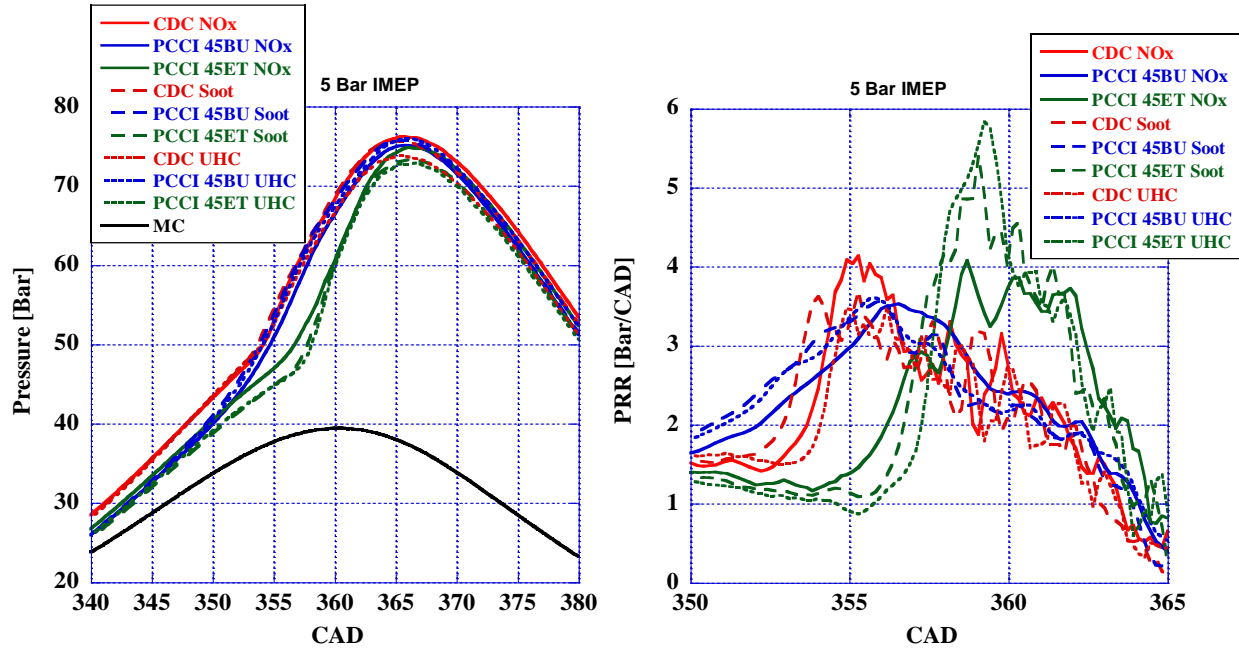


Figure 46: In-cylinder Pressure and PRR of All Trials at 5 Bar IMEP

In Figure 47, the in-cylinder pressure and PRR traces can be observed for the 3 optimal points (CDC Soot, PCCI 45BU Soot, and PCCI 45ET UHC) conducted at a load of 5 bar IMEP. Yet again it was seen that PCCI with ethanol had lower in-cylinder pressure than both CDC and PCCI with n-butanol as was previously observed at 4 bar IMEP indicating that as load is increased the lower reactivity of ethanol diminishes the increase of pressure greater than n-butanol as Lambda decreases. This observation indicates that the increase in volumetric injection of ethanol in comparison to n-butanol has greater effect on the reduction of in-cylinder pressures as lambda decreases. While at lower loads where lambda is greater, the quantity of ethanol injected does not provide the desired decrease of reactivity but provides additional oxygen to the combustion event that greatly effects the PRR observed from combustion.

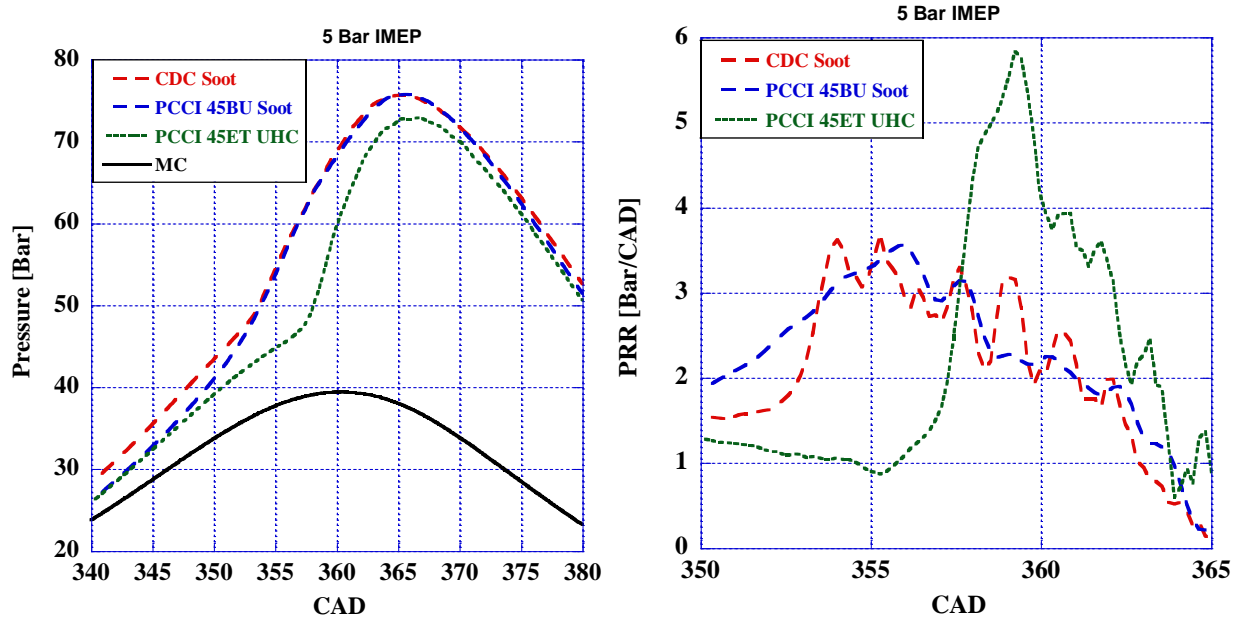


Figure 47: In-cylinder Pressure and PRR of The Best 3 Trials at 5 Bar IMEP

### Ringing Intensity

The RI was calculated for all the 28 combustion tests conducted over the loads 3, 4, and 5 bar IMEP using the maximum temperature, peak pressure, and PPRR as seen in Equation 10.

$$RI = \frac{(\beta(\frac{dP}{dt})_{max})^2}{(2\gamma P_{max})} \sqrt{\gamma R T_{max}} \quad \text{Equation 10}$$

It was seen in Figure 48 that, most PCCI with ethanol tests had higher RI than CDC for the 3 loads tested while PCCI with n-butanol had mostly lower RI than CDC except at a load of 3 bar IMEP. This phenomenon is due to the higher PPRR that PCCI with ethanol has in comparison to all the other tests, as the value of PPRR has the greatest influence on RI.

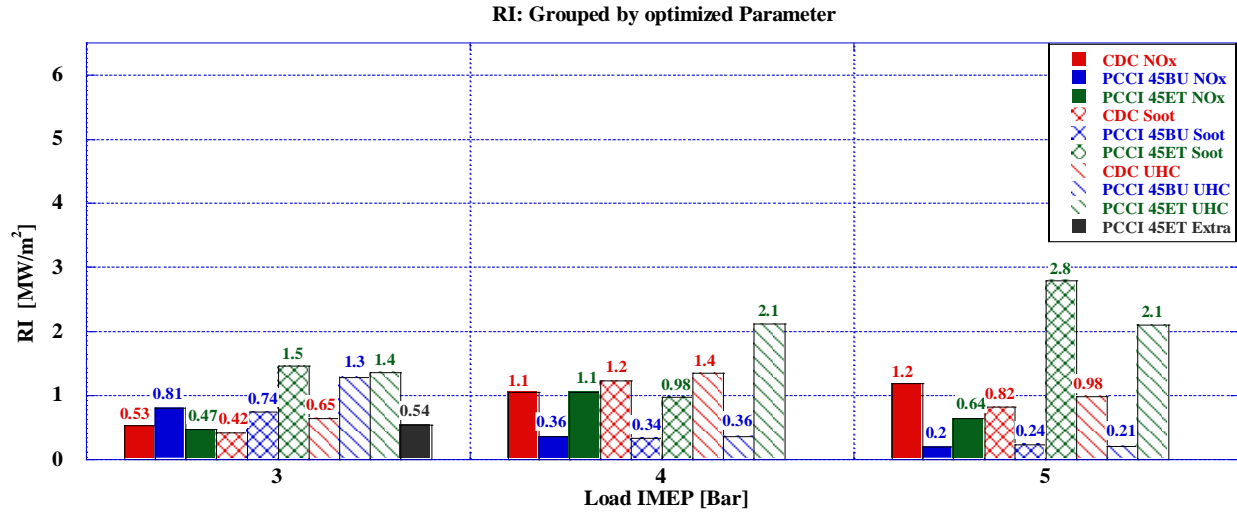


Figure 48: RI for All Combustion Tests Conducted at 3 bar IMEP

The RI and % difference from CDC for the 3 optimal test points per load can be seen in Table 16. It was observed that PCCI with ethanol had a higher RI than CDC by 28.6% at 3 bar and 156.1% at 5 bar while at 4 bar IMEP RI was reduced by 30%. For PCCI with n-butanol only the test conducted at 3 bar IMEP had a higher RI than CDC by 92.8%, however at loads of 4 and 5 bar IMEP the RI was reduced by 75.7% and 70.7% respectively. These results confirm the observation made with Figure 48, that RI is typically greater for PCCI with ethanol despite its lower reactivity than n-butanol as a result of the higher oxygen content increasing the PPRR greater than that of CDC or PCCI with n-butanol.

Table 16: RI of 3 Optimal Points per Load Tested

Combustion Test	RI @ 3 Bar IMEP	RI @ 4 Bar IMEP	RI @ 5 Bar IMEP
CDC	0.42	1.4	0.82
PCCI 45BU	0.81	0.34	0.24
PCCI 45ET	0.54	0.98	2.1
Combustion Test	$\Delta\%$ from CDC @ 3 Bar IMEP	$\Delta\%$ from CDC @ 4 Bar IMEP	$\Delta\%$ from CDC @ 5 Bar IMEP
PCCI 45BU	92.8%	-75.7%	-70.7%
PCCI 45ET	28.6%	-30.0%	156.1%

### In-Cylinder Temperature

The in-cylinder temperatures seen in Figure 49 were calculated using the in-cylinder pressure of each one of the combustion tests conducted at 3 bar IMEP. It was observed that CDC had the greatest maximum temperature of the combustion tests evaluated with a variation of a peak of 1200°C (CDC UHC) to 1050°C (CDC NO<sub>x</sub>). In contrast, PCCI with either ethanol or n-butanol was found to have smaller variations of maximum temperature spanning a range of 1120°C to 1020°C for PCCI with ethanol and a range of 1150°C to 1100°C for PCCI with n-butanol. This indicates that overall PCCI with either ethanol or n-butanol typically has greater combustion temperatures than CDC but at a smaller range. In addition, the cooling effect of the intake charge that is typically seen with PFI of alcohols is not observed here possibly due to the overall lower usage of fuel mass at lower loads.

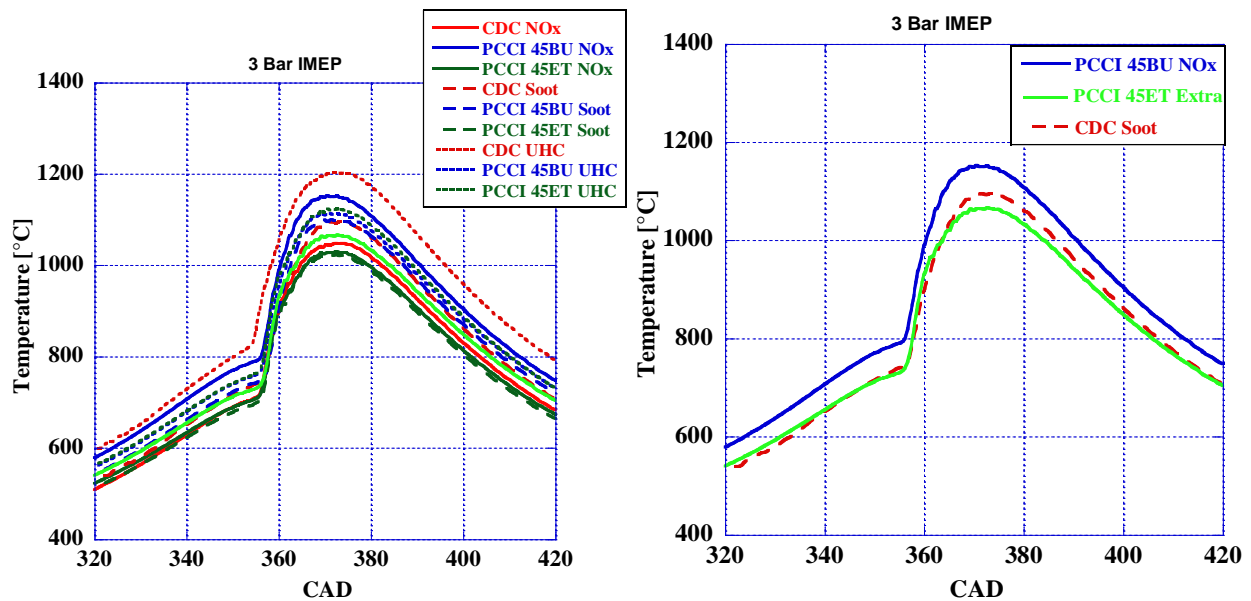


Figure 49: In-cylinder Temperature for Combustion Tests Conducted at 3 Bar IMEP

For the 3 optimal combustion tests conducted at 3 bar IMEP, it was seen that PCCI with ethanol had a lower maximum in-cylinder temperature compared to both CDC and PCCI with n-butanol while PCCI with n-butanol had the greatest in-cylinder temperatures of the 3 tests. This could be attributed to the lower EGR% of 15% utilized for PCCI 45BU NO<sub>x</sub> not being able to

reduce the temperature as greatly as the other tests conducted at 25% EGR (PCCI 45ET Extra) and 20% (CDC Soot).

The in-cylinder temperatures for the tests conducted at 4 bar IMEP can be seen in Figure 50 where the trend previously observed at 3 bar IMEP is inverted to CDC having the narrowest range of temperatures recorded. It was seen that CDC had a variation of maximum temperature between tests of 30°C whereas PCCI with ethanol had the greatest range of maximum temperatures of 95°C. PCCI with n-butanol had a range of maximum temperatures of 75°C, furthermore PCCI with either fuel was observed to have a decrease of temperature prior to combustion due to the cooling effect of PFI.

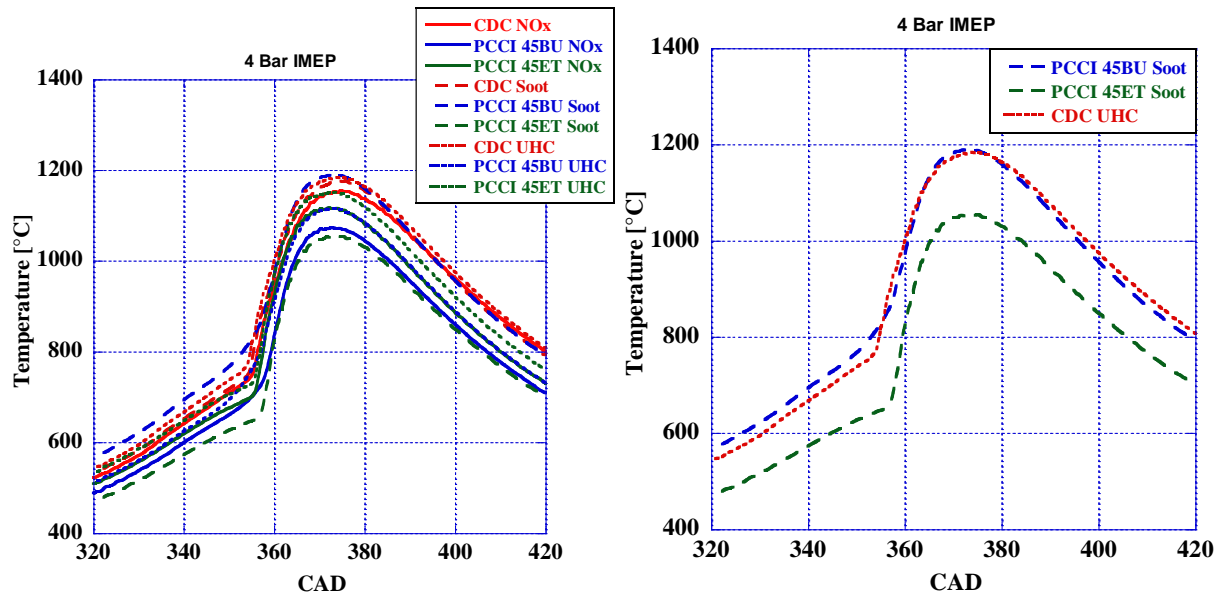


Figure 50: In-cylinder Temperature for Combustion Tests Conducted at 4 Bar IMEP

The 3 optimal points for a load of 4 bar IMEP were observed in Figure 50, where it was seen that PCCI 45ET Soot had both the lowest maximum in-cylinder temperatures but also the lowest temperature prior to combustion. Although PCCI with n-butanol (PCCI 45BU Soot) had the same PFI % by fuel mass as PCCI with ethanol, only PCCI with ethanol had shown a reduction to the intake air fuel charge as seen by the temperature prior to combustion. This observation can be attributed to the greater volume of ethanol that is injected (indicated by an increase in PFI duration) and the higher latent heat of vaporization of ethanol. As a result of this and ethanol's lower reactivity, maximum in-cylinder temperatures were reduced however this may not indicate

a reduction of NO<sub>x</sub> emissions as the greater oxygen content of ethanol may lead to greater NO<sub>x</sub> emissions.

It was observed in Figure 51, that the variation in maximum temperatures and the intensity had increased at a load of 5 bar IMEP for most of the combustion tests conducted in comparison to 4 bar IMEP. CDC had the greatest range of peak temperatures spanning a range of 360°C whereas PCCI with ethanol only had a range of 76°C between tests. PCCI with n-butanol unlike ethanol expressed a greater range of temperatures encompassing a range 176°C between its maximum temperatures. However, unlike the observation made at 4 bar IMEP, PCCI with n-butanol was seen to have a decrease in cylinder temperatures prior to combustion due to the reduction of temperature of the intake air-fuel charge due to a greater mass of fuel injected when compared to 4 bar IMEP.

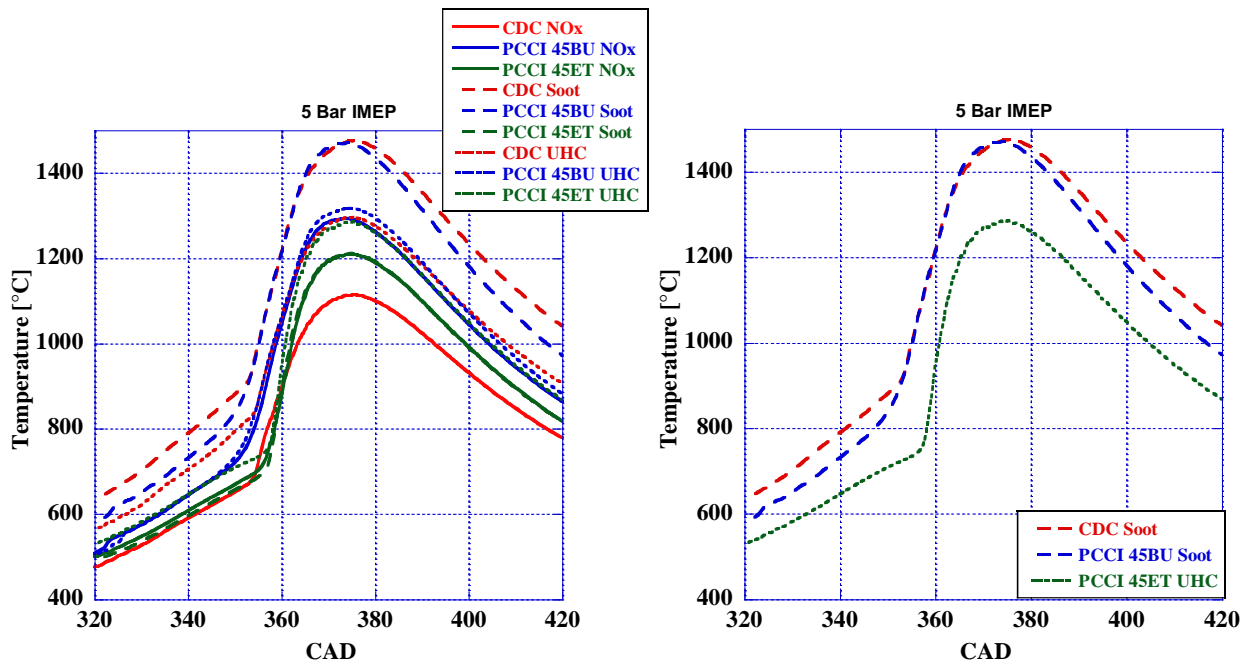


Figure 51: In-cylinder Temperature for Combustion Tests Conducted at 5 Bar IMEP

As for the 3 optimal combustion tests at 5 bar IMEP (CDC Soot, PCCI 45BU Soot, and PCCI 45ET UHC), it was observed yet again that PCCI with ethanol had the lowest maximum in-cylinder temperature of the 3 combustion tests while PCCI with n-butanol had similar maximum temperature to CDC. However, the temperature prior to combustion was observed to be reduced

compared to CDC as the increased fuel mass injected (from 4 bar IMEP, still at 45% PFI by mass) was able to further reduce the temperature of the intake air-fuel charge though not to the same magnitude as ethanol.

### Apparent Heat Release Rate

The AHRR for each test conducted was calculated using Equation 11 which was governed by the first law of thermodynamics. As is the case, the system was considered a closed system with appropriate compensations made for fuel mass introduced from DI events and mass lost due to blow-by. With this consideration in mind, the model was only utilized during the time in which the intake valve was closed as well as the exhaust valve.

$$\frac{dQ}{d\theta} = \frac{1}{[\gamma - 1]} V \frac{dP}{d\theta} + \frac{\gamma}{[\gamma - 1]} P \frac{dv}{d\theta} \quad \text{Equation 11}$$

The AHRR of tests conducted at a load of 3 bar IMEP can be seen in Figure 52, where it can be seen that most tests conducted had similar peak AHRR as well as the shape of it despite the usage of different fuels in PCCI. In addition, it was observed that most PCCI tests had sharper peak AHRR compared to CDC and is especially evident in PCCI with ethanol. While this trend was generally observed, CDC UHC had the lowest peak AHRR with a much broader area of combustion.



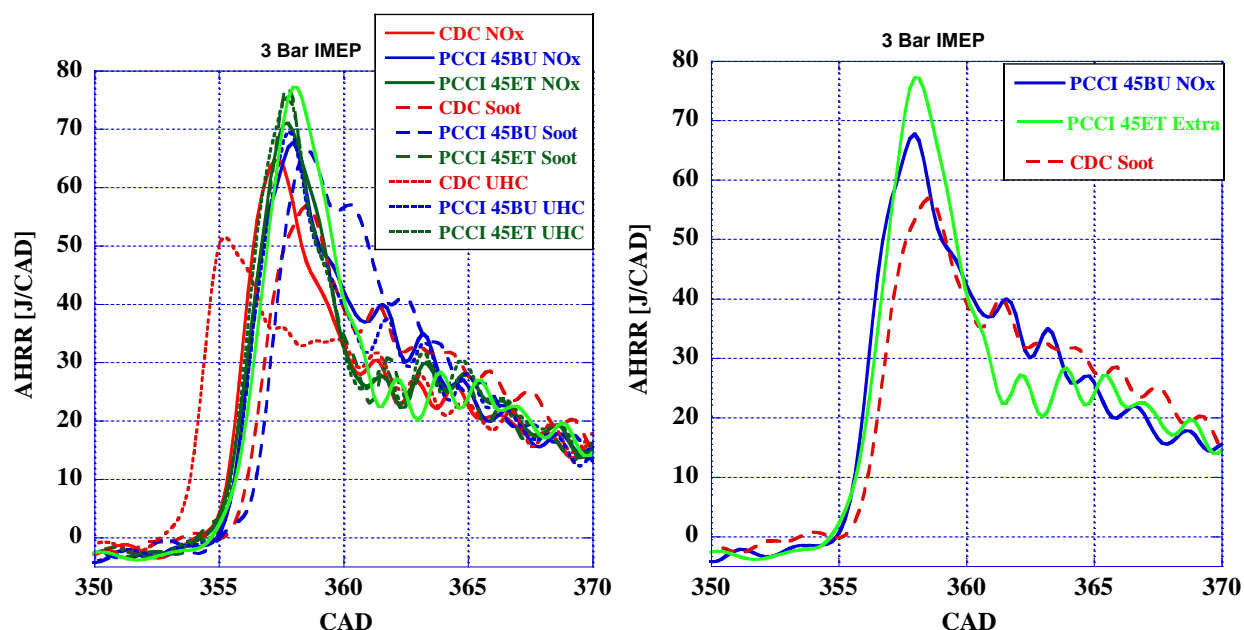


Figure 52: AHRR for Combustion Tests Conducted at 3 Bar IMEP

In conjunction, the 3 optimal test points for 3 bar IMEP (CDC Soot, PCCI 45ET Extra, and PCCI 45BU NO<sub>x</sub>) all had similar sharp AHRR, with PCCI with ethanol having the most notable of the 3. It was observed that PCCI with ethanol had a 35.75% increase in peak AHRR followed by PCCI with n-butanol having a 19.07% increase in peak AHRR from CDC. This indicates that the additional oxygen provided from the PFI increases peak AHRR at lower loads which could come at a detriment to NO<sub>x</sub> emissions as this is typically indicative of higher NO<sub>x</sub> formation.

Figure 53 contains the AHRR of the tests conducted at 4 bar IMEP where it was observed that apart from PCCI with ethanol, the shape of the AHRR was changed from 3 bar IMEP as the peak was diminished but the duration is increased. For the 3 optimal combustion points at 4 bar IMEP (CDC UHC, PCCI 45ET Soot, and PCCI 45BU Soot), the same trend was observed where only PCCI with ethanol had a more pronounced peak AHRR. This indicates that although ethanol has a lower reactivity than n-butanol, ethanol's higher oxygen content increases the intensity of combustion causing it to have a more pronounced peak and shorter duration. This may however be detrimental to NO<sub>x</sub> emissions as it may lead to an increase despite lower in-cylinder temperatures. PCCI with n-butanol however was similar to CDC having no distinguished peak AHRR but however occurring over a shorter duration. When compared to one another, PCCI with n-butanol had a 1.3% decrease in peak AHRR while PCCI with ethanol had an increase of 63.5%.

In addition, it was noted that all PCCI with n-butanol tests exhibited auto-ignition of the homogenous air-fuel mixture prior to SOI-2 injection timing.

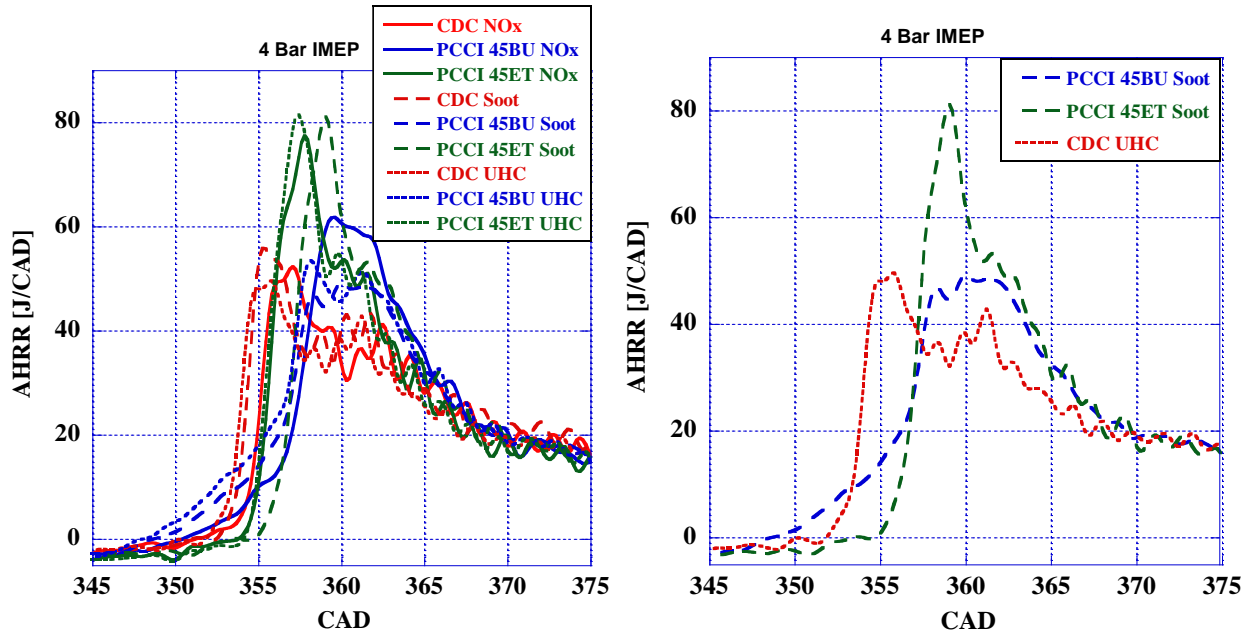


Figure 53: AHRR for Combustion Tests Conducted at 4 Bar IMEP

As the load was increased to 5 bar IMEP, it was observed in Figure 54 that the same trend previously observed at 4 bar IMEP with peak AHRR remained the same and auto-ignition occurring prior to SOI-2. PCCI with ethanol had a distinguished sharp peak AHRR compared to the other combustion tests as well as a lower duration than CDC and PCCI with n-butanol. In contrast to this, PCCI with n-butanol had an AHRR similar to CDC.

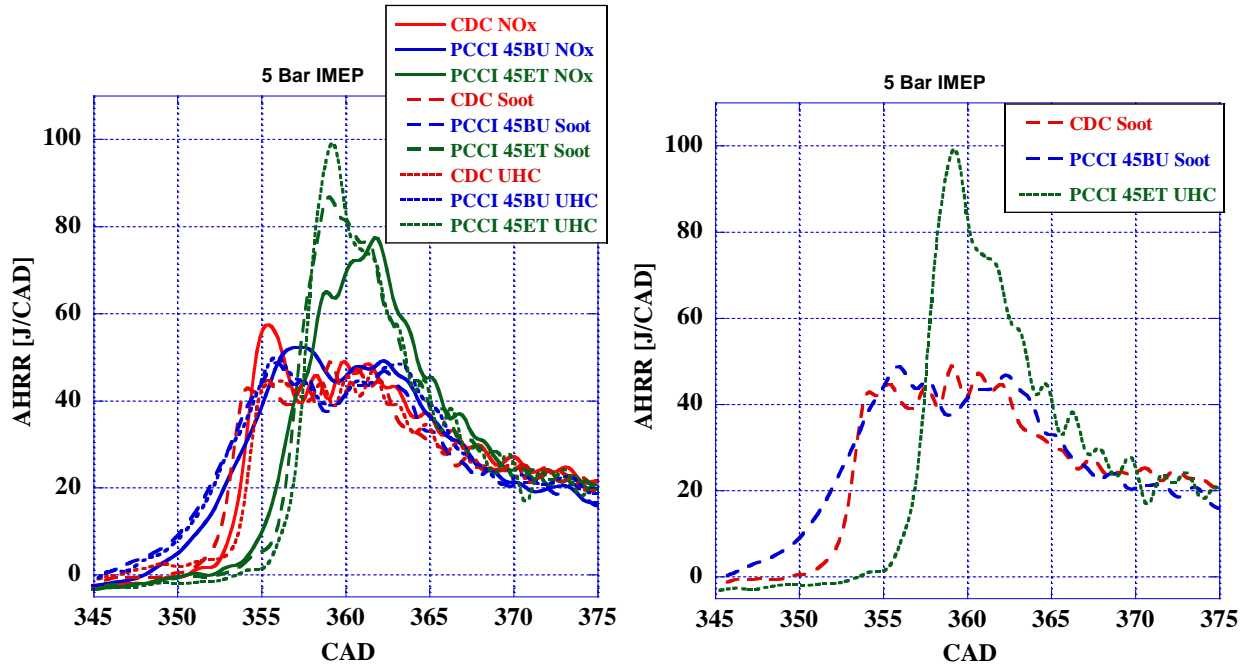


Figure 54: AHRR for Combustion Tests Conducted at 5 Bar IMEP

It was further observed for the 3 optimal combustion tests conducted (CDC Soot, PCCI 45BU Soot, and PCCI 45ET UHC) that CDC and PCCI with n-butanol had similar AHRR with no distinguished peaks but rather a relatively flat AHRR. Although PCCI with n-butanol only had a -0.4% difference in peak AHRR when compared to CDC, PCCI with ethanol had 103% increase in peak AHRR compared to CDC. In addition, PCCI with n-butanol exhibited auto-ignition prior to SOI-2 timing of 6° BTDC. With this observation and the other made at lower loads, it is abundantly clear that despite the lower reactivity of ethanol, PCCI with ethanol's combustion characteristics is predominantly governed by its higher oxygen content. As a result, the higher oxygen content increases the intensity of combustion and therefore increases peak AHRR and simultaneously reduces the duration of AHRR.

#### Mass Fraction Burned

The MFB was calculated from the integration of the AHRR at the start of HTHR, the UHC and CO emissions were also used for calculating the maximum combustion efficiency per combustion event. For this study, an indicated CA50 of 5° BTDC (from the AVL Indicomp) was utilized for determining the appropriate injection timing for maintaining the same combustion

phasing between tests. However, due to the variability of the combustion events on a per cycle basis, and the shortened time frame in which tests could be conducted due to hardware constraints, the measured CA50 was determined to be at an average of  $9^\circ$  ATDC with a tolerance of  $\pm 2$  CAD.

However due to the quantity of data available and the subpar combustion performance of the tests conducted at 4 and 5 bar IMEP, an in-depth analysis was only conducted for the 3 optimal points at 5 bar IMEP. With this in mind, the MFB of the optimal test points conducted at a load of 5 bar IMEP were analyzed in detail as to ascertain the combustion performance of each point. It was seen in Figure 55 that CDC had the latest CA50 of the three tests conducted although having the earliest injection timing of the 3. It was also noted that combustion for PCCI with ethanol appeared to occur at a slower rate than all of the other optimal points prior to CA10. However, once this threshold is breached PCCI with ethanol has a greater mass fraction consumption rate till approximately 70% of the fuel mass is consumed. This phenomenon is supported by the observations made in AHRR and the PRR where prior to this critical juncture, ethanol's lower reactivity prevents any LTHR from occurring. However, once the oxygen within the ethanol is separated at a sufficient quantity, HTHR occurs at a rapid rate due to the oxygenated air-fuel mixture.

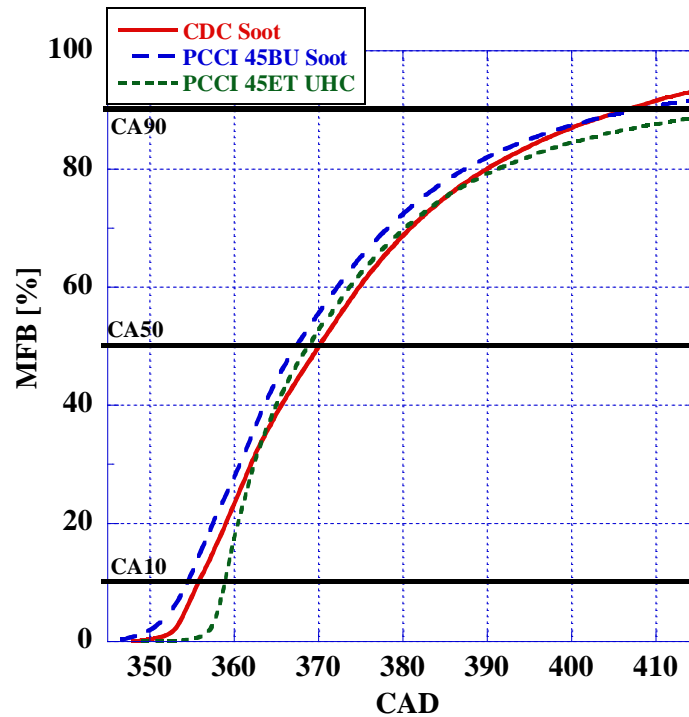


Figure 55: MFB of Optimal Points at 5 Bar IMEP

As mentioned previously, the in-depth analysis of the MFB was only done on the optimal points conducted at 5 bar IMEP as PCCI with either ethanol or n-butanol was found to have a combustion efficiency lower than 90% despite the additional boost provided over CDC. This data can be observed in the Annex section where various properties including the combustion efficiency of the other tests conducted can be observed. With this in mind, as seen in Table 17, the maximum MFB (Combustion Efficiency) observed was between 89.8% (PCCI 45ET UHC) and 94.8% (CDC Soot) at a load of 5 bar IMEP. This indicates that in order to achieve greater maximum MFB, higher loads should be considered for PCCI, although lower loads may be able to sustain greater maximum MFB with either greater combustion ratios or greater boost pressures.

Nevertheless, for the optimal points conducted it was observed that CDC soot and PCCI 45ET UHC had the same ID while PCCI 45BU Soot had an ID of 0 CAD. As indicated from the AHRR, PCCI with n-butanol was found to have auto-ignition occur prior to SOI-2 injection occurring, thus the ID was calculated to be 0 CAD as CA10 was obtained shortly after the DI event. This characteristic of PCCI with n-butanol was observed as well at a load of 4 bar IMEP, indicating that n-butanol is more susceptible to auto-ignition than PCCI with ethanol as load is increased. This however can be mitigated with either greater EGR% or the elimination or reduction of the pilot injection done at 60° BTDC.

Table 17: ID and CD for Optimal Points at 5 Bar IMEP

Combustion Test	CA10 [CAD]	CA50 [CAD]	CA90 [CAD]	ID [CAD]	CD [CAD]	MAX MFB [%]
CDC Soot	4 °BTDC	10 °ATDC	46 °ATDC	8 °	50 °	94.8
PCCI 45BU Soot	6 °BTDC	7 °ATDC	48 °ATDC	0 °	54 °	92.2
PCCI 45ET UHC	1 °BTDC	9 °ATDC	NA	8 °	NA	89.8

### Heat Flux and Heat Losses

Due to the fundamental change in combustion characteristics of LTC methods in comparison to CDC, an investigation on the heat flux and associated heat losses was conducted. Due to the quantity of tests conducted in this study, only 3 points were selected for an in-depth analysis and were selected due to their high combustion efficiency. The heat flux and heat losses were calculated utilizing Equation 12 and Equation 13 based off a study by (Borman and Nishiwaki 1987). In addition, modifications were made to the model in order to best encapsulate the properties/characteristics of the experimental engine as seen previously by (Soloiu, Moncada, Gaubert, Muiños, et al. 2018). The model used is able to recognize the heat transfers associated with the convection of gasses within the combustion chamber and the radiative heat of both particulate matter and diffusion combustion. In Equation 12 the overall heat flux ( $\dot{q}$ ) was determined utilizing the wall temperature ( $T_w$ ) (assumed to be an average temperature), the combustion temperatures ( $T_A$ ), and the air thermal conductivity ( $\lambda_A$ ). The viscosity of the combustion chamber air was obtained using the Southerland model ( $\mu$ ), the results of which were used for calculating the Reynolds number in Equation 13.

$$\dot{q}(\alpha) = A \frac{\lambda_A(\alpha)}{D} Re^{0.7} (T_A(\alpha) - T_w) + \sigma * \varepsilon (T_A^4(\alpha) - T_w^4) \quad \text{Equation 12}$$

$$Re(\alpha) = \rho(\alpha) \frac{S * N * D}{30\mu(\alpha)} \quad \text{Equation 13}$$

It was seen in Figure 56 that PCCI 45BU Soot had the highest total heat flux of the 3 optimal combustion test points conducted at 5 bar IMEP. While PCCI 45ET UHC had the lowest total heat fluxes by a significant magnitude. It was shown that CDC and PCCI with n-butanol had similar heat losses with the discrepancies lying after TDC where convection and radiation losses after 10° ATDC begin to diverge from one another with CDC being greatest. This indicates that the intensity of the combustion for PCCI 45BU Soot is greater than CDC Soot as a result of both a diffusion and premixed flame occurring simultaneously and thus consuming greater fuel mass earlier than CDC as was indicated with the MFB section. However, this led to a slight decrease in combustion efficiency as the quenched areas of the flames may have been greater due to less exposure time from the premixed flame that had propagated from the auto-ignition of n-butanol. This was indicated from the increase in convection losses of PCCI with n-butanol between 365

CAD and 370 CAD from CDC. However, the heat fluxes from PCCI 45ET UHC are noteworthy, as they are a direct result of the diminished duration of AHRR and the sharp rise of AHRR seen previously. This indicates that although combustion efficiency for PCCI with ethanol was lower, heat losses are diminished as a result of the rapid combustion and the location of this combustion occurring close to TDC thus reducing the surface area available for heat loss to occur. Although in regard to PCCI 45ET, the lower radiation heat flux could be as a result of lower soot formation.

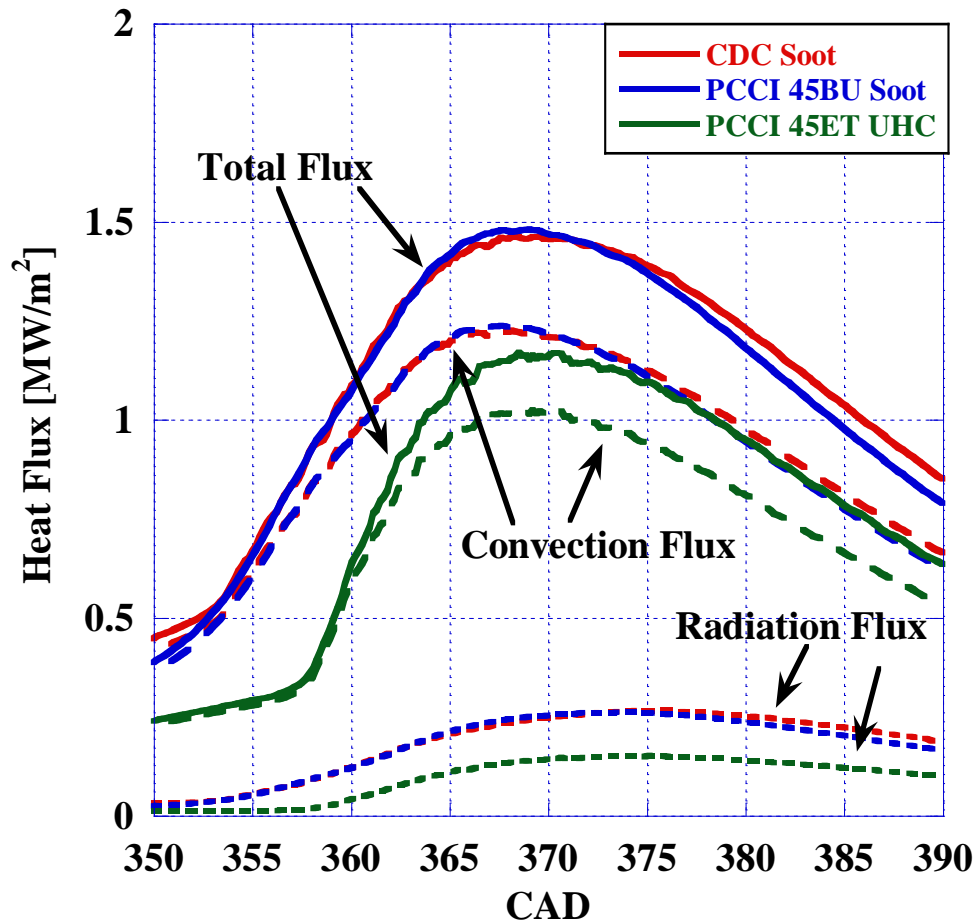


Figure 56: Heat Flux of Optimal Points at 5 Bar IMEP

In Figure 57 and Table 18, the heat losses for each optimal combustion test conducted at 5 bar IMEP can be observed, it was seen that CDC had the greatest heat losses of the three tests conducted. This was a result of the greater heat flux durations observed in Figure 56 in comparison to the other 2 tests, however PCCI with n-butanol had similar heat losses as CDC. As a result,

PCCI 45BU Soot had a negligible difference of heat losses from CDC at 0.39% less radiation loss, 0.01% less convection loss, and 0.04% less crevice loss than CDC.

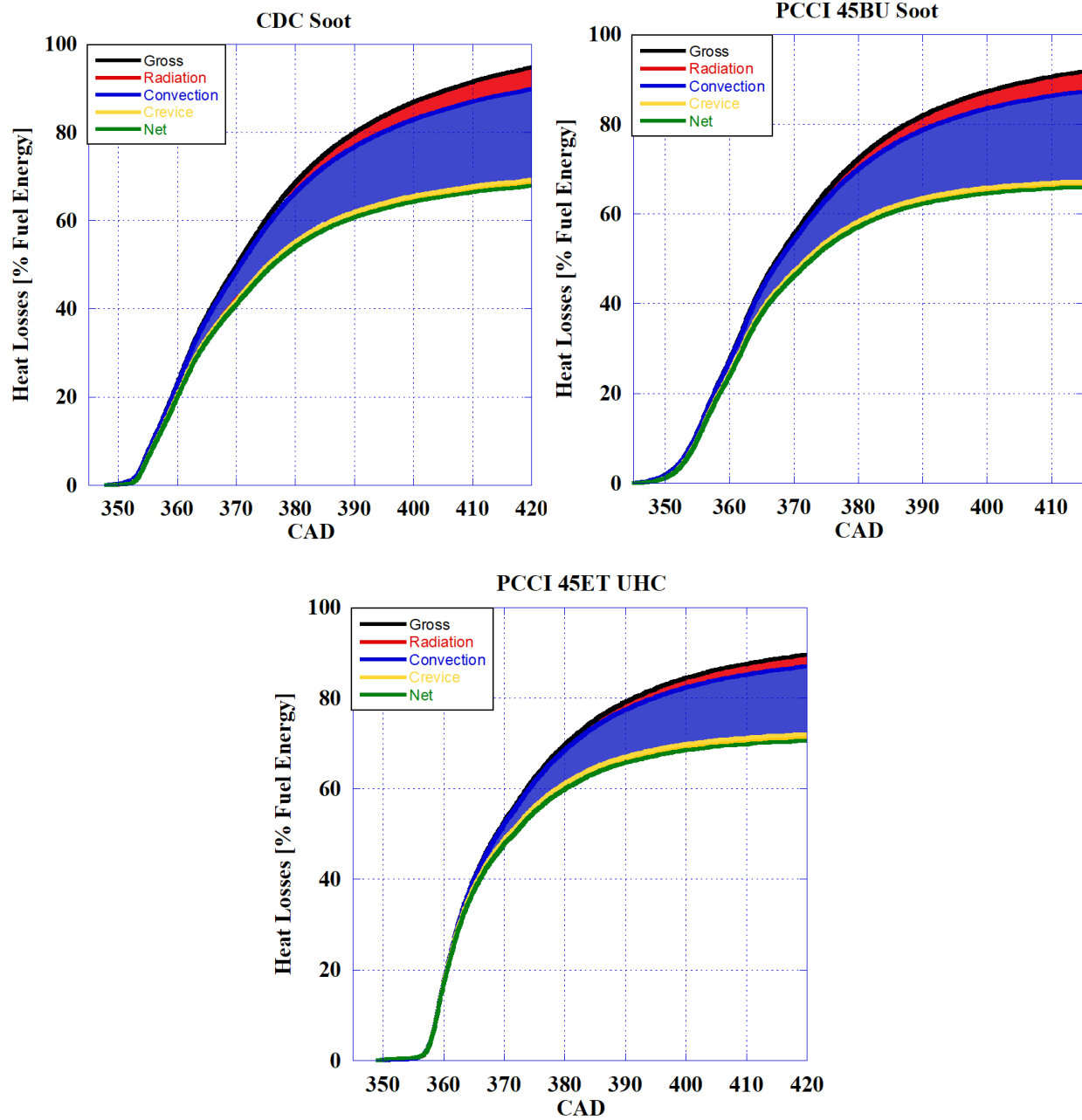


Figure 57: Heat Losses of Optimal Points at 5 Bar IMEP

PCCI with ethanol on the other hand had a greater reduction of losses from CDC partially due to its lower combustion efficiency and from its lower heat fluxes. It was observed that PCCI



45ET UHC had, 2.31% less radiation loss, 3.21% less convection loss, and an increase of 0.05% crevice loss from CDC. This is a result of the greater magnitude of the AHRR of PCCI with ethanol and its occurrence closer to TDC therefore minimizing the heat lost to the surrounding engine components.

Table 18: Percent Losses of Optimal Points at 5 Bar IMEP

Test Name	Radiation Loss [%]	Convection Loss [%]	Crevice Loss [%]
CDC Soot	4.94	17.10	1.36
PCCI 45BU Soot	4.55	17.09	1.32
PCCI 45ET UHC	2.63	13.89	1.41

### Emissions Analysis

An emissions analysis was conducted on the 28 combustion tests conducted over a span of loads ranging from 3 bar IMEP to 5 bar IMEP utilizing an AVL SESAM FTIR V4 for the gaseous species and an AVL Microsoot 483 for the soot Emissions. For each one of the emissions analyses, a table was created detailing the optimal combustion tests conducted per load emissions and their comparison to CDC.

### Nitrogen Oxide Emissions

The NO<sub>x</sub> emissions for each of the 28 combustion tests conducted are shown in Figure 58, each tests NO<sub>x</sub> emissions were measured with an AVL SESAM FTIR V4 at an accuracy of  $\pm 2.0\%$  for the appropriate PPM range. It was observed that most PCCI tests had lower NO<sub>x</sub> emissions than CDC with most exemptions occurring at a load of 3 bar IMEP or PCCI with ethanol. It was generally observed that on average PCCI with n-butanol had a 4.52% reduction of NO<sub>x</sub> emissions in comparison to CDC while PCCI with ethanol was observed to have an average 5.07% increase in NO<sub>x</sub> emissions at 3 bar IMEP. This reiterates the observation made previously that the oxygen content of ethanol more heavily governs the intensity of AHRR and the subsequent NO<sub>x</sub> emissions than the reactivity of the fuel in PCCI combustion. For the tests conducted at 4 and 5 bar IMEP, on average the NO<sub>x</sub> emissions were lowered for PCCI combustion with either fuel in comparison to CDC. The reduction of NO<sub>x</sub> emissions at 4 bar IMEP ranged from 7.45% (PCCI with ethanol)

to 30.63% (PCCI with n-butanol) and at 5 bar IMEP the reduction ranged from 15.18% (PCCI with ethanol) to 50.07% (PCCI with n-butanol).

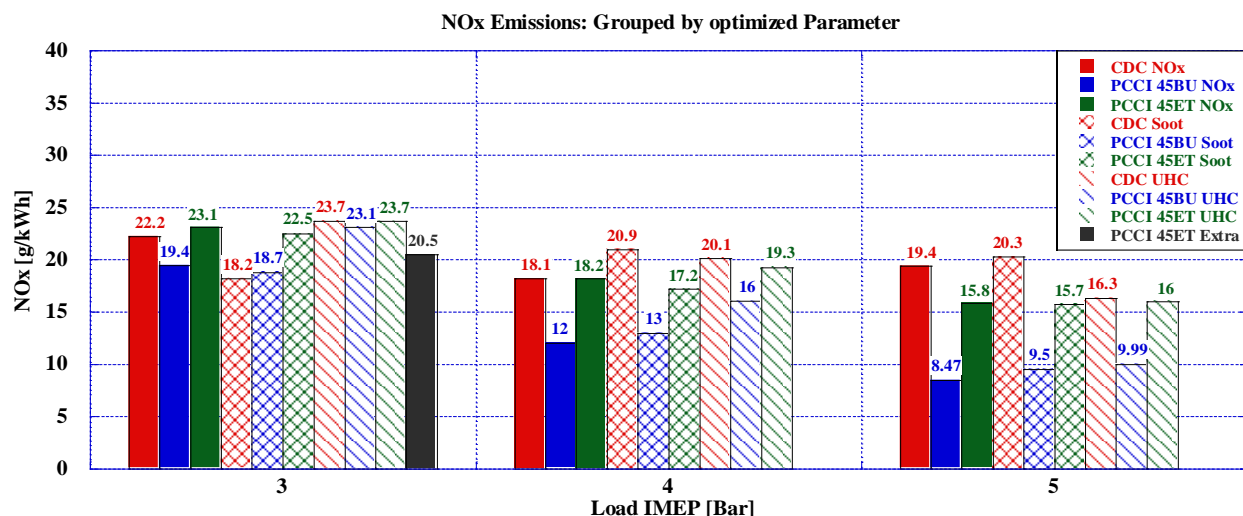


Figure 58: NO<sub>x</sub> Emissions of All Combustion Tests Conducted

The NO<sub>x</sub> emissions of the optimal combustion tests conducted per load can be seen in Table 19. It was observed, the NO<sub>x</sub> emissions for PCCI with either ethanol or n-butanol were reduced at loads 4 and 5 bar IMEP while increasing at a load of 3 bar IMEP in comparison to CDC. This discrepancy is due to the increase in peak AHRR observed at 3 bar IMEP despite CDC having higher in-cylinder temperatures than PCCI with ethanol. As for the PCCI tests conducted at 4 bar IMEP, the NO<sub>x</sub> emissions were lowered by 14.4% for PCCI with ethanol and 35.3% for PCCI with n-butanol in comparison to CDC. At 5 bar IMEP further reductions were seen with PCCI with ethanol having a 21.2% reduction while PCCI with n-butanol had a reduction of 53.2% in comparison to CDC.

Table 19: NO<sub>x</sub> Emissions of Optimal Points

Combustion Test	NO <sub>x</sub> @ 3 Bar IMEP	NO <sub>x</sub> @ 4 Bar IMEP	NO <sub>x</sub> @ 5 Bar IMEP
CDC	18.2	20.1	20.3
PCCI 45BU	19.4	13.0	9.5
PCCI 45ET	20.5	17.2	16.0
Combustion Test	Δ% from CDC @ 3 Bar IMEP	Δ% from CDC @ 4 Bar IMEP	Δ% from CDC @ 5 Bar IMEP
PCCI 45BU	6.6%	-35.3%	-53.2%
PCCI 45ET	12.6%	-14.4%	-21.2%

With this in mind, it was seen from this study that PCCI should be utilized for loads greater than 3 bar IMEP in order to facilitate the reduction of NO<sub>x</sub> emissions without the usage of aftertreatment systems.

#### Soot Emissions

The soot emissions were measured utilizing an AVL Microsoot 483 system for each one of the 28 combustion tests conducted. In Figure 59 it can be seen that the usage of oxygenated fuels in PCCI combustion reduces the soot emitted in comparison to CDC with greatest reductions occurring at the higher loads. It was seen that at a load of 3 bar IMEP, PCCI with n-butanol had a 34.94% reduction of soot emissions while PCCI with ethanol had a 53.01% decrease in comparison to CDC. The trend of PCCI with ethanol having greater reductions of soot emissions than PCCI with n-butanol was further exemplified at loads of 4 and 5 bar IMEP. It was observed that at a load of 4 bar IMEP, PCCI 45BU and PCCI 45ET reduced soot emissions by 42.35% and 71.76% respectively while at 5 bar IMEP reductions of 32.82% and 75.57 of soot emissions were observed respectively.

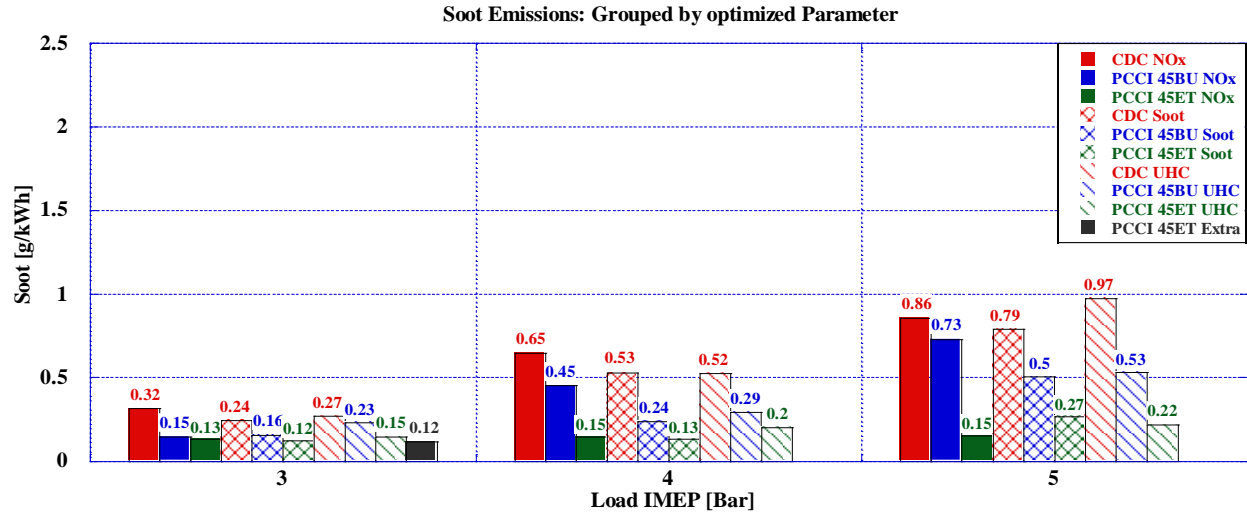


Figure 59: Soot Emissions of All the Combustion Tests Conducted

For the optimal combustion tests conducted through the loads of 3-5 bar IMEP, the soot emissions as well as the reduction seen between PCCI, and CDC are shown in Table 20. It was seen that throughout the load range PCCI with ethanol had greater reductions of soot emissions than PCCI with n-butanol spanning a range of -55.5% reduction (at 3 bar IMEP) and 75.0% reduction from CDC (at 4 bar IMEP). While PCCI with n-butanol did achieve soot emissions reductions ranging from 53.8% (at 4 bar IMEP) to 36.7% (at 5 bar IMEP), PCCI with ethanol was proven to be the fuel of choice for targeting soot emissions. This is attributed to the higher oxygen content of ethanol reducing the soot formation occurring at the diffusion combustion of the DI plume.

Table 20: Soot Emissions of Optimal Points

Combustion Test	Soot @ 3 Bar IMEP	Soot @ 4 Bar IMEP	Soot @ 5 Bar IMEP
CDC	0.27	0.52	0.79
PCCI 45BU	0.15	0.24	0.5
PCCI 45ET	0.12	0.13	0.22
Combustion Test	$\Delta\%$ from CDC @ 3 Bar IMEP	$\Delta\%$ from CDC @ 4 Bar IMEP	$\Delta\%$ from CDC @ 5 Bar IMEP
PCCI 45BU	-44.4%	-53.8%	-36.7%
PCCI 45ET	-55.5%	-75.0%	-72.2%

### Unburnt Hydrocarbon Emissions

The UHC emissions of LTC methods is often an area of great interest as typically LTC methods such as PCCI struggle with reducing the quantity of UHC. As is the case, Figure 60 contains the UHC emissions from each of the 28 combustion tests conducted in this study. It was noted that, UHC were greater for all PCCI tests conducted regardless of the PFI fuel used with the magnitude of this increase diminishing as load increases. Generally, it was observed that PCCI with ethanol had greater UHC emissions than PCCI with n-butanol despite the usage of greater boost pressures.

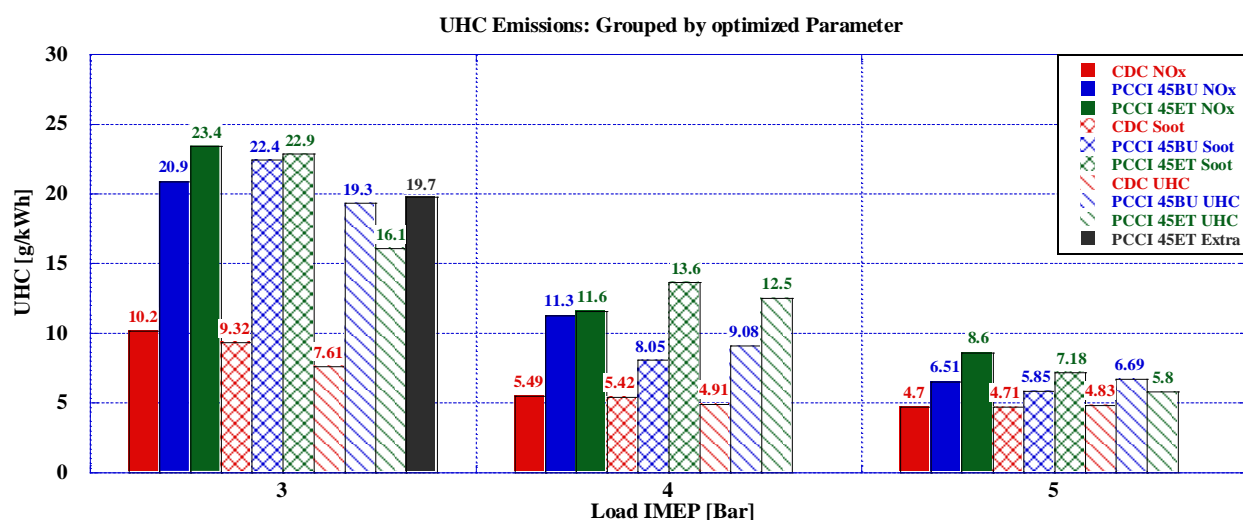


Figure 60: UHC Emissions of All the Combustion Tests Conducted

As seen in Table 21, the UHC emissions of PCCI were subpar at loads of 3 and 4 bar IMEP due to insufficient combustion chamber pressures/temperatures necessary for a more complete combustion process. As a result, UHC emissions remained elevated in comparison to CDC thought the load range with only a minimum increase of 23.1% observed at 5 bar IMEP for PCCI 45ET. This indicates for the usage of PCCI at lower loads either a substantial increase in boost must be utilized or be implanted in an engine with a greater compression ratio.

Table 21: UHC Emissions of Optimal Points

Combustion Test	UHC @ 3 Bar IMEP	UHC @ 4 Bar IMEP	UHC @ 5 Bar IMEP
CDC	9.32	4.91	4.71
PCCI 45BU	20.9	8.05	5.85
PCCI 45ET	19.7	13.6	5.8
Combustion Test	$\Delta\%$ from CDC @ 3 Bar IMEP	$\Delta\%$ from CDC @ 4 Bar IMEP	$\Delta\%$ from CDC @ 5 Bar IMEP
PCCI 45BU	124.2%	63.9%	24.2%
PCCI 45ET	111.4%	176.9%	23.1%

### Carbon Monoxide Emissions

The CO emissions for all the 28 combustion tests conducted over the loads 3, 4, and 5 bar IMEP are shown in Figure 61 where it was seen that CO emissions for PCCI combustion with either fuel had higher CO emissions than CDC. In addition, CO emissions were shown to be higher for PCCI with n-butanol in comparison to PCCI with ethanol for most tests at 3 and 4 bar with the opposite being true at 5 bar IMEP.

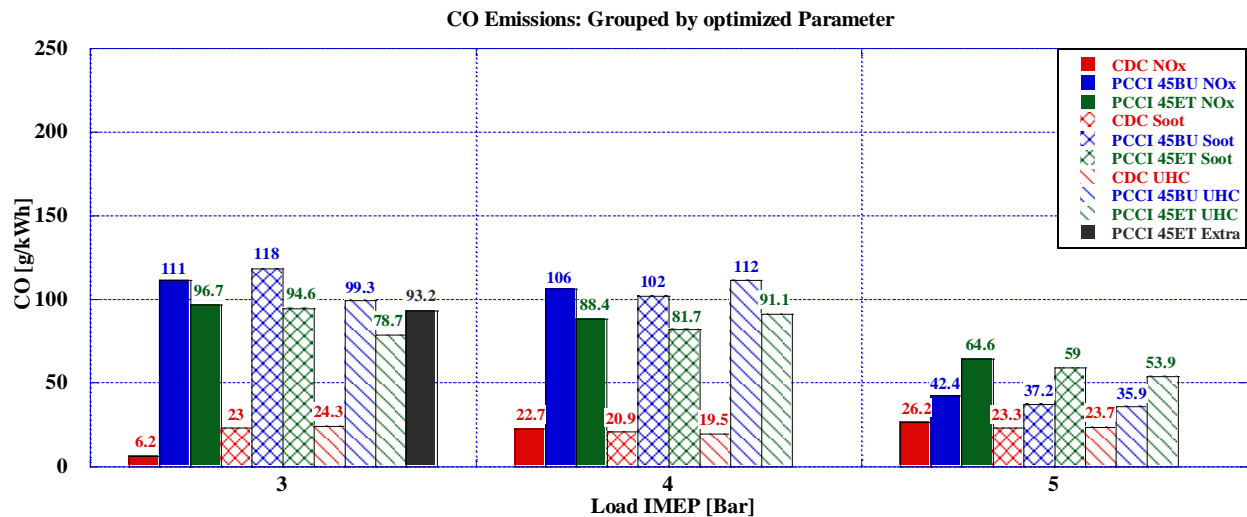


Figure 61: CO Emissions of All the Combustion Tests Conducted

The optimal combustion points for each load are shown in Table 22, where the same trend was observed that PCCI with n-butanol had greater CO emissions at 3 and 4 bar IMEP while PCCI with ethanol had lower CO emissions at 5 bar IMEP. As is the case, the minimum increase in CO emissions was seen at 5 bar IMEP for PCCI 45BU with 59.7% in comparison to CDC.

Table 22: CO Emissions of Optimal Points

Combustion Test	CO @ 3 Bar IMEP	CO @ 4 Bar IMEP	CO @ 5 Bar IMEP
CDC	23.0	19.5	23.3
PCCI 45BU	111	102	37.2
PCCI 45ET	93.2	81.7	53.9
Combustion Test	$\Delta\%$ from CDC @ 3 Bar IMEP	$\Delta\%$ from CDC @ 4 Bar IMEP	$\Delta\%$ from CDC @ 5 Bar IMEP
PCCI 45BU	382%	423%	59.7%
PCCI 45ET	305%	319%	131%

#### Formaldehyde and Aldehyde Emissions

Formaldehyde and aldehyde emissions although unregulated by most emissions standards, is often reported on for alternate combustion techniques that utilize biofuels. The formaldehyde emissions for the 28 combustion tests conducted over 3-5 bar IMEP are shown in Figure 62, in addition to this the optimal combustion tests per load are shown in Table 23. It was observed that formaldehyde emissions for PCCI with ethanol were higher than PCCI with n-butanol at loads of 4 and 5 bar IMEP. However, at 3 bar IMEP, the formaldehyde emissions were nearly the same for both PCCI techniques. As for the 3 optimal combustion tests per load seen in Table 23, the lowest increase in formaldehyde emissions was 46.3% greater than CDC for PCCI 45BU at a load of 5 bar IMEP.

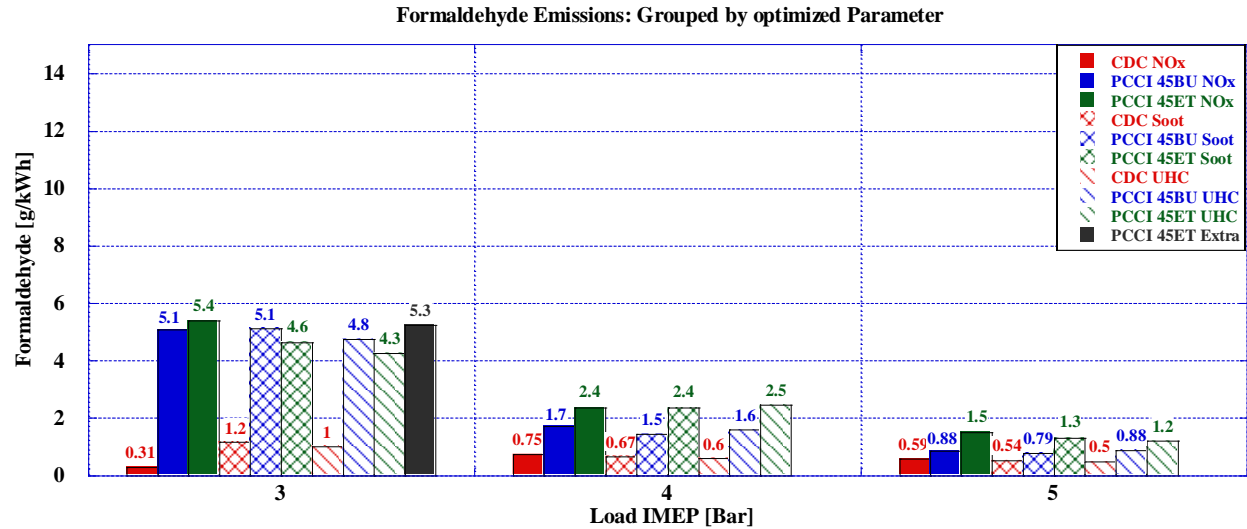


Figure 62: Formaldehyde Emissions of All the Combustion Tests Conducted

Table 23: Formaldehyde Emissions of Optimal Points

Combustion Test	Formaldehyde @ 3 Bar IMEP	Formaldehyde @ 4 Bar IMEP	Formaldehyde @ 5 Bar IMEP
CDC	1.2	0.6	0.54
PCCI 45BU	5.1	1.5	0.79
PCCI 45ET	5.3	2.4	1.2
Combustion Test	$\Delta\%$ from CDC @ 3 Bar IMEP	$\Delta\%$ from CDC @ 4 Bar IMEP	$\Delta\%$ from CDC @ 5 Bar IMEP
PCCI 45BU	325%	150%	46.3%
PCCI 45ET	342%	300%	122%

A similar trend was observed for aldehyde emissions in Figure 63 and Table 24 where PCCI had considerably higher aldehyde emissions than CDC at each load. Although it was noted that as load increased, aldehyde emissions decreased at a considerable rate for all PCCI tests. As seen in Table 24, the lowest increase in aldehyde emissions was observed at 5 bar IMEP for PCCI 45BU at 238% in comparison to CDC.



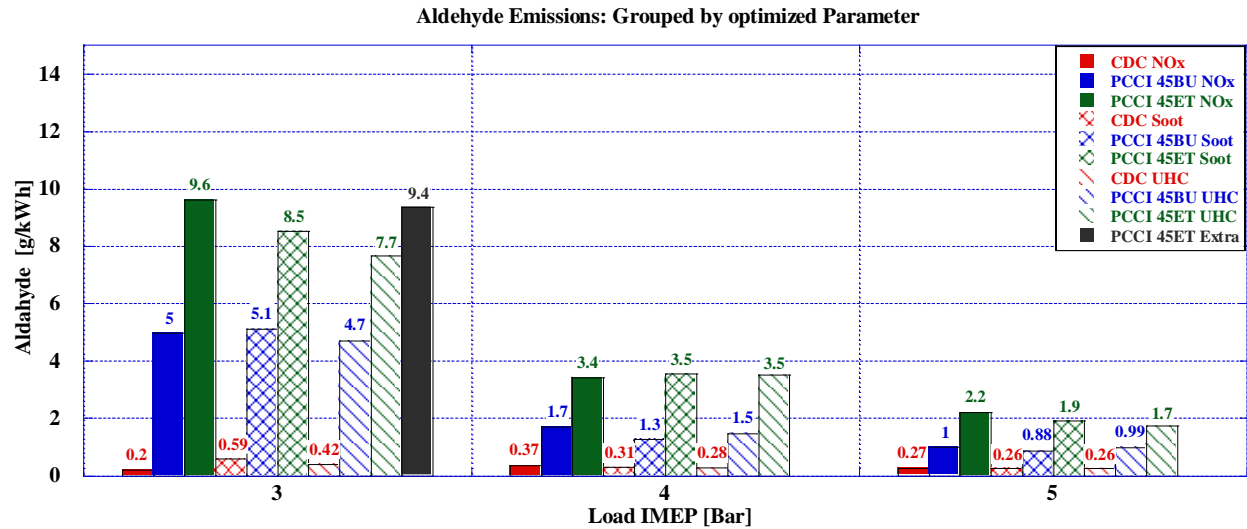


Figure 63: Aldehyde Emissions of All the Combustion Tests Conducted

Table 24: Aldehyde Emissions of Optimal Points

Combustion Test	Aldehyde @ 3 Bar IMEP	Aldehyde @ 4 Bar IMEP	Aldehyde @ 5 Bar IMEP
CDC	0.59	0.28	0.26
PCCI 45BU	5.0	1.3	0.88
PCCI 45ET	9.4	3.5	1.7
Combustion Test	$\Delta\%$ from CDC @ 3 Bar IMEP	$\Delta\%$ from CDC @ 4 Bar IMEP	$\Delta\%$ from CDC @ 5 Bar IMEP
PCCI 45BU	747%	364%	238%
PCCI 45ET	1493%	1150%	554%

### Carbon Dioxide Emissions and Carbon Environmental Impact Index

The CO<sub>2</sub> emissions for each one of the combustion tests conducted in this study are shown in Figure 64 where it was observed that at 3 and 4 bar IMEP CO<sub>2</sub> emissions were lowered by an average of 4.17% (PCCI 45BU) to 12.42% (PCCI 45ET) at 3 bar and 5.25% (PCCI 45BU) to 5.84% (PCCI 45ET) respectively. Although at 5 bar IMEP CO<sub>2</sub> emissions were raised by 9.30% (PCCI 45BU) to 10.71% (PCCI 45ET), the overall environmental impact is not equivalent with

CDC due to the usage of renewable fuel sources which will be discussed in further detail in a later section.

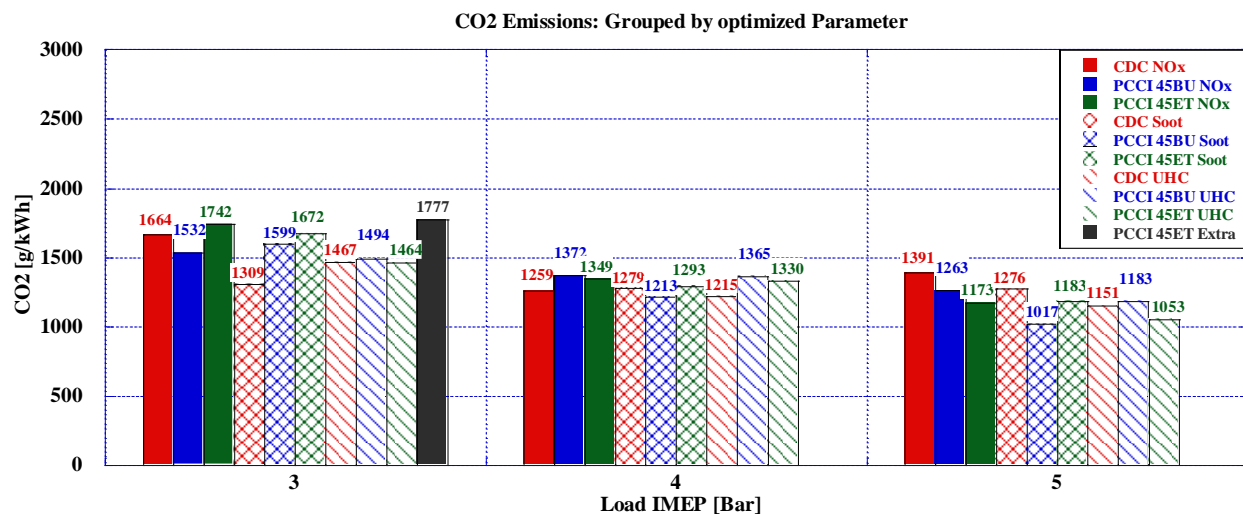


Figure 64: CO<sub>2</sub> Emissions of All the Combustion Tests Conducted

It was observed however that for the optimal combustion points seen in Table 25, the greatest reductions to CO<sub>2</sub> emissions occurred at 5 bar IMEP by as much as 20.3% for PCCI 45BU in comparison to CDC. This indicates that at higher loads for the points that are optimal for NO<sub>x</sub>, soot, and combustion efficiency CO<sub>2</sub> emissions are lowered considerably than at other loads. However as previously stated, the CO<sub>2</sub> emissions for PCCI with either n-butanol or ethanol cannot be equivocally compared as 45% of the fuel mass is derived from renewable sources.

Table 25: CO<sub>2</sub> Emissions of All the Optimal Combustion Tests Conducted

Combustion Test	CO <sub>2</sub> @ 3 Bar IMEP	CO <sub>2</sub> @ 4 Bar IMEP	CO <sub>2</sub> @ 5 Bar IMEP
CDC	1309	1215	1276
PCCI 45BU	1532	1213	1017
PCCI 45ET	1777	1293	1053
Combustion Test	Δ% from CDC @ 3 Bar IMEP	Δ% from CDC @ 4 Bar IMEP	Δ% from CDC @ 5 Bar IMEP
PCCI 45BU	17.0%	-0.16%	-20.3%
PCCI 45ET	35.8%	6.42%	-17.5%

As seen in Table 26, a comparison was made of the non-renewable carbon reduction of PCCI combustion to CDC and the quantity of moles per hour of non-renewable carbon emitted per hour. This Renewable Carbon Index was created in order to best compare the environmental impact of each biofuel utilized in PCCI combustion in comparison to CDC. A consideration was made of the difference between first generation biofuels (ethanol) and second-generation biofuels (n-butanol) sustainability within the Renewable Carbon Index (RCI). As seen in Equation 14, the RCI was calculated based off the moles of carbon per hour of CDC ( $M_{CDC}$ ), the moles of non-renewable carbon of the biofuel combustion test per hour ( $M_{Bio}$ ), and the constant associated with the biofuel generation utilized ( $S_{gen}$ ). The constant  $S_{gen}$  was defined as 1 for non-renewable fuel, 0.9 for first generation biofuel, 0.75 for second generation biofuel, and 0.5 for third generation biofuels. As a result, an RCI of 10 signifies a comparable carbon footprint to CDC while any number lower this signifies a reduction of the carbon footprint.

$$N_{RCI} = \left( \frac{(M_{Bio} * S_{gen})}{M_{CDC}} \right) * 10 \quad \text{Equation 14}$$

It was observed in Table 26 that at a load of 3 bar IMEP, PCCI 45BU had 58% non-renewable carbon reduction in comparison to CDC while PCCI 45ET had a 65% reduction on non-renewable carbon. The same reductions were observed at 4 bar IMEP although at 5 bar IMEP the reductions slightly changed to 59% reduction for PCCI 45BU and 64% for PCCI 45ET. This slight change in carbon reduction can be attributed to the higher combustion efficiency observed at 5 bar

IMEP resulting in less fuel mass needed for power production. In terms of the RCI of the optimal combustion tests, the range of the RCI varied from 4.11 at 3 bar IMEP to 4.47 at 5 bar IMEP for PCCI 45BU. It was also observed that the RCI for PCCI 45ET ranged from 5.15 at 3 bar IMEP to 5.8 at 5 bar IMEP. This implies that as load is increased for each PCCI combustion test the RCI increases due to an overall increase in fuel needed to sustain power needs. However, each combustion test was considerably lower than CDC with PCCI 45BU having the lowest RCI due to the second-generation bio alcohol n-butanol having an overall lower environmental impact than first generation bio alcohol ethanol.

Table 26: Renewable Carbon Index of All the Optimal Combustion Tests Conducted

	Non-Renewable Carbon Reduction		
Combustion Test	3 Bar IMEP	4 Bar IMEP	5 Bar IMEP
PCCI 45BU	58%	58%	59%
PCCI 45ET	65%	65%	64%
Combustion Test	Moles of Non-Renewable Carbon per hour @ 3 Bar IMEP	Moles of Non-Renewable Carbon per hour @ 4 Bar IMEP	Moles of Non-Renewable Carbon per hour @ 5 Bar IMEP
CDC	3.27	4.20	4.90
PCCI 45BU	1.79	2.38	2.92
PCCI 45ET	1.87	2.66	3.16
Combustion Test	Carbon Index at 3 Bar IMEP	Carbon Index at 4 Bar IMEP	Carbon Index at 5 Bar IMEP
PCCI 45BU	4.11	4.25	4.47
PCCI 45ET	5.15	5.7	5.80

### Fuel Consumption and Efficiency

#### Energy Specific and Brake Specific Fuel Consumption

The ESFC and BSFC was collected for each one of the 28 combustion tests conducted in this study in order to gauge the performance of PCCI of either biofuel in comparison to CDC. In

Figure 65, the ESFC was shown for the 28 tests conducted over 3,4, and 5 bar IMEP. It was shown that the average ESFC was similar between all the tests falling within a range of 4.61% of one another. PCCI with ethanol however was shown to have a slight decrease in ESFC in comparison to CDC for each load while PCCI with n-butanol having a slight increase at 3 bar IMEP and slight decrease at 4 and 5 bar IMEP. This is a direct result of the lower calorific content of the PFI fuels than ULSD#2.

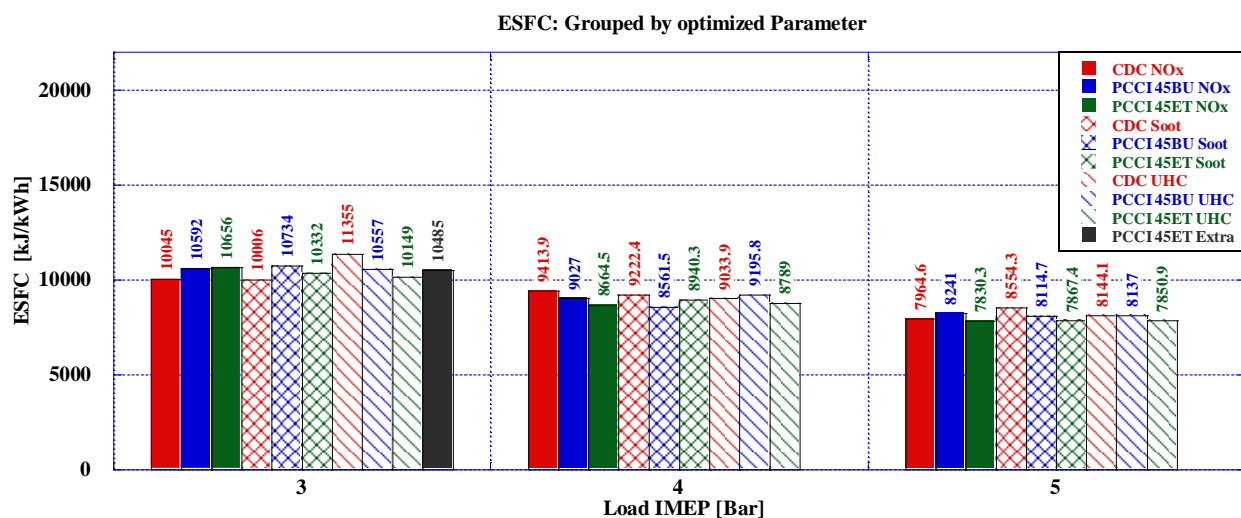


Figure 65: ESFC of All the Combustion Tests Conducted

For the optimal points conducted, the ESFC was shown in Table 27 where it was observed that at a load of 4 and 5 bar IMEP PCCI had less ESFC than CDC while having a greater ESFC at 3 bar IMEP. As the load was increased from 4 to 5 bar IMEP, PCCI 45ET was shown to have a greater reduction of ESFC from 1.04% to 8.22% from CDC while PCCI 45BU was stable at 5% reduction from CDC with only a 0.09% variation between tests.

Table 27: ESFC of Optimal Points

Combustion Test	ESFC @ 3 Bar IMEP	ESFC @ 4 Bar IMEP	ESFC @ 5 Bar IMEP
CDC	10006	9033.9	8554.3
PCCI 45BU	10592	8561.5	8114.7
PCCI 45ET	10485	8940.3	7850.9
Combustion Test	$\Delta\%$ from CDC @ 3 Bar IMEP	$\Delta\%$ from CDC @ 4 Bar IMEP	$\Delta\%$ from CDC @ 5 Bar IMEP
PCCI 45BU	5.86%	-5.23%	-5.14%
PCCI 45ET	4.79%	-1.04%	-8.22%

As for the BSFC, it was seen in Figure 66 that on average the BSFC of PCCI with either fuel was greater than CDC for all loads spanning a range of 5.57% (PCCI 45BU at 4 bar IMEP) to 21.55% (PCCI 45ET at 3 bar IMEP). This was caused from the decreased energy density of the PFI fuels and the lower combustion efficiency of PCCI combustion, as a subsequent result BSFC increased for PCCI combustion with either fuel in comparison to CDC.

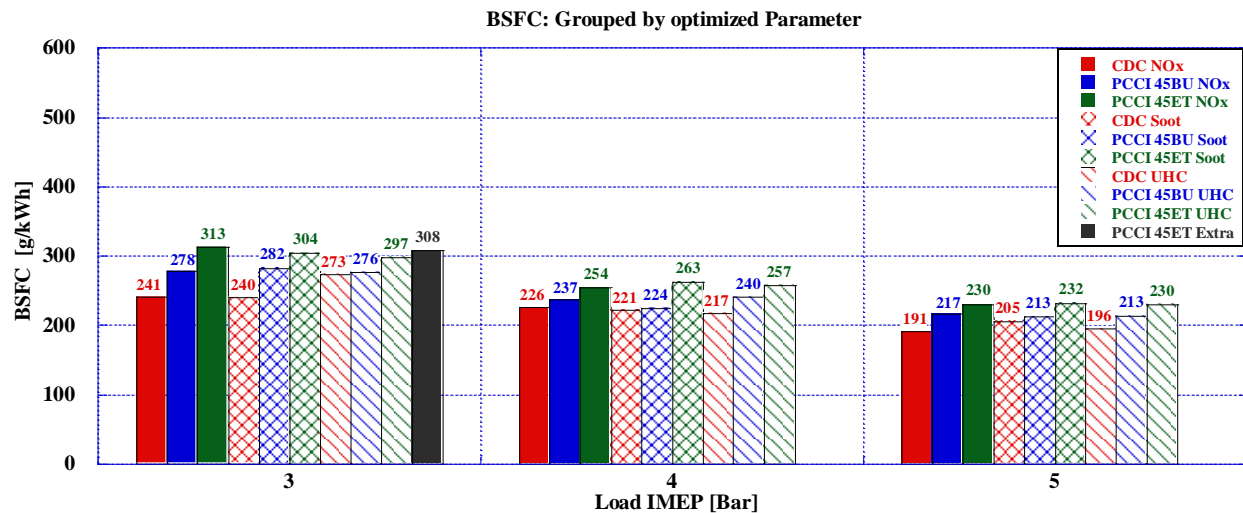


Figure 66: BSFC of All the Combustion Tests Conducted

The BSFC for the 3 optimal tests per load studied is shown in Table 28 where it was observed that PCCI 45BU had a lower increase in BSFC than PCCI 45ET at each load. It was seen

that as load increased BSFC was rise above CDC reduced from 28.3% to 12.2% for PCCI 45ET while PCCI 45BU went from 15.8% rise to 3.9%.

Table 28: BSFC of Optimal Points

Combustion Test	BSFC @ 3 Bar IMEP	BSFC @ 4 Bar IMEP	BSFC @ 5 Bar IMEP
CDC	240	217	205
PCCI 45BU	278	224	213
PCCI 45ET	308	263	230
Combustion Test	$\Delta\%$ from CDC @ 3 Bar IMEP	$\Delta\%$ from CDC @ 4 Bar IMEP	$\Delta\%$ from CDC @ 5 Bar IMEP
PCCI 45BU	15.8%	3.2%	3.9%
PCCI 45ET	28.3%	21.2%	12.2%

### Indicated Thermal Efficiency

The ITE of all the tests conducted in this study are shown in Figure 67, where it was seen that PCCI with either ethanol or n-butanol had greater thermal efficiency than CDC at each load. The ITE for each point was higher than usual due to the externally driven fuel pumps and supercharger used in the experimental CI engine. It was also observed that generally PCCI with ethanol had greater thermal efficiency than PCCI with n-butanol as this was caused by the shorter duration of intense AHRR and a subsequent decrease in heat losses.

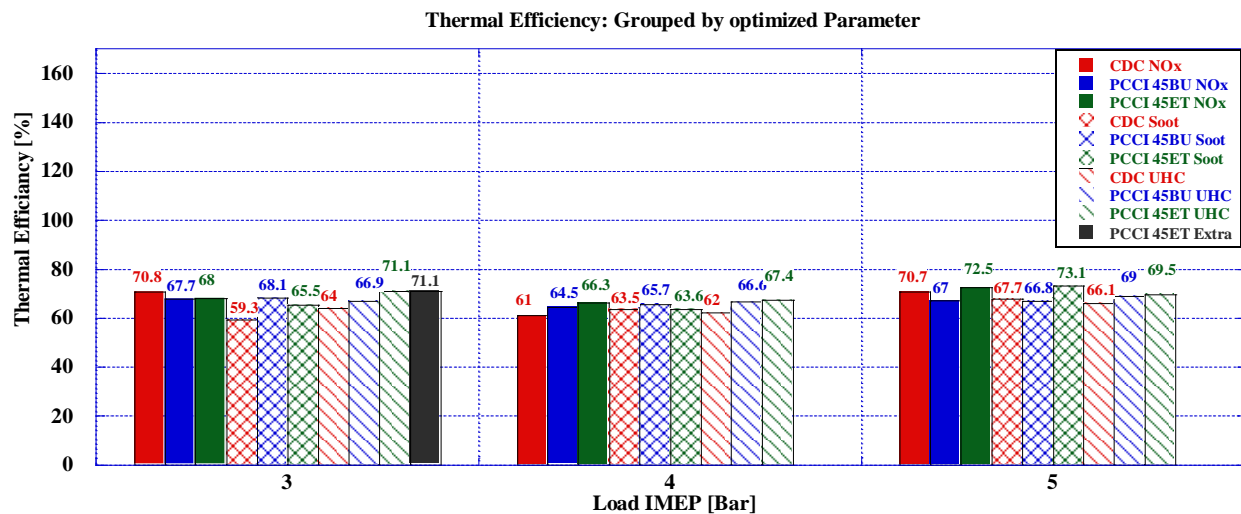


Figure 67: ITE of All the Combustion Tests Conducted

As for the optimal combustion tests points conducted per load, it was shown in Table 29 that the ITE for PCCI was greatest at lower loads in comparison to CDC with diminishing gains as load increased. PCCI with ethanol had the greatest ITE at loads of 3 and 5 bar in comparison to PCCI with n-butanol. This trend can be explained by the decrease in heat losses, increase in the usage of boost pressure

Table 29: ITE of Optimal Points

Combustion Test	Thermal Efficiency @ 3 Bar IMEP	Thermal Efficiency @ 4 Bar IMEP	Thermal Efficiency @ 5 Bar IMEP
CDC	59.3	62.0	67.7
PCCI 45BU	67.7	65.7	66.8
PCCI 45ET	71.1	63.6	69.5
Combustion Test	$\Delta\%$ from CDC @ 3 Bar IMEP	$\Delta\%$ from CDC @ 4 Bar IMEP	$\Delta\%$ from CDC @ 5 Bar IMEP
PCCI 45BU	14.2%	5.9%	-1.3%
PCCI 45ET	19.9%	2.6%	2.7%



## CHAPTER 5

### FINDINGS, CONCLUSION, AND RECOMMENDATIONS

#### Conclusions

An investigation was conducted on the optimal engine parameters for facilitating lower  $\text{NO}_x$  and soot emissions of PCCI with either ethanol or n-butanol as the PFI fuel of choice at loads of 3, 4, and 5 Bar IMEP. 28 total combustion tests were conducted over the span of loads with variations made to the EGR% and boost pressure for each test in order to find the optimal point for simultaneous emissions reduction.

The hypothesis for this research states: *With an optimal EGR and boost strategy, PCCI can obtain a  $\text{NO}_x$  and soot emissions reduction of at least 10% for 2 out of the 3 loads without the need of a non-neat ULSD#2 DI fuel.* The hypothesis was proven correct for PCCI tests conducted at 4 and 5 bar as a minimal reduction of 36.7% soot reduction had occurred for PCCI with n-butanol at 5 bar IMEP and a minimal reduction of 14.4%  $\text{NO}_x$  emissions for PCCI with ethanol at 4 bar IMEP.

During the course of this investigation multiple combustion/emissions metrics were analyzed in order to gain insight on what operating points were considered to be optimal for each load for CDC, PCCI with 45% PFI by mass of n-butanol (PCCI 45BU), and PCCI with 45% PFI by mass of ethanol. It was found during this study that PCCI 45ET required greater EGR% and boost pressure than PCCI 45BU at each load tested in order to overcome the lower reactivity of ethanol. However, despite the lower reactivity of ethanol, it was seen at 3 bar IMEP that PCCI 45ET had greater combustion pressures than CDC by 3.95 bar while PCCI 45BU had an increase of 6.1 bar in comparison to CDC. As load was increased it was observed that PCCI 45BU and CDC had increases in combustion pressure greater than PCCI 45ET, as such PCCI 45ET had a peak combustion pressure 1.66 bar less than CDC at 4 bar IMEP and 2.76 bar at 5 bar IMEP.

Despite this observed trend, the PPRR and subsequent AHRR reflected a greater difference between CDC and PCCI 45BU to PCCI 45ET at each given load with greater deviations as the load was increased. At 3 bar IMEP, both PCCI 45BU and PCCI 45ET had greater PPRR than CDC by 0.84 bar/CAD and 1.32 bar/CAD respectively while the AHRR reflected a similar trend. The max AHRR for PCCI 45ET and PCCI 45BU was increased by 20.32 J/CAD and 10.84 J/CAD respectively indicating that at such a light load the intensity of combustion from the global lean

mixture of either ethanol or n-butanol intensified combustion. However, as load was increased it was observed at 4 and 5 bar IMEP that only PCCI 45ET exhibited this trait with increasing magnitude while PCCI 45BU resembled CDC in terms of AHRR and PRR. As is the case at 4 bar IMEP PCCI 45ET had a peak AHRR greater than CDC by 31.51 J/CAD and an increased PRRR of 1.22 bar/CAD. At 5 bar IMEP, the max AHRR of PCCI 45ET was increased by 50.38 J/CAD from CDC and had a PRRR 2.14 bar/CAD greater than CDC. With this information in mind, it was noted that although ethanol has a lower DCN than n-butanol, because of its higher oxygen content the intensity of combustion was increased as a direct consequence and was observed to occur once 10% of fuel mass had been consumed.

Despite the intensity of combustion of PCCI 45ET, NO<sub>x</sub> emissions were reduced at 4 and 5 bar IMEP by 14.4% and 21.2% respectively in comparison to CDC. PCCI 45BU however had even greater reductions at 4 and 5 bar by 35.3% and 53.2% respectively from CDC. In addition to this PCCI 45ET did have greater soot emissions reductions at 4 and 5 bar IMEP at 75% and 72.2% respectively as a direct result of the fuels higher oxygen content thereby increasing the local lambda at the DI diffusion burn of ULSD#2. Despite this PCCI 45BU did however have a considerable reduction of soot emissions of 53.8% at 4 bar and 36.7% at 5 bar IMEP in comparison to CDC. As for the environmental impact of each combustion method, it was shown that at 3 and 4 bar IMEP PCCI 45BU had a 58% reduction of non-renewable carbon and PCCI 45ET had a 65% reduction of non-renewable carbon. As the load was increased to 5 bar IMEP, the non-renewable carbon was reduced by 59% and 64% respectively to PCCI 45BU and PCCI 45ET.

Although PCCI with n-butanol had a lesser reduction of non-renewable carbon than PCCI with ethanol, due to the inherent benefits of second-generation biofuels PCCI 45BU had a reduced Renewable Carbon Index (RCI) of 4.11, 4.25, and 4.47 to PCCI 45ET RCI of 5.15, 5.7, and 5.8 over the span of loads conducted. With all of the combustion/emissions metrics gathered in this study it was determined that PCCI with n-butanol is a superior combustion method of choice for simultaneously reducing the NO<sub>x</sub> and soot emissions of a CI engine while simultaneously facilitating further reduction of the environmental impact of ICE.

### Future Work

Although much progress has been done on the optimization of PCCI with n-butanol in regard to  $\text{NO}_x$  and soot emissions, research is needed for the suppression of increased BSFC and lowered combustion efficiency. To facilitate the optimization of PCCI in future studies, it is recommended that a simulation be built in order to optimize other engine parameters not covered in depth by this study (CRDI pressure, intake temperature, target CA50, pilot injection timing and duration, DI fuel blended with PFI fuel, and the usage of additional DI injection events). In addition to this, in order to further reduce BSFC and increase combustion efficiency, a new cooling system for the existing centrifugal supercharger gearbox or a higher capacity supercharger would be desirable for increasing boost pressures further than done so in this study. If these parameters and supporting engine systems are incorporated, PCCI with n-butanol could have a promising future for the reduction of ICE impact on the environment.

### Special Thanks

I acknowledge the technical support of the following: Barry Waters from Claxton Oil Company for supplying the experimental fuels, Christopher Mileski, Charles McGuffy, Michael Rankin, Denise Mukes, Jacques Lapeyre, from PACLP, and Joseph von Wolfgang from Malvern Lasers. Tanner Smith, Tony Frazer, Ryan Salmon, and Alfonso Moreira from Brüel and Kjær. Bob Petit, Doug Dykens, Arley Bedillion from Mastry engines Center LLC, Mike Smith of Exergy Engineering LLC, Timothy Martin, Joe Tran, Chad Wilson, Donna West, & Bret MacGregor from MKS Instruments, Sam Olesky from Kistler, Matt Viele from Viatech, Daniel Stockton, Tim Domin, Christopher Williams, Jeffrey Lewis, Don Apple, Richard Locke III, Paul Enger & Steven Rougeou from AVL, Richard Frazee from Singularity Scientific, Jon Palek from EMS, & Coty Harrison from Yokogawa. This paper is based upon work supported by the National Science Foundation Grant No. 1950207.

## REFERENCES

- Albertus, Paul, Venkataramani Anandan, Chunmei Ban, Nitash Balsara, Ilias Belharouak, Josh Buettner-Garrett, Zonghai Chen, Claus Daniel, Marca Doeff, Nancy J. Dudney, Bruce Dunn, Stephen J. Harris, Subramanya Herle, Eric Herbert, Sergiy Kalnaus, Joesph A. Libera, Dongping Lu, Steve Martin, Bryan D. McCloskey, Matthew T. McDowell, Y. Shirley Meng, Jagjit Nanda, Jeff Sakamoto, Ethan C. Self, Sanja Tepavcevic, Eric Wachsman, Chunsheng Wang, Andrew S. Westover, Jie Xiao, and Thomas Yersak. 2021. "Challenges for and Pathways toward Li-Metal-Based All-Solid-State Batteries." *ACS Energy Letters* 6 (4):1399-1404. doi: 10.1021/acsenergylett.1c00445.
- Altun, F., S. A. Tekin, S. Gürel, and M. Cernat. 2019. "Design and Optimization of Electric Cars. A Review of Technological Advances." 2019 8th International Conference on Renewable Energy Research and Applications (ICRERA), 3-6 Nov. 2019.
- Ansari, Ehsan, Mahdi Shahbakhti, and Jeffrey Naber. 2018. "Optimization of performance and operational cost for a dual mode diesel-natural gas RCCI and diesel combustion engine." *Applied Energy* 231:549-561. doi: <https://doi.org/10.1016/j.apenergy.2018.09.040>.
- Babayev, Rafig, Arne Andersson, Albert Serra Dalmau, Hong G. Im, and Bengt Johansson. 2021. "Computational characterization of hydrogen direct injection and nonpremixed combustion in a compression-ignition engine." *International Journal of Hydrogen Energy* 46 (35):18678-18696. doi: <https://doi.org/10.1016/j.ijhydene.2021.02.223>.
- Beita, Jadeed, Midhat Talibi, Suresh Sadasivuni, and Ramanarayanan Balachandran. 2021. "Thermoacoustic Instability Considerations for High Hydrogen Combustion in Lean Premixed Gas Turbine Combustors: A Review." *Hydrogen* 2 (1). doi: 10.3390/hydrogen2010003.
- Boehm, Randall C., Logan C. Scholla, and Joshua S. Heyne. 2021. "Sustainable alternative fuel effects on energy consumption of jet engines." *Fuel* 304:121378. doi: <https://doi.org/10.1016/j.fuel.2021.121378>.
- Borman, Gary, and Kazuie Nishiwaki. 1987. "Internal-combustion engine heat transfer." *Progress in Energy and Combustion Science* 13 (1):1-46. doi: [https://doi.org/10.1016/0360-1285\(87\)90005-0](https://doi.org/10.1016/0360-1285(87)90005-0).
- Brookfield, Amtek. "Brookfield viscometer DVII+pro." [http://brookfield-benelux.com/Brookfield\\_DVII+PRO\\_viscometer.html](http://brookfield-benelux.com/Brookfield_DVII+PRO_viscometer.html).
- Cao, Dao Nam, Anh Tuan Hoang, Hong Quan Luu, Van Ga Bui, and Thi Thu Huong Tran. 2020. "Effects of injection pressure on the NOx and PM emission control of diesel engine: A review under the aspect of PCCI combustion condition." *Energy Sources, Part A: Recovery, Utilization, and Environmental Effects*:1-18. doi: 10.1080/15567036.2020.1754531.
- Chandler, David L. 2022. "A method for stabilizing the interfaces in solid-state lithium-ion batteries opens new possibilities." MIT News. <https://news.mit.edu/2022/solid-state-batteries-interface-stability-0308>.

- Davis, Sarah C., William J. Parton, Stephen J. Del Grosso, Cindy Keough, Ernest Marx, Paul R. Adler, and Evan H. DeLucia. 2012. "Impact of second-generation biofuel agriculture on greenhouse-gas emissions in the corn-growing regions of the US." *Frontiers in Ecology and the Environment* 10 (2):69-74. doi: <https://doi.org/10.1890/110003>.
- DC Bradley, LL Stillings, BW Jaskula, L Munk, and AD McCauley, 'Lithium' Chapter K in KJ Schulz, JH DeYoung, RR Seal. 2018. Critical Mineral Resources of the United States: Economic and Environmental Geology and Prospects for Future Supply. edited by United States Geological Survey.
- Deere, John. 2022. "Diesel Engine Technology - See the Evolution." <https://www.deere.com/en/campaigns/engines-and-drivetrain/diesel-engine-technology/>.
- Doustdar, Omid, Soheil Zeraati-Rezaei, Jose M. Herreros, Athanasios Tsolakis, Karl D. Dearn, and Mirosław L. Wyszynski. 2021. "Tribological Performance of Biomass-Derived Bio-Alcohol and Bio-Ketone Fuels." *Energies* 14 (17). doi: 10.3390/en14175331.
- Dwivedi, Puneet, Weiwei Wang, Tara Hudiburg, Deepak Jaiswal, William Parton, Stephen Long, Evan DeLucia, and Madhu Khanna. 2015. "Cost of Abating Greenhouse Gas Emissions with Cellulosic Ethanol." *Environmental Science & Technology* 49 (4):2512-2522. doi: 10.1021/es5052588.
- Elfasakhany, Ashraf, and Abdel-Fattah Mahrous. 2016. "Performance and emissions assessment of n-butanol–methanol–gasoline blends as a fuel in spark-ignition engines." *Alexandria Engineering Journal* 55 (3):3015-3024. doi: <https://doi.org/10.1016/j.aej.2016.05.016>.
- Ellsmoor, James. 2019. "Electric Vehicles Are Driving Demand For Lithium - With Environmental Consequences." Forbes. <https://www.forbes.com/sites/jamesellsmoor/2019/06/10/electric-vehicles-are-driving-demand-for-lithium-with-environmental-consequences/?sh=2a9854062e2b>.
- EPA. 2021a. "Acid Rain Program Results." United States Environmental Protection Agency, Last Modified March 31, 2021, accessed 02/19/2022. <https://www.epa.gov/acidrain/acid-rain-program-results>.
- EPA. 2021b. "Diesel Fuel Standards and Rulemakings." United States Environmental Protection Agency, Last Modified September 24, 2021, accessed 2/19/2022. <https://www.epa.gov/diesel-fuel-standards/diesel-fuel-standards-and-rulemakings>.
- EPA. 2021c. "Particle Pollution and Respiratory Effects." United States Environmental Protection Agency, Last Modified May 27, 2021, accessed 2/20/2022. <https://www.epa.gov/particle-pollution-and-your-patients-health/health-effects-pm-patients-lung-disease>.
- Frampton, Utell, Zareba,, Cox Oberdörster, Huang,, Lee Morrow, Chalupa,, and Speers Frasier, and Stewart. 2004. Effects of Exposure to Ultrafine Carbon Particles in Healthy Subjects and Subjects with Asthma. Accessed February 22, 2022.
- Frankel, Todd C. 2016. "THE COBALT PIPELINE

- Tracing the path from deadly hand-dug mines in Congo to consumers' phones and laptops." Washington Post. <https://www.washingtonpost.com/graphics/business/batteries/congo-cobalt-mining-for-lithium-ion-battery/>.
- Gao, Jianbing, Xiaochen Wang, Panpan Song, Guohong Tian, and Chaochen Ma. 2022. "Review of the backfire occurrences and control strategies for port hydrogen injection internal combustion engines." *Fuel* 307:121553. doi: <https://doi.org/10.1016/j.fuel.2021.121553>.
- Goh, Brandon Han Hoe, Cheng Tung Chong, Hwai Chyuan Ong, Tine Seljak, Tomaž Katrašnik, Viktor Józsa, Jo-Han Ng, Bo Tian, Srinibas Karmarkar, and Veeramuthu Ashokkumar. 2022. "Recent advancements in catalytic conversion pathways for synthetic jet fuel produced from bioresources." *Energy Conversion and Management* 251:114974. doi: <https://doi.org/10.1016/j.enconman.2021.114974>.
- H. Bockhorn, A. D'Anna, A. F. Sarofim, H. Wang. 2009. "Combustion Generated Fine Carbonaceous Particles." In *Combustion Generated Fine Carbonaceous Particles*, edited by KIT Scientific Publishing, 1-2, 9-12. Original edition, 2009.
- Han, Gi Bo, Jung Hee Jang, Min Hwei Ahn, and Byung Hun Jung. 2019. "Recent Application of Bio-Alcohol: Bio-Jet Fuel." In *Alcohol Fuels-Current Technologies and Future Prospects*. IntechOpen.
- Hannu Jääskeläinen, Magdi K. Khair. 2020. "EGR Systems & Components." [https://dieselnet.com/tech/engine\\_egr\\_sys.php](https://dieselnet.com/tech/engine_egr_sys.php).
- Hawley, J. G., F. J. Wallace, A. Cox, R. W. Horrocks, and G. L. Bird. 1999. "Reduction of Steady State NO<sub>x</sub> Levels from an Automotive Diesel Engine Using Optimised VGT/EGR Schedules." 1999-03-01.
- Hergueta, C., A. Tsolakis, J. M. Herreros, M. Bogarra, E. Price, K. Simmance, A. P. E. York, and D. Thompsett. 2018. "Impact of bio-alcohol fuels combustion on particulate matter morphology from efficient gasoline direct injection engines." *Applied Energy* 230:794-802. doi: <https://doi.org/10.1016/j.apenergy.2018.08.076>.
- Ho, Shih-Hsin, Chun-Yen Chen, Duu-Jong Lee, and Jo-Shu Chang. 2011. "Perspectives on microalgal CO<sub>2</sub>-emission mitigation systems — A review." *Biotechnology Advances* 29 (2):189-198. doi: <https://doi.org/10.1016/j.biotechadv.2010.11.001>.
- Hoang, Anh Tuan. 2020. "Critical review on the characteristics of performance, combustion and emissions of PCCI engine controlled by early injection strategy based on narrow-angle direct injection (NADI)." *Energy Sources, Part A: Recovery, Utilization, and Environmental Effects*:1-15. doi: 10.1080/15567036.2020.1805048.
- Hosseini, Seyed Ehsan, and Mazlan Abdul Wahid. 2016. "Hydrogen production from renewable and sustainable energy resources: Promising green energy carrier for clean development." *Renewable and Sustainable Energy Reviews* 57:850-866. doi: <https://doi.org/10.1016/j.rser.2015.12.112>.
- Huang, Jin, Yinming Du, Teng Bao, Meng Lin, Jufang Wang, and Shang-Tian Yang. 2019. "Production of n-butanol from cassava bagasse hydrolysate by engineered *Clostridium*

- tyrobutyricum overexpressing adhE2: Kinetics and cost analysis." *Bioresource Technology* 292:121969. doi: <https://doi.org/10.1016/j.biortech.2019.121969>.
- Johnson, Jane M. F., Alan J. Franzluebbbers, Sharon Lachnicht Weyers, and Donald C. Reicosky. 2007. "Agricultural opportunities to mitigate greenhouse gas emissions." *Environmental Pollution* 150 (1):107-124. doi: <https://doi.org/10.1016/j.envpol.2007.06.030>.
- Kang, Qian, Lise Appels, Tianwei Tan, and Raf Dewil. 2014. "Bioethanol from Lignocellulosic Biomass: Current Findings Determine Research Priorities." *The Scientific World Journal* 2014:298153. doi: 10.1155/2014/298153.
- Kasmuri, N. H., S. K. Kamarudin, S. R. S. Abdullah, H. A. Hasan, and A. Md Som. 2017. "Process system engineering aspect of bio-alcohol fuel production from biomass via pyrolysis: An overview." *Renewable and Sustainable Energy Reviews* 79:914-923. doi: <https://doi.org/10.1016/j.rser.2017.05.182>.
- Kaunda, Rennie B. 2020. "Potential environmental impacts of lithium mining." *Journal of Energy & Natural Resources Law* 38 (3):237-244. doi: 10.1080/02646811.2020.1754596.
- Kouremenos, D. A., D. T. Hountalas, and K. B. Binder. 2001. "The Effect of EGR on the Performance and Pollutant Emissions of Heavy Duty Diesel Engines Using Constant and Variable AFR." *SAE Transactions* 110:225-238.
- Lawrence, Mark G., and Paul J. Crutzen. 1999. "Influence of NO<sub>x</sub> emissions from ships on tropospheric photochemistry and climate." *Nature* 402 (6758):167-170. doi: 10.1038/46013.
- Li, Yaopeng, Ming Jia, Yachao Chang, Zhen Xu, Guangfu Xu, Hong Liu, and Tianyou Wang. 2018. "Principle of determining the optimal operating parameters based on fuel properties and initial conditions for RCCI engines." *Fuel* 216:284-295. doi: <https://doi.org/10.1016/j.fuel.2017.12.010>.
- Liang, Xin, Anhao Zhong, Zuoyu Sun, and Dong Han. 2019. "Autoignition of n-heptane and butanol isomers blends in a constant volume combustion chamber." *Fuel* 254:115638. doi: <https://doi.org/10.1016/j.fuel.2019.115638>.
- Liu, Xinlei, Sage Kokjohn, Yu Li, Hu Wang, Hailin Li, and Mingfa Yao. 2019. "A numerical investigation of the combustion kinetics of reactivity controlled compression ignition (RCCI) combustion in an optical engine." *Fuel* 241:753-766. doi: <https://doi.org/10.1016/j.fuel.2018.12.068>.
- Maiboom, Alain, Xavier Tauzia, and Jean-François Hétet. 2008. "Experimental study of various effects of exhaust gas recirculation (EGR) on combustion and emissions of an automotive direct injection diesel engine." *Energy* 33 (1):22-34. doi: <https://doi.org/10.1016/j.energy.2007.08.010>.
- Maity, Jyoti Prakash, Jochen Bundschuh, Chien-Yen Chen, and Prosun Bhattacharya. 2014. "Microalgae for third generation biofuel production, mitigation of greenhouse gas emissions and wastewater treatment: Present and future perspectives – A mini review." *Energy* 78:104-113. doi: <https://doi.org/10.1016/j.energy.2014.04.003>.

- Majewski, W. Addy. 2016. "Diesel Catalysts." Diesel Net.  
[https://dieselnet.com/tech/cat\\_diesel.php](https://dieselnet.com/tech/cat_diesel.php).
- Maurya, Rakesh Kumar. 2019. "Introduction." In *Reciprocating Engine Combustion Diagnostics: In-Cylinder Pressure Measurement and Analysis*, edited by Rakesh Kumar Maurya, 1-35. Cham: Springer International Publishing.
- Miller, Caleb. 2022. "First Toyota with Solid-State Batteries Will Be a Hybrid." Car and Driver.  
<https://www.caranddriver.com/news/a38711469/toyota-solid-state-batteries-2025/>.
- Morgan, Sam. 2019. "WHY EUROPE'S ROADS ARE NOT YET SWARMING WITH ELECTRIC CARS." *E&T*, May 2019, 12-13.
- NOAA. 2016. "TOAR: Assessing the Science of Ozone Pollution." NOAA.  
[https://csl.noaa.gov/news/2016/178\\_0114.html](https://csl.noaa.gov/news/2016/178_0114.html).
- Oceania, Shimadzu. "DTG-60/DTG-60A." <https://shimadzu.com.au/dtg-60dtg-60a>.
- Pan, Wang, Metin Korkmaz, Joachim Beeckmann, and Heinz Pitsch. 2020. "Nonlinear Identification Modeling for PCCI Engine Emissions Prediction Using Unsupervised Learning and Neural Networks." 2020-04-14.
- Pitz JW, Westbrook CK. 2011. "Combustion Chemistry."
- Price, D., R. Birnbaum, R. Batiuk, M. McCullough, and R. Smith. 1997. Nitrogen oxides: Impacts on public health and the environment. United States.
- Raganati, Francesca, Alessandra Procentese, Giuseppe Olivieri, Maria Elena Russo, Piero Salatino, and Antonio Marzocchella. 2020. "Bio-butanol recovery by adsorption/desorption processes." *Separation and Purification Technology* 235:116145. doi: <https://doi.org/10.1016/j.seppur.2019.116145>.
- Raut, A., B. K. Irdmoussa, and M. Shahbakhti. 2018. "Dynamic modeling and model predictive control of an RCCI engine." *Control Engineering Practice* 81:129-144. doi: <https://doi.org/10.1016/j.conengprac.2018.09.004>.
- Richter, Felix. 2021. "Rising Commodity Prices Slow EV Battery Price Drop." Statista.  
<https://www.statista.com/chart/7713/electric-car-battery-prices/>.
- Roser, Hannah Ritchie and Max. 2020. "CO<sub>2</sub> and Greenhouse Gas Emissions." *Our World in Data*.
- Shim, Euijoon, Hyunwook Park, and Choongsik Bae. 2020. "Comparisons of advanced combustion technologies (HCCI, PCCI, and dual-fuel PCCI) on engine performance and emission characteristics in a heavy-duty diesel engine." *Fuel* 262:116436. doi: <https://doi.org/10.1016/j.fuel.2019.116436>.
- Singh, Akhilendra Pratap, Vikram Kumar, and Avinash Kumar Agarwal. 2020. "Evaluation of comparative engine combustion, performance and emission characteristics of low temperature combustion (PCCI and RCCI) modes." *Applied Energy* 278:115644. doi: <https://doi.org/10.1016/j.apenergy.2020.115644>.



- Soloiu, Valentin, Cesar E. Carapia, Justin T. Wiley, Jose Moncada, Remi Gaubert, Aliyah Knowles, Marcel Ilie, and Mosfequr Rahman. 2019. "RCCI Investigations With n-Butanol and ULSD." ASME 2019 Internal Combustion Engine Division Fall Technical Conference.
- Soloiu, Valentin, Jose D. Moncada, Remi Gaubert, Aliyah Knowles, Gustavo Molina, Marcel Ilie, Spencer Harp, and Justin T. Wiley. 2018. "Reactivity Controlled Compression Ignition combustion and emissions using n-butanol and methyl oleate." *Energy* 165:911-924. doi: <https://doi.org/10.1016/j.energy.2018.09.181>.
- Soloiu, Valentin, Jose D. Moncada, Remi Gaubert, Martin Muiños, Spencer Harp, Marcel Ilie, Andrew Zdanowicz, and Gustavo Molina. 2018. "LTC (low-temperature combustion) analysis of PCCI (premixed charge compression ignition) with n-butanol and cotton seed biodiesel versus combustion and emissions characteristics of their binary mixtures." *Renewable Energy* 123:323-333. doi: <https://doi.org/10.1016/j.renene.2018.02.061>.
- Styring, Peter, George R. M. Dowson, and Isabel O. Tozer. 2021. "Synthetic Fuels Based on Dimethyl Ether as a Future Non-Fossil Fuel for Road Transport From Sustainable Feedstocks." *Frontiers in Energy Research* 9.
- Tian, Zhi, Xudong Zhen, Yang Wang, Daming Liu, and Xiaoyan Li. 2020. "Combustion and emission characteristics of n-butanol-gasoline blends in SI direct injection gasoline engine." *Renewable Energy* 146:267-279. doi: <https://doi.org/10.1016/j.renene.2019.06.041>.
- VISNIC, BILL. 2021. "Toyota promising big battery, EV action, but circumspect on absolutes." SAE International. <https://www.sae.org/news/2021/09/toyota-details-significant-battery-investment-plan>.
- VP-Racing-Fuels. 2019. "Specification Sheet: X-98." Last Modified 10/04/2019. [https://vpracingfuels.com/wp-content/uploads/2019/12/X98-Spec-Sheets\\_100419A-1.pdf](https://vpracingfuels.com/wp-content/uploads/2019/12/X98-Spec-Sheets_100419A-1.pdf).
- Weber, Christian, Alexander Farwick, Feline Benisch, Dawid Brat, Heiko Dietz, Thorsten Subtil, and Eckhard Boles. 2010. "Trends and challenges in the microbial production of lignocellulosic bioalcohol fuels." *Applied Microbiology and Biotechnology* 87 (4):1303-1315. doi: 10.1007/s00253-010-2707-z.
- Xiao, Helin, Fengyun Guo, Shengjun Li, Ru Wang, and Xiaolong Yang. 2019. "Combustion performance and emission characteristics of a diesel engine burning biodiesel blended with n-butanol." *Fuel* 258:115887. doi: <https://doi.org/10.1016/j.fuel.2019.115887>.
- Yoshimoto, Yasufumi, Enkhjargal Tserenochir, Eiji Kinoshita, and Takeshi Otaka. 2018. "Combustion Improvements by C4/C5 Bio-Alcohol Isomer Blended Fuels Combined with Supercharging and EGR in a Diesel Engine." *International Journal of Mechanical, Industrial and Aerospace Sciences* 11.0 (10). doi: 10.5281/zenodo.1474930.
- Zheng, Zunqing, Mingtao Xia, Haifeng Liu, Xiaofeng Wang, and Mingfa Yao. 2018. "Experimental study on combustion and emissions of dual fuel RCCI mode fueled with biodiesel/n-butanol, biodiesel/2,5-dimethylfuran and biodiesel/ethanol." *Energy* 148:824-838. doi: <https://doi.org/10.1016/j.energy.2018.02.015>.